ANALYTICAL INVESTIGATIONS ON COLLAPSE OF CYLINDRICAL SUBMARINE SHELLS

G9047

A THESIS

UNIVERSITY LIBRARY ★ COCHIN UNIVERSITY OF SCIENCE AND TECHNOLOGY ★
G9047
Cochin - 682 022

Submitted by

ALICE MATHAI

for the award of the degree

of

DOCTOR OF PHILOSOPHY

DEPARTMENT OF SHIP TECHNOLOGY
COCHIN UNIVERSITY OF SCIENCE AND TECHNOLOGY
KOCHI-682 022

NOVEMBER 2004

Certificate

I here by certify that, to the best of my knowledge, the thesis entitled ***Analytical Investigations on Collapse of Cylindrical Submarine Shells*** *is a record of bona fide research carried out by* ***Alice Mathai,*** *Part time research student, Reg. No.2046 under my supervision and guidance, as the partial fulfilment of the requirement for the award of Ph.D degree in the faculty of technology. The results presented in this thesis or parts of it have not been presented for the award of any other degree.*

Kochi –22,
10–11–04.

Dr. C.G. Nandakumar,
Research Guide,
Dept. of Ship Technology,
Cochin University of Science &
Technology, Kochi –22.

DECLARATION ABOUT THE AUTHENTICITY OF THE RESEARCH WORK BY THE RESEARCH STUDENT

I here by declare that the thesis entitled ***Analytical Investigations on Collapse of Cylindrical Submarine Shells*** *is an authentic record of the research work carried by me under the supervision and guidance of Dr. C.G. Nandakumar, Department of Ship Technology, CUSAT, in the partial fulfilment of the requirement for the award of Ph.D degree in the faculty of technology and no part thereof has been presented for the award of any other degree.*

Kochi –22,
10-11-04.

Alice Mathai,
Part time Research Scholar,
Reg. No. 2046,
Dept. of Ship Technology,
CUSAT, Kochi-22.

Dedicated To My Father,

Who Inspired Me

ACKNOWLEDGEMENTS

I express my sincere gratitude to Dr. C.G. Nandakumar, Department of Ship Technology, Cochin University of Science and Technology, for his valuable guidance, constant support and encouragement without which this thesis work would not have been materialised. Words are not enough to describe how much I am indebted to him in the process of conception, execution and completion of this work.

I would like to thank Dr. K.P. Narayanan, Head of the Department of Ship Technology for having provided the support – both in his official and personal capacities for this work. I am very much grateful to my senior colleague, Smt. Jayasree Ramanujan, Lecturer, Mar Athanasius College of Engineering, for her whole - hearted help in this endeavour.

My sincere gratitude is extended to all the faculty members and office staff of the Department of Ship Technology, CUSAT. Special mention should be made about Smt. Seenath and Smt. Ajitha for their support. I owe much to the valuable insight given by Mr. Unnithan C., Research Scholar, I I T Madras, in the area of nonlinear analysis.

I would like to acknowledge the faculty members of Mar Athanasius College of Engineering, Kothamangalam, who in various capacities rendered their help. Very special thanks to Principal, Dr. Paul K. Mathew, Prof. P. Salome Varghese and Dr. M.G. Grasius for their encouragement.

Last but not the least, I am very much indebted to my husband George, for his encouragement and sons, John and Mathew for their patience and to ease a mother's guilt from spending too little time with them.

CONTENTS

Abstract vi

Nomenclature vii

List of Figures xi

List of Tables xvi

Chapter 1. Introduction

1.1 General 1

1.2 Hull Geometry 1

1.3 Structural Behaviour 1

1.4 Structural Analysis of Cylindrical Shells 2

1.5 Finite Element Analysis of Stiffened Cylindrical Shells 2

1.6 Finite Element Modeling of Unstiffened Cylindrical Shells 3

1.7 Finite Element Modeling of Stiffened Cylindrical Shells 4

1.8 Types of Analyses Performed 5

1.8.1 Linear Static Analysis 6

1.8.2 Linear Buckling Analysis 6

1.8.3 Geometric Nonlinear Analysis 8

1.9 Follower Force Effect of Hydrostatic Pressure 9

1.10 Design Aspects of Submarine Hulls 10

1.11 Organisation of the Thesis 11

Chapter 2. Review of Literature

2.1 Introduction 13

2.2 Classical Solutions 13

2.2.1 Shell Buckling 13

2.2.2 Shell Yielding 14

2.2.3 General Instability 15

2.3 Axisymmetric Cylindrical Shell Finite Elements 17

2.3.1 Unstiffened Shells 17

2.3.2 Stiffened Shells 19

2.4 Ring Stiffened Cylindrical Shells with Other Types of Finite Elements .. 21

2.5 Follower Force Effect 21

2.6 Design Aspects of Submarine Hulls 23
2.7 Scope and Objectives 24

Chapter 3. Linear Static Analysis

3.1 General 26
3.2 Finite Element Modeling of Cylindrical Shell 26
3.2.1 Geometry, Displacement Field and Shape Functions 26
3.2.2 Strain Matrix 27
3.2.3 Constitutive Matrix 28
3.2.4 Linear Elastic Stiffness Matrix 29
3.2.5 Load Vector 30
3.2.6 Evaluation of Displacement 30
3.2.7 Recovery of Stress Resultants and Principal Stresses 30
3.3 Finite Element Modeling of Stiffened Cylindrical Shell 31
3.3.1 Discrete Ring Stiffener Element 31
3.3.2 Elastic Stiffness Matrix of Ring Stiffener Element 31
3.3.3 Transformation Matrix for Stiffener 32
3.3.4 Formulation of Stiffness Matrix of Stiffened Shell Element 32
3.4. Assembly of Global Matrix 32
3.4.1 Stiffness Matrix 32
3.4.2 Load Vector 32
3.5 Software Development 33
3.5.1 Flow Chart 33
3.5.2 Program MAIN 35
3.5.3 Description of Functions 35
3.6 Numerical Investigations 36
3.6.1 Validation 36
3.6.2 Linear Static Analysis of Submarine Models 37
3.7 Results and Discussion 41

Chapter 4. Linear Buckling Analysis

4.1 Introduction 52
4.2 Hydrostatic Pressure as Radial Pressure Load 52
4.2.1 Development of Geometric Stiffness Matrix 52

4.2.2 Geometric Stiffness Matrix of the Shell Element 53
4.2.3 Geometric Stiffness Matrix of the Discrete Stiffener Element 54
4.2.4 Prediction of Linear Buckling Pressure 54
4.3 Follower Force Effect due to Hydrostatic Pressure 55
4.3.1 Development of Pressure Stiffness Matrix 55
4.3.2 Buckling Pressure Prediction 57
4.4 Development of Software 57
4.4.1 Flow Chart 57
4.4.2 Program MAIN 60
4.4.3 Description of Functions 60
4.5 Numerical Investigations 61
4.6 Results and Discussion 63
4.6.1 Interstiffener Buckling Analysis of BMP2 63
4.6.2 Influence of Nodal Degrees of Freedom, which are Derivatives of Displacement 66
4.6.3 Analysis of Stiffened Cylindrical Shell of BMP3 66
4.6.4 Interstiffener Buckling Analysis of Submarine Models 69
4.6.5 Interdeepframe Buckling Analysis of Submarine Models 72
4.6.6 Interbulkhead Buckling Analysis of Submarine Models 75
4.6.7 Follower Force Effect of Hydrostatic Pressure 77

Chapter 5. Geometric Nonlinear Analysis

5.1 Introduction 86
5.2 Hydrostatic Pressure as Radial Pressure Load 86
5.2.1 Methodology 86
5.2.2 Corotational Kinematics and Generation of Total Tangent Stiffness Matrix 89
5.2.3 Transformation Matrix 92
5.2.4 Tangent Stiffness Matrix 93
5.3 Follower Force Effect of Hydrostatic Pressure 94
5.4 Software Development 94
5.4.1 Flow Chart 94
5.4.2 Description of the Program MAIN 98

5.4.3 Description of Functions 98
5.5 Numerical Investigations 100
5.6 Results and Discussion 102
5.6.1 Validation 102
5.6.2 Interstiffener Analysis of BMP2 104
5.6.3 Analysis of Stiffened Cylindrical Shell of BMP3 107
5.6.4 Interstiffener Analysis of Submarine Models 109
5.6.5 Interdeepframe Analysis of Submarine Models 117
5.6.6 Interbulkhead Analysis of Submarine Models 121
5.6.7 Follower Force Effect of Hydrostatic Pressure 126
5.6.8 Combined Effect of Geometric Nonlinearity and Follower Force on Buckling Pressure 133
5.6.9 Safety Factor 135

Chapter 6. Conclusions

6.1 General 138
6.2 Linear Static Analysis 138
6.3 Linear Buckling Analysis 139
6.4 Geometric Nonlinear Analysis 142
6.5 Overall Reduction in Buckling Pressure 144
6.6 Safety Factor from Classical Solutions and Design Pressure from Rulebook Provisions 145
6.7 Scope for Future Work 145

References 147

Appendix A. Elements of Stiffness Matrices of All-Cubic Axisymmetric Element and Discrete Ring Stiffener Element

A.1 Upper Triangular Elements of Elastic Stiffness Matrix [k] of the Shell Element 156
A.2 Elements of Stress Resultant Matrix [S] 159
A.3 Upper Triangular Elements of Elastic Stiffness Matrix [k_S] of the Stiffener Element 161
A.4 Upper Triangular Elements of Geometric Stiffness Matrix [k_g] of the Shell Element 161

A.5 Upper Triangular Elements of Geometric Stiffness Matrix [k_{gS}] of the Stiffener Element 162
A.6 Upper Triangular Elements of Pressure Stiffness Matrix [k_p] of the Shell Element 162

Appendix B. Classical Solutions and Rulebook Provisions

B.1. General 164
B.2. Classical Solutions for Short Stiffened Cylindrical Shell with External Pressure 164
B.2.1 Radial Deflection 164
B.2.2 Stress Resultants 165
B.2.3 Shell Buckling 165
B.2.4 Shell Yielding 166
B.2.5 General Instability 166
B.3 Software Development 166
B.4 Numerical Investigations 166
B.5 Discussion of Results 167

Publications based on the research work 169

ABSTRACT

Submarine hull structure is a watertight envelope, under hydrostatic pressure when in operation. Stiffened cylindrical shells constitute the major portion of these submarine hulls and these thin shells under compression are susceptible to buckling failure. Normally loss of stability occurs at the limit point rather than at the bifurcation point and the stability analysis has to consider the change in geometry at each load step. Hence geometric nonlinear analysis of the shell forms becomes a necessity. External hydrostatic pressure will follow the deformed configuration of the shell and hence follower force effect has to be accounted for.

Computer codes have been developed based on all-cubic axisymmetric cylindrical shell finite element and discrete ring stiffener element for linear elastic, linear buckling and geometric nonlinear analysis of stiffened cylindrical shells. These analysis programs have the capability to treat hydrostatic pressure as a radial load and as a follower force.

Analytical investigations are carried out on two attack submarine cylindrical hull models besides standard benchmark problems. In each case, the analysis has been carried out for interstiffener, interdeepframe and interbulkhead configurations. The shell stiffener attachment in each of this configuration has been represented by the simply supported-simply supported, clamped-clamped and fixed-fixed boundary conditions in this study.

The results of the analytical investigations have been discussed and the observations and conclusions are described. Rotation restraint at the ends is influential for interstiffener and interbulkhead configurations and the significance of axial restraint becomes predominant in the interbulkhead configuration. The follower force effect of hydrostatic pressure is not significant in interstiffener and interdeepframe configurations where as it has very high detrimental effect on buckling pressure on interbulkhead configuration. The geometric nonlinear interbulkhead analysis incorporating follower force effect gives the critical value of buckling pressure and this analysis is recommended for the determination of collapse pressure of stiffened cylindrical submarine shells.

NOMENCLATURE

B	-	Ratio of shell area under the frame faying flange to total frame area plus shell area under frame faying flange
$[\overline{B}]$	-	Strain matrix
[B]	-	Linear strain matrix
$[B_{nl}]$	-	Nonlinear strain matrix
D	-	Diameter to midplane of shell
[D]	-	Constitutive Matrix
e	-	Eccentricity of the stiffener
E	-	Modulus of elasticity
F	-	Internal force vector
{F}	-	Equivalent resistive forces
G	-	Shear Modulus
[G]	-	Matrix from derivative of shape functions
H	-	Transcendental function that define bending effect in shell reflected at midspan
i,j,k	-	Unit vectors in mutually orthogonal directions
I	-	Moment of inertia of the frame including one frame spacing of shell plating
[k]	-	Linear elastic stiffness matrix
$[k_g]$	-	Geometric stiffness matrix
$[k_P]$	-	Pressure stiffness matrix
$[k_S]$	-	Linear elastic stiffness matrix of the stiffener
$[k_{gS}]$	-	Geometric stiffness matrix of the stiffener
K	-	Transcendental function
$[K_o]$	-	Global elastic stiffness matrix in the original configuration
${}^t[K]$	-	Global elastic stiffness matrix in the current configuration

$[K_g]$	-	Global geometric stiffness matrix in the original configuration
$[K_{gp}]$	-	Stiffness matrix incorporating geometric and pressure stiffnesses
$[K_G]$	-	Global geometric stiffness matrix at the particular stress level
$[K_{nl}]$	-	Large displacement stiffness matrix
$[K_P]$	-	Pressure stiffness matrix in the original configuration
$[K_T]$	-	Total tangent stiffness matrix in the original configuration
${}^t[K_T]$	-	Total tangent stiffness matrix in the current configuration
l,m,n	-	Direction cosines
L	-	Unsupported length of shell plating
L_s	-	Length between bulk heads
n	-	Circumferential wave number
[N]	-	Shape function
$N_x, N_\theta, N_{x\theta}$	-	Stress resultants
$M_x, M_\theta, M_{X\theta}$	-	Moment resultants
O, O_0, O_R	-	Origin in base, corotated and current configurations
p	-	Pressure intensity
Pi	-	Effective pressure acting on the stiffened shell
P	-	Discrete load
P_y	-	Pressure, Corresponding to frame yielding
P_c	-	Collapse Pressure corresponding to shell buckling
P_{cr}	-	Critical pressure associated with general instability
{Q}	-	Nodal load vector.
r	-	External load vector
R	-	Radius to midplane of shell
R_r	-	Radius to the centroid of the stiffener
{R}	-	Equivalent nodal loads

t	-	Minimum thickness of the shell
T	-	Transformation matrix of the stiffener
$[T_R]$	-	Transformation matrix for the element
$[T_r]$	-	Coordinate rotation matrix
u	-	Displacement vector
$\bar{u}$	-	Purely deformational displacements
u^e	-	Deformational displacements in local coordinates
u_R	-	Rigid body displacements
u,v,w	-	Meridional, tangential and radial displacement field
u_x,v_x,φ	-	Derivatives of displacements with respect to x
u_r,v_r,w_r,φ_r	-	Centroidal degrees of freedom of discrete ring stiffener element
U	-	Total strain energy
ux_1,ux_2,ux_0	-	Translation in global X direction
uy_1,uy_2,uy_0	-	Translation in global Y direction
uz_1,uz_2,uz_0	-	Translation in global Z direction
W	-	Work done by the prebuckling stresses on the nonlinear buckling displacement
(x_o^e,y_o^e,z_o^e)	-	Local coordinate system in the initial stage
(x_e,y_e,z_e)	-	Local coordinate system in the corotated stage
(x_R^e,y_R^e,z_R^e)	-	Corotated coordinate system
(x,y,z)	-	Global coordinates in the deformed configuration
(X,Y,Z)	-	Global coordinates in the original configuration
α_1, α_2	-	Pre-buckling stress coefficient
β	-	Numerical factor
β_f	-	Degree of flexibility provided by the frame
$\{\delta\}$	-	Displacement matrix

δ^{I}	-	Net deflection of the stiffened cylinder
$\{\delta_r\}$	-	Displacement vector at the centroidal degrees of freedom of stiffeners
ϵ	-	Total strain
ϵ_L	-	Linear strain
ϵ_{nL}	-	Nonlinear strain
$\{\epsilon_\theta\}_{nL}$	-	Nonlinear buckling strain
$\epsilon_x, \epsilon_\theta, \epsilon_{x\theta}$	-	In surface strains of cylindrical shell
θ	-	Angular variation in circumferential direction
λ	-	Nondimensional pressure
λ_b	-	Nondimensional buckling pressure
σ_{yN}	-	Specified minimum yield stress
σ_x, σ_θ	-	Prebuckling stresses
$\{\sigma\}$	-	Stress level
ν, μ	-	Poisson's ratio
ξ	-	Nondimensional meridional coordinate
$\psi_x, \psi_\theta, \psi_{x\theta}$	-	Curvatures of the cylindrical shell
Ω	-	Work done during pressure rotation phase
εD	-	Displacement convergence tolerance
Π	-	Total potential

LIST OF FIGURES

Fig. No	Title	Page
1.1	Bifurcation buckling	6
3.1	All-cubic cylindrical shell finite element	27
3.2	Discrete ring stiffener element	31
3.3a	Schematic diagram for linear static analysis	33
3.3b	Flowchart for linear static analysis	34
3.4	Geometric features of ring stiffened cylindrical shell BMP1	37
3.5	Finite element model of ring stiffened cylindrical shell BMP1	37
3.6a	Stiffened cylindrical shell of M1 between two bulkheads	39
3.6b	Stiffened cylindrical shell of M1 with deep frames	39
3.7a	Stiffened cylindrical shell of M2 between two bulkheads	39
3.7b	Stiffened cylindrical shell of M2 with deep frames	40
3.8	Variation of radial deflection for BMP1	41
3.9	Variation of circumferential stress for BMP1	41
3.10	Variation of meridional moment for BMP1	42
3.11	Variation of radial deflection for M1 for interstiffener configuration	43
3.12	Variation of major and minor principal stresses in the outer and the middle layers for M1 for interstiffener configuration	43
3.13	Variation of longitudinal and circumferential stress resultants for M1 for interstiffener configuration	44
3.14	Variation of longitudinal and circumferential moments for M1 for interstiffener configuration	44
3.15	Variation of radial deflection for M2 for interstiffener configuration	45
3.16	Variation of major and minor principal stresses in the outer and the middle layers for M2 for interstiffener configuration	45
3.17	Variation of longitudinal and circumferential stress resultants for M2 for interstiffener configuration	45

3.18	Variation of longitudinal and circumferential moments for M2 for interstiffener configuration	45
3.19	Variation of radial deflection for M1 for interdeepframe configuration	46
3.20	Variation of major and minor principal stresses in the outer and the middle layers for M1 for interdeepframe configuration	46
3.21	Variation of longitudinal and circumferential stress resultants for M1 for interdeepframe configuration	46
3.22	Variation of longitudinal and circumferential moments for M1 for interdeepframe configuration	46
3.23	Variation of radial deflection for M2 for interdeepframe configuration	47
3.24	Variation of major and minor principal stresses in the outer and the middle layers for M2 for interdeepframe configuration	47
3.25	Variation of longitudinal and circumferential stress resultants for M2 for intersdeepframe configuration	47
3.26	Variation of longitudinal and circumferential moments for M2 for interdeepframe configuration	47
3.27	Variation of radial deflection for M1 for interbulkhead configuration	48
3.28	Variation of major and minor principal stresses in the outer and the middle layers for M1 for interbulkhead configuration	48
3.29	Variation of longitudinal and circumferential stress resultants for M1 for interbulkhead configuration	48
3.30	Variation of longitudinal and circumferential moments for M1 for interbulkhead configuration	48
3.31	Variation of radial deflection for M2 for interbulkhead configuration	49
3.32	Variation of major and minor principal stresses in the outer and the middle layers for M2 for interbulkhead configuration	49
3.33	Variation of longitudinal and circumferential stress resultants for M2 for interbulkhead configuration	49
3.34	Variation of longitudinal and circumferential moments for M2 for inter bulkhead configuration	49

3.35	Variation of radial deflection for interbulkhead configuration of M1 with and without stiffeners	50
3.36	Variation of radial deflection for interbulkhead configuration of M2 with and without stiffeners	51
4.1a	Schematic diagram for linear buckling analysis	58
4.1b	Flowchart for linear buckling analysis	59
4.2a	Geometric features of BMP2	61
4.2.b	Finite element model of interstiffener portion of BMP2	61
4.3a	Geometric features of BMP3	62
4.3b	Cross sectional details of the stiffeners	62
4.3c	Finite element model of BMP3	62
4.4	Determinant Vs buckling pressure of BMP2 for interstiffener linear buckling analysis for s.s-s.s for minimum buckling pressure with circumferential wave no. 12	63
4.5	Interstiffener linear buckling pressures of BMP2 for various boundary conditions	65
4.6	Linear buckling pressures of BMP3 for various boundary conditions	67
4.7	Interstiffener linear buckling pressures for M1 for various boundary conditions with and without follower force effect	70
4.8	Interstiffener linear buckling pressures for M2 for various boundary conditions with and without follower force effect	71
4.9	Interdeepframe linear buckling pressures for M1 for various boundary conditions	73
4.10	Interdeepframe linear buckling pressures for M2 for various boundary conditions	74
4.11	Interbulkhead linear buckling pressures for M1 for various boundary conditions	76
4.12	Interbulkhead linear buckling pressures for M2 for various boundary conditions	77
5.1	Load control incremental- iterative procedure	87
5.2	Corotational kinemtics	90

5.3a	Schematic diagram of geometric nonlinear analysis	95
5.3b	Flowchart for geometric nonlinear analysis	96
5.4.	Geometric features of ring stiffened cylindrical shell (BMP4)	100
5.5	Nonlinear buckling pressures corresponding to wave numbers for BMP4.	103
5.6	Linear and nonlinear load deflection curve of BMP4 for s.s-s.s boundary conditions (n=6)	103
5.7	Nonlinear interstiffener buckling pressures corresponding to wave numbers for BMP2 for various boundary conditions	105
5.8	Minimum linear and nonlinear buckling pressures for various boundary conditions for BMP2	106
5.9	Equilibrium path and linear load deflection curve of BMP2 for f-f boundary conditions (n=11)	106
5.10	Nonlinear buckling pressures corresponding to wave numbers of stiffened cylindrical shell of BMP3 for various boundary conditions	108
5.11	Minimum linear and nonlinear buckling pressures for various boundary conditions for BMP3	108
5.12	Linear and nonlinear load deflection curve of BMP3 for f-f boundary condition for circumferential wave number 12	109
5.13	Nonlinear interstiffener buckling pressures for M1 with and without follower force effect for various boundary conditions	111
5.14	Minimum linear and nonlinear buckling pressures for various configurations and boundary conditions with and without follower force effect for M1	112
5.15	Linear load deflection curve and equilibrium path with and without follower force effect for shell between stiffeners of M1 for f-f boundary condition	113
5.16	Nonlinear interstiffener buckling pressures of M2 with and without follower force effect for various boundary conditions	114
5.17	Minimum linear and nonlinear buckling pressures for various configurations and boundary conditions with and without follower force effect for M2	115

5.18	Linear load deflection curve and equilibrium path with and without follower force effect for shell between stiffeners of M2 for f-f boundary condition (n=16)	116
5.19	Nonlinear interdeepframe buckling pressures corresponding to wave numbers with and without follower force effect of M1 for various boundary conditions	118
5.20	Linear load deflection curve and equilibrium path with and without follower force effect of shell between deepframes of M1 for f-f boundary condition	119
5.21	Nonlinear interdeepframe buckling pressures for M2 with and without follower force effect for various boundary conditions	120
5.22	Linear load deflection curve and equilibrium path with and without follower force effect for shell between deepframes of M2 for f-f boundary condition (n=15)	121
5.23	Nonlinear interbulkhead buckling pressures corresponding to wave numbers of M1 with and without follower force effect for various boundary conditions	122
5.24	Linear load deflection curve and equilibrium path with and without follower force effect for shell between bulkheads of M1 for f-f boundary condition (n=2)	123
5.25	Nonlinear interbulkhead buckling pressures corresponding to wave numbers of M1 with and without follower force effect for various boundary conditions	124
5.26	Linear load deflection curve and equilibrium path with and without follower force effect of shell between bulkheads of M2 for f-f boundary condition (n=2)	125

LIST OF TABLES

Table. No	Title	Page
3.1	Design specifications of submarine models M1 & M2	38
3.2	Geometric features of submarine models MI &M2	38
3.3	The L/R values for three configurations and R/t values for M1 and M2	40
3.4	Comparison with Flugge's results	42
3.5	Comparison with classical solutions for radial deflection for long shells	51
4.1	Linear interstiffener buckling pressures of BMP2 for various boundary conditions and finite element models	64
4.2	Comparison with Kendrick's and von Mises' results for BMP2	65
4.3	Influence of derivatives of displacements u_x and v_x in interstiffener buckling analysis of BMP2	66
4.4	Linear buckling pressures of BMP3 for various boundary conditions	67
4.5	Comparison with Kendrick's and Bryant's results for BMP3	68
4.6	Interstiffener linear buckling pressures for M1 for various boundary conditions	69
4.7	Interstiffener linear buckling pressures of M2 for various boundary conditions	71
4.8	Interdeepframe linear buckling pressures for M1 for various boundary conditions	73
4.9	Interdeepframe linear buckling pressures for M2 for various boundary conditions.	74
4.10	Interbulkhead buckling pressures of stiffened cylindrical shell for M1 for various boundary conditions	75
4.11	Interbulkhead buckling pressures of stiffened cylindrical shell for M2 for various boundary conditions	76
4.12	Interstiffener linear buckling pressures for M1 for various boundary conditions with follower force effect	78

4.13	Interstiffener linear buckling pressures for M2 for various boundary conditions with follower force effect	79
4.14	Effect of follower force on interstiffener minimum linear buckling pressures of M1	80
4.15	Effect of follower force on interstiffener minimum linear buckling pressures of M2	80
4.16	Interdeepframe linear buckling pressures for M1 for various boundary conditions	81
4.17	Interdeepframe linear buckling pressures for M2 for various boundary conditions	82
4.18	Effect of follower force on interdeepframe minimum linear buckling pressures of M1	83
4.19	Effect of follower force on interdeepframe minimum linear buckling pressures of M2	83
4.20	Interbulkhead linear buckling pressures for M1 for various boundary conditions	84
4.21	Interbulkhead linear buckling pressures for M2 for various boundary conditions	84
4.22	Effect of follower force on interbulkhead minimum linear buckling pressures of M1	85
4.23	Effect of follower force on interbulkhead minimum linear buckling pressures of M2	85
5.1	Nonlinear buckling pressures corresponding to wave numbers for BMP4	102
5.2	Nonlinear interstiffener buckling pressures corresponding to wave numbers for BMP2 for various boundary conditions	104
5.3	Comparison of linear and nonlinear buckling pressures of BMP2 for various boundary conditions	105
5.4	Nonlinear buckling pressures corresponding to wave numbers for BMP3 for various boundary conditions	107
5.5	Comparison of linear and nonlinear buckling pressures of BMP3 for f-f, c-c and s.s-s.s boundary conditions	108
5.6	Nonlinear interstiffener buckling pressures corresponding to wave numbers for M1 for various boundary conditions	110

5.7	Comparison of linear and nonlinear interstiffener buckling pressures of M1 for f-f, c-c and s.s-s.s boundary conditions	111
5.8	Nonlinear interstiffener buckling pressures corresponding to wave numbers for M2 for various boundary conditions	114
5.9	Comparison of linear and nonlinear interstiffener buckling pressures for M2 for f-f, c-c and s.s-s.s boundary conditions	115
5.10	Nonlinear interdeepframe buckling pressures corresponding to wave numbers for M1 for various boundary conditions	117
5.11	Comparison of linear and nonlinear interdeepframe buckling pressures for M1 for f-f, c-c and s.s-s.s boundary conditions	118
5.12	Nonlinear interdeepframe buckling pressures corresponding to wave numbers for M2 for various boundary conditions	119
5.13	Comparison of linear and nonlinear interdeepframe buckling pressures of M2 for f-f, c-c and s.s-s.s boundary conditions	120
5.14	Nonlinear interbulkhead buckling pressures corresponding to wave numbers for M1 for various boundary conditions	122
5.15	Comparison of linear and nonlinear interbulkhead buckling pressures for M1 for f-f, c-c and s.s-s.s boundary conditions	123
5.16	Nonlinear interbulkhead buckling pressures corresponding to wave numbers for M2 for various boundary conditions	124
5.17	Comparison of linear and nonlinear interbulkhead buckling pressures of M2 for f-f, c-c and s.s-s.s boundary conditions	125
5.18	Nonlinear interstiffener buckling pressures for M1 with follower force effect for various boundary conditions	126
5.19	Effect of follower force on nonlinear interstiffener buckling pressures for M1 for f-f, c-c and s-s boundary conditions	127
5.20	Nonlinear interstiffener buckling pressures with follower force effect for M2 for various boundary conditions	127
5.21	Effect of follower force on nonlinear interstiffener buckling pressures corresponding to wave numbers for M2 for f-f, c-c and s.s-s.s boundary conditions	128
5.22	Nonlinear interdeepframe buckling pressures with follower force effect corresponding to wave numbers for M1 for various boundary conditions	129

5.23	Effect of follower force on nonlinear interdeepframe buckling pressures for M1 for f-f, c-c and s.s-s.s boundary conditions	129
5.24	Nonlinear interdeepframe buckling pressures corresponding to wave numbers with follower force effect for M2 for various boundary conditions	130
5.25	Effect of follower force on interdeepframe nonlinear buckling pressures for M2 for f-f, c-c and s.s-s.s boundary conditions	130
5.26	Nonlinear interbulkhead buckling pressures with follower force effect for M1 for various boundary conditions	131
5.27	Effect of follower force on nonlinear interbulkhead buckling pressures for M1 for f-f, c-c and s.s-s.s boundary conditions	132
5.28	Nonlinear interbulkhead buckling pressures corresponding to wave numbers with follower force effect for M2 for various boundary conditions	132
5.29	Effect of follower force on nonlinear buckling pressures for shell between bulkheads of M2 for f-f, c-c and s.s-s.s boundary conditions	133
5.30	The overall % reduction in buckling pressures on considering the geometric nonlinearity and follower force effect for M1 &M2	134
5.31	Safety factor against buckling for various configurations and boundary conditions for M1 &M2	135
5.32	Collapse pressure predicted and safety factors from classical solutions for M1 and M2	136
5.33	Design pressure predicted by Rulebooks for M1 and M2	137
B.1	Design pressure predicted by Rulebooks for M1 and M2	167
B.2	Collapse pressure predicted and safety factors from classical solutions for M1 and M2	167

CHAPTER 1
INTRODUCTION

1.1 GENERAL

More than two third of the earth's surface is covered with water. Submersibles are primarily employed to observe and explore the subsea environment. Submarine is a submersible which operates in deep waters and can be defined as hydrodynamically designed one atmos. pressure chamber, and which maintains its structural integrity at the chosen diving depth and functions as a floating vessel on surfacing.

Besides the submarines for warfare there are commercial submarines, which are used in the offshore industry for underwater exploration, repair and maintainence. For the functional environment for the crew, submarines are essentially designed as atmospheric pressure chambers and consequently the hull has to withstand safely the hydrostatic pressure prevailing at the operational depth.

1.2 HULL GEOMETRY

High hydrostatic pressure is best withstood by axisymmetric structural forms (Jackson, 1983). The pressure hull of a submarine is often constructed from various combinations of cylinders, cones and domes. The pressure hull is mainly a cylindrical pressure vessel and the changes in hull diameter are accomplished through conical sections. The fore and aft ends of the hull consist of domed and/or conical end closures. These hull forms are hydrodynamically efficient and possess better overall strength. Usually the cylinders are stiffened with rings and/or stringers (Burcher and Rydill, 1994).

1.3 STRUCTURAL BEHAVIOUR

Stiffened cylindrical shells are essential components in various hydrospace, aerospace and terrestrial structures. Cylindrical shell structures by virtue of their

shell geometry carry the applied loads primarily by direct stresses lying in their plane accompanied by a little or no bending. External hydrostatic pressure induces compressive stress resultants in the cylindrical shells and may cause buckling at a pressure, much lower than the axisymmetric yield. Subsequently analytical investigation on buckling of such shell forms is the major problem to be addressed. The introduction of stiffeners considerably increases the buckling strength of the shell and is a satisfactory solution for increasing the strength of the shell.

The primary modes of failure of a stiffened cylindrical shell are considered to be buckling of shell between ring stiffeners identified by dimples or lobes around the periphery of shell plating; yielding of shell between ring stiffeners usually appearing as axisymmetric accordion pleats and general instability characterized by large dished-in portions of stiffened cylinder wherein the shell and the stiffeners deflect bodily as a single unit (Cormstock, 1988). Third mode of collapse is sensitive to spacing of bulkheads or deepframes and the scantlings of supporting ring frames. The general instability is very much sensitive to initial imperfections.

The simultaneous occurrence of all modes of failures described earlier has been argued by theoreticians as being the only criterion to be considered for the optimum design.

1.4 STRUCTURAL ANALYSIS OF CYLINDRICAL SHELLS

Classical methods are available for deflections, stresses and buckling pressures of ring stiffened cylindrical shells under hydrostatic pressure. But these are not applicable to actual submarines with stiffeners of various shapes and nonuniform spacing and shells with complex boundary conditions. Numerical solution schemes like finite difference and finite element methods can effectively be employed in these situations.

1.5 FINITE ELEMENT ANALYSIS OF STIFFENED CYLINDRICAL SHELLS

Finite element method is an efficient numerical technique for the study of the behaviour of various structural forms. The finite element method requires the actual submarine structure to be replaced by a finite element model, made up of

structural elements of known elastic and geometric properties. The objective therefore, is to develop a model, which simulates the elastic behaviour of continuous structure as closely as required. The finite element modeling of stiffened cylindrical shells can be done either using a smeared model or stiffener shell model. Various finite element models of stiffened cylindrical shells, viz., orthotropic shell model, discrete stiffener model and superelement model are generally used in the analysis.

The hydrostatic pressure can be idealized as uniformly distributed external load acting on the periphery of the shell, which can be converted into consistent load vector. Since hydrostatic pressure is a displacement dependant load, nonlinear analysis has become a necessity and hence finite element method is preferably adopted.

1.6 FINITE ELEMENT MODELING OF UNSTIFFENED CYLINDRICAL SHELLS

Unstiffened cylindrical shells subjected to external hydrostatic pressure can be modeled using axisymmetric elements, facet elements or general shell elements.

Singly curved shell finite elements were first developed in axisymmetric form for the analysis of shells of revolution. Since the hull of the submarine is stiffened cylindrical shell under axisymmetric loading, axisymmetric shell finite elements can be effectively used for analysis. Elements with axisymmetric geometry and asymmetric displacement functions (designated as rotational finite elements) can be effectively used for stability and geometric nonlinear analyses. In these types of elements shell nodes are nodal circles. The shape functions are obtained by combining polynomials along meridional direction and trigonometric functions in circumferential direction. Axisymmetric structures subjected to nonaxisymmetric loading can also be analysed using these elements.

Generally axisymmetric elements are efficient in achieving a state of constant strain and rigid body modes and in eliminating membrane locking and shear locking problems compared to general shell elements (Cook et al, 1989). The major

drawback of these elements is that proper analysis is not possible in the presence of irregularities or discontinuities within the shell.

In facet element modeling, the assembly of elements gives a geometry, which approximates the actual shell surface. The shell behaviour is achieved by the superposition of stretching behaviour (membrane element) and bending behaviour (plate bending element). The concept of the use of such elements in shell analysis was suggested by Greene et al (1961). The attractive features of this modeling are simplicity in formulation, easiness to mix with other types of elements and the capacity of modeling rigid body motion. Geometric nonlinear analysis based on corotational kinematics can be done effectively using these elements (Ramm, 1982). However, there are some drawbacks such as the lack of coupling between stretching and bending within the element and the discontinuity of slope between adjacent plate elements, which may produce bending moments in the regions where they do not exist. These are available in rectangular, quadrilateral and triangular shape together with coordinate transformations.

The curved elements have been developed with a view to overcome the limitations of facet elements and are generally used for general shells or shells with geometric discontinuity. Based on basic assumptions and theories, two types of curved elements have been formulated, viz., elements based on classical shell theories and degenerated shell elements.

1.7 FINITE ELEMENT MODELING OF STIFFENED CYLINDRICAL SHELLS

Various finite element models of stiffened cylindrical shells are orthotropic shell model; discrete stiffener model and superelement model and are described subsequently.

In the orthotropic approach, the ring stiffeners are blended with the shell such that the ring-stiffened shell is represented as an unstiffened but orthotropic cylindrical shell having different constitutive relationships in longitudinal and circumferential directions.

In the orthotropic shell modeling, stiffeners are assumed to interact to such a degree that these can be smeared into the shell. The compatibility of the plate and the stiffener gives rise to internal stresses, which results in change in constitutive relations in two mutually perpendicular directions. These constitutive relations can be effectively derived from the compatibility of the shell and the stiffener. The orthotropic approximation is applicable to geometries where there are a large number of closely and equally spaced rings and\or stringers, in which the stiffened hull is modeled using orthotropic shell elements.

In discrete stiffener model the stiffener is modeled as rings or an assembly of curved beam finite elements defined by cross sectional area and eccentricity of the cross section from the shell middle surface. In this model the stiffeners are assumed to be concentrated along the nodes of the shell elements. This model introduces certain inconsistencies such as the lumped stiffeners, indicating a coupling only along the nodes to which it is connected. Secondly the stiffeners inside the shell element are shifted to a new position in the lumped model.

The superelement modeling generally consists of merging a group of subelements into an assembly followed by the reduction of internal degrees of freedom that are local to a given superelement. The remaining degrees of freedom are termed as retained or super degrees of freedom. It is the process of substructuring technique followed by static condensation. The degrees of freedom normally retained are those, which are required to connect the superelement. The superelements may in turn be used as subelements for new assemblies on higher level. In this way a multilevel hierarchy of superelement may be established. The highest level in such a hierarchy will represent the complete structure. Hybrid beam elements (in which axial and bending stiffnesses are based on different cross sections) or eccentric beam elements (in which element nodes are not located along the stiffener centroidal axis) can be effectively used as the special elements or superelements (Hughes, 1986).

1.8 TYPES OF ANALYSES PERFORMED

Finite element analyses performed for the stiffened cylindrical shells of submarine are linear static analysis, linear buckling analysis and geometric nonlinear analysis.

1.8.1 Linear Static Analysis

Linear static analysis is the strength analysis in which the principle of super position is valid. It is based on the small deflection theory where stress strain relations and strain displacement relations are linear. In this method of analysis the change in geometry of the structure is not taken into account while deriving the equilibrium equations. The linear static analysis of the stiffened cylindrical shell can be performed by solving the general finite element equilibrium equations, consisting of linear elastic stiffness matrix and load vector. Deformation pattern and stress resultants can be calculated.

1.8.2 Linear Buckling Analysis

Buckling phenomenon is the major failure mode associated with thin walled cylindrical structures subjected to external pressure. The structure can suffer instability at a pressure, which may be only a small fraction to cause material failure. The buckling phenomenon associated with thin walled circular cylindrical shell subjected to uniform external pressure can be explained using the load deflection curve shown in fig. 1.1 (Rajagopalan, 1993).

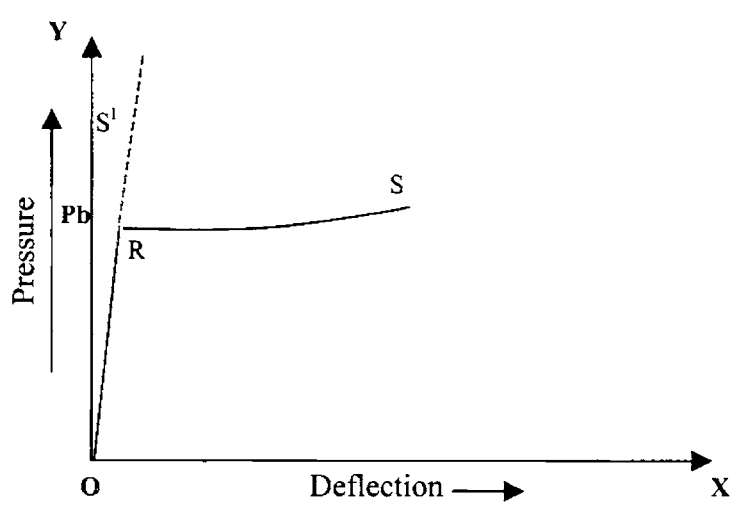

Fig. 1.1 Bifurcation buckling

The first regime OR, called the prebuckling state, determines the axisymmetric state of stress due to axisymmetric pressure load on the perfect

cylinder. The prebuckling path is linear. The second regime RS, called the buckling stage and the load deflection curve for a perfectly circular cylinder subjected to uniform external pressure splits into two at the point R. At this point the load deflection curve can be either RS or RS^I and the pressure Pb is called bifurcation-buckling pressure.

In the linear prebuckling analysis, change in geometry prior to buckling is neglected. The prebuckling deformations are neglected and hence stiffness matrices are evaluated at the original undeformed configuration.

Bifurcation buckling pressure is determined from linear buckling analysis. Linear buckling analysis is performed by constructing linear elastic stiffness matrix signifying the internal strain energy and geometric stiffness matrix representing the work done by the prebuckling stresses on the buckling displacement of the complete structure. The elastic stiffness matrix, $[K_o]$ and the geometric stiffness matrix $[K_g]$ are evaluated at the original undeformed configuration. The geometric stiffness matrix at any load level $[K_G]$ is linearly related to the initial geometric stiffness matrix $[K_g]$ by a parameter λ, which is a nondimensional function of load applied (Felippa, 1999).

$$[K_G] = \lambda [K_g] \qquad \text{.....(1.1)}$$

During buckling the total stiffness matrix becomes singular or the determinant of the total stiffness matrix vanishes. The eigen value problem of instability is therefore formulated as

$$([K_o] + [K_G]) \{\delta\} = 0 \qquad \text{..... (1.2)}$$

$$([K_o] + \lambda_b [K_g]) \{\delta\} = 0 \qquad \text{..... (1.3)}$$

The buckling pressure is evaluated for the condition

$$\left| [K_o] + \lambda_b [K_g] \right| = 0 \qquad \text{.....(1.4)}$$

where λ_b is the nondimensional buckling pressure.

In the solution, eigen values will be the buckling pressure and eigen vectors will be the buckling mode. Linear prebuckling analysis has the advantage of avoiding a full nonlinear analysis, which may be expensive and time consuming. This method

is effective in cases of cylinder subjected to hydrostatic loading, in which prebuckling deformations are small. Linear prebuckling analysis is effective in cylindrical shell structures made of steel in which buckling occurs in the elastic range. Cylindrical shell under hydrostatic pressure is not much sensitive to initial imperfections and hence linear buckling analysis can be adopted.

Linear buckling analysis predicts the collapse pressure at the bifurcation point and the postbuckling regime is left untouched. Geometric nonlinear analysis has been recommended to make the investigations of buckling behaviour complete.

1.8.3 Geometric Nonlinear Analysis

In structural mechanics a problem is nonlinear if the stiffness matrix or load vector depend on displacements. The cause of nonlinearity may be material or geometric. The material nonlinearity may be due to nonlinear stress-strain relations and geometric nonlinearity may be due to nonlinear kinematic relations i.e. nonlinear strain-displacement relations (large displacements) and large strains.

The prebuckling deformations of the cylindrical shell causes rotation of the structural elements and primary equilibrium path will be nonlinear from the outset. The ring stiffened shell with high degree of orthotropy may experience significant nonlinear prebuckling deformations. The critical load could not be determined with sufficient accuracy if prebuckling nonlinearity is neglected. Normally the loss of stability occurs at the limit point rather than at the bifurcation point. In such cases the critical load must be determined through the solutions of nonlinear system of equations.

The geometric nonlinearity in which the nonlinear effect arising from nonlinear strain displacement relations and nonlinearity due to follower force effect of hydrostatic pressure are to be taken into consideration for stiffened cylindrical shell subjected to hydrostatic pressure. These two are smooth nonlinearites and incremental iterative procedure can effectively be used as solution strategy.

The key component of the finite element nonlinear analysis is the solution of nonlinear algebraic equations that arise upon discretization. This difficulty is

overcome by the concept of continuation, which is also called incremental analysis (Crisfield, 1980). In this method the analysis is started from an easily computable solution (for e.g. the linear solution) and try to follow the behaviour of the system, as actions applied to it are changed by small steps called increments. In the incremental iterative methods one or more iteration steps are included to eliminate or reduce the drifting error, which are there in purely incremental methods (Felippa, 1999).

Out of three types of incremental iterative procedures, viz., load control, displacement control and arc length control, load control method is the basic one, and is generally adopted in the analyses mentioned earlier.

The essential feature of geometric nonlinear analysis is that the equilibrium equations must be written with respect to the deformed geometry, which is not known in advance (Bathe, 2001). Corotational kinematics is adopted for the generation of equilibrium equation at the deformed configuration i.e., for the generation of tangent stiffness matrix and the load vector at the deformed configuration. The reference configuration is split. Strains and stresses are measured from the corotated configuration where as the base configuration is maintained as a reference for measuring rigid body motion.

1.9 FOLLOWER FORCE EFFECT OF HYDROSTATIC PRESSURE

Conventional structural analysis involves loads that do not change their direction during deformation process and such loads are called conservative loads. The direction of the external loads such as water pressure or wind forces in the real situation may be changed during the deformation and the forces induced by such loads are called follower forces or polygenetic forces. These forces remain normal to the surface upon which they act throughout the load displacement history. Follower force effects are to be considered in the analysis of practical structures such as pressure vessels, cooling towers etc.

In the case of follower force the direction of the applied force is dependent on displacement, and to account for this additional stiffness terms, pressure stiffness

matrix must be added to the conventional stiffness matrix to take care of the pressure rotation effects.

Normally structures with follower force do not have proximate equilibrium position. These structural systems change to instability directly from the prebuckled equilibrium configuration and geometric nonlinear analysis becomes a necessity. The linear prebuckling analysis is restricted to static criterion, which is restricted to conservative loads. But for structures not having any loaded free edges or if a constant pressure is acting on a fully enclosed volume (like submarine pressure hull), polygenetic force effect will be weak and hence the structure is amenable to bifurcation buckling analysis. So the pressure rotation effects can also be handled within the realm of bifurcation buckling analysis.

Pressure rotation effects are important in cylindrical shells only when the shell buckles with a smaller number of waves in the circumferential direction, a phenomenon that occurs on long shells. Hence there is sufficient scope for including follower force effect originating from hydrostatic pressure in the collapse pressure prediction of submarine shells

1.10 DESIGN ASPECTS OF SUBMARINE HULLS

A landmark paper on submarine design is presented by Arentzen and Mandel (1960). The design procedure forwarded by Kendrick (1970) has received acceptance in European codes (BS 5500 and DnV). According to Kendrick the advantage in submarine strength prediction is that the hydrostatic loading is well defined. Under static conditions the ring-framed cylinder may fail by general instability, inter frame buckling or yielding of the plate between frames. Overall collapse between bulkheads or general instability is a low order-buckling phenomenon due to insufficiently strong frames in relation to the compartment length. Reducing the effective compartment length and/ or introducing stronger ring frames can markedly increase the buckling pressure. Kendrick has published about half a dozen design papers. His design method is based on the philosophy that it is more practical to arrange the prime mode of collapse that determine the main weight and cost of the vessel should have an adequate but not excessive strength margin. But

other forms of collapse mode that require considerable analytical effort for accurate collapse prediction but little material to avoid premature buckling can be avoided by using generous margins of elastic buckling pressure for the appropriate mode.

A rational submarine hull design proposes scantlings for an optimum structural form, which has adequate safety at the operational diving depth. The designer has to take into account many uncertainties and unavoidable situations like slight variation in material characteristics, deviations from circularity and other departures from ideal, which may occur in construction or service. Residual stresses particularly in frames, stress concentrations, inaccuracies in computing statically indeterminate systems and possibility of submarine exceeding its operational depth due to control malfunctions or as a deliberate manoeuvre to avoid attack as reported by Daniel (1983) etc., are also to be taken into account. There has to be reasonable stress analysis or strength estimation done before arriving at the final scantlings.

The stiffeners are the principal structural members that support the shell membrane and maintain its integrity. Actually externally welded frames are more stable than internal frames (Gorman & Louie, 1994). It also allows better utilization of internal spaces. However, these experience tensile stresses in a corrosive environment and are more likely to have separation from shell plating under dynamic loading and hence not adopted usually. From the hydrodynamic point of view internal frames are preferred.

1.11 ORGANISATION OF THE THESIS

This thesis is presented in six chapters. In the first chapter an introduction for submarines, structural action of underwater shells and method of structural analysis employed are given. Brief description of type of finite element analyses of stiffened cylindrical shells is presented.

In the second chapter a review of literature on finite element analysis of cylindrical shell is presented and the objectives of the present study are given here.

Third chapter describes the linear static analysis of stiffened cylindrical shells. The description of the all-cubic element and discrete stiffener element used in

the analysis are given. The validation of computer code developed and numerical investigations of stiffened cylindrical shell models of submarines are included.

Fourth chapter describes the linear buckling analysis of stiffened cylindrical shells, which predicts the collapse pressure of submarine hull. Validation and analytical investigation of submarine cylindrical shell models are included subsequently.

The description of the nonlinear analysis of stiffened cylindrical shell is given in the fifth chapter. Development of software and results of numerical investigations are described. Conclusions and scope for future work are given in chapter 6.

The details of elements of stiffness matrices are given in Appendix A and classical solutions and Rulebook provisions for the analysis of stiffened cylindrical shells are depicted in Appendix B.

CHAPTER 2
REVIEW OF LITERATURE

2.1 INTRODUCTION

Stiffened cylindrical shell forms are extensively used as structural components in naval and offshore industry. Buckling analysis of these shell forms are very relevant in subsea applications since the hydrostatic pressure induces compressive stress resultants in shell membrane. An attempt has been made here to realize the state of art in the analysis and design of cylindrical shells. Literature describing early classical closed form solutions as well as finite element analysis of stiffened cylindrical shells are reviewed and presented under subheadings classical methods, axisymmetric cylindrical shell finite elements, follower force effect and design aspects.

2.2 CLASSICAL SOLUTIONS

Classical solutions for linear and buckling analysis of unstiffened cylindrical shells are available through Timoshenko (1961), Flugge (1962), Donnell (1976), Novozhilov (1959), Kraus (1967) and Brush and Almroth (1975).

2.2.1 Shell Buckling

The buckling pressure of an unstiffened shell with uniform thickness with simply supported boundary condition is given by von Mises as eqn. 2.1.

$$P_c = \left(\frac{[2E(t/D)]}{(n^2+m^2/2-1)} \right) \left(\frac{(t/D)^2 [(n^2+m^2)^2 - 2n^2+1]}{3(1-\mu^2)} + \frac{m^4}{(n^2+m^2)^2} \right) \quad \text{.....} (2.1)$$

Where $m = \pi R/L_s$

von Mises' expression is still widely used because it has been presented in a relatively simple form and gives slightly conservative values (Faulkner, 1983). Windenburg and Trilling (1934) have developed another simplified equation based

on von Mises' to predict the collapse pressure under hydrostatic pressure loading and this is given as eqn.2.2.

$$P_c = \frac{2.24E(t/D)^{5/2}}{(1-\mu^2)^{3/2}[L/D-4.5\,(t/D)^{1/2}]} \qquad \text{.....} (2.2)$$

Analytical solutions for buckling analysis of unstiffened cylindrical shells are given by Batdorf (1947) and Nash (1954).

Reis and Walker (1984) have analysed the local buckling strength of ring stiffened cylindrical shells under external pressure. The collapse pressure is calculated by assuming failure to occur when the material reaches a plastic stress state. Ross (2000) has observed that many vessels buckle at a pressure that are considerably less than those predicted by elastic theory and introduced a plastic knockdown factor PKD by which the theoretical elastic instability buckling pressure is to be divided, to get the predicted buckling pressure. The value of PKD can be taken from the semi empirical chart developed by Ross.

2.2.2 Shell Yielding

Von Sanden and Gunther (Cormstock, 1988) have developed two equations to predict the pressure at which yielding of the shell occurs at frame and midbay.

For yielding at frame

$$P = \frac{2\sigma_Y\,(t/D)}{0.5+1.815K((0.85-B)/(1+\beta))} \qquad \text{.....} (2.3)$$

For yielding at midbay

$$P = \frac{2\sigma_Y(t/D)}{1+H\,((0.85-B)/(1+\beta))} \qquad \text{.....} (2.4)$$

More exact analysis has been made by Salerno and Pulos to include the effect of axial loading (Jackson, 1992).

2.2.3 General Instability

Classical solutions for general instability of ring-stiffened shells under hydrostatic pressure are given by Kendrick (1953), Bijlaard (1957) and Galletly (1957). Kendrick has presented a classical variational formulation of the differential equation of buckling analysis of ring stiffened cylindrical shells. By assuming a half sine wave between supports as the buckling deformation and proper allowance for shell distortions between frames, collapse pressure has been predicted by Kendrick (1965) using Ritz's procedure for simply supported – simply supported boundary conditions and has been extended for clamped boundary condition by Kaminsky (1954). Displacement field used by Kendrick has been modified by Ross (1965) and general instability analysis of ring stiffened cylindrical shells has been performed incorporating various degrees of rotational restraint at the boundary.

Bresse has developed an expression for elastic collapse of infinitely long ring-framed compartments (Timoshenko, 1961). Bryant has modified the formula developed by Kendrick by combining von Mises' and Bresse's relations for the determination of the overall buckling pressure of ring stiffened cylindrical shell with simply supported boundary conditions and is available in the form as,

Buckling pressure of stiffened cylindrical shell $P_c = P_{cf} + P_{cs}$ ..... (2.5)

$$\left.\begin{aligned} &P_{cf} = \text{buckling pressure of ring stiffeners} = \{[n^2-1]\, EI/R^3L\} \\ &P_{cs} = \text{buckling pressure of shell} = Et/R\ \{m^4/([n^2-1+(m^2/2)][n^2+m^2]^2)\} \\ &\text{and } m = \pi R/L_s \end{aligned}\right\} \quad \text{..... (2.6)}$$

Bryant's two-term approximation to the overall buckling pressure has gained wide acceptance because of its simplicity (Faulkner, 1983). The effect of imperfections on buckling pressure has been investigated and an expression has been developed by Bijlaard (1957).

The critical pressure for general instability of ring stiffened, stringer stiffened and ring and stringer stiffened cylindrical shells are computed by Bodner (1957). Baruch and Singer (1963) have carried out general instability analysis of stiffened cylindrical shell by considering the distributed eccentric ring stiffeners and stringers separately. The well-known superiority of rings over stringers for

cylindrical shells under external pressure is very clearly brought out. The effect of eccentricity of stiffeners is more pronounced for rings than for stringers. Voce (1969) has developed a solution procedure based on energy method for general instability of orthotropic ring stiffened cylinders under external hydrostatic pressure for simply supported boundary condition. Kempner et al (1970) have developed a procedure to determine the stresses and deflections incorporating the effects of large rotations, initial deflections and thick shell effects. Singer (1982) has extended buckling analysis for imperfect stiffened shells. Wu and Zhang (1991) have developed a nonlinear theoretical analysis for predicting the buckling and post buckling loads of discretely stiffened cylindrical shells.

Karabalis (1992) has made a simplified analytical procedure, which can be used as an effective method in checking the design of stiffening frames of cylindrical fuselages with or without cutouts for failure by general instability. The general instability mode of failure of cylindrical shell is independent of geometric discontinuity like cutouts. Any loss in moment of inertia due to the cutouts must be proportionately compensated by gain in bending stiffness, which can be realized by the addition of reinforcement possibly at the edges of the cutouts. However large reinforced cutouts would fail due to local instability at the edges of the cutouts. It is recommended that the proposed criteria can be used for design and calculation in the absence rigorous finite element analysis. Huang and Wierzbicki (1993) have developed a simple analytical model that describes the plastic behaviour of a curved cylindrical panel with ring stiffeners. Energy methods are used to analyse the plastic tripping response of the structure. In order to derive a closed form solution to the problem, a number of simplifications are made such as the material is treated as fully plastic and the energy corresponding to lateral bending of stiffeners are neglected.

Tian et al (1999) have carried out elastic buckling analysis of ring stiffened cylindrical shells using Ritz's procedure, which can be used as a reference source for checking the validity of other numerical methods and software for buckling of cylindrical shells.

Barlag and Rothert (2002) have developed an idealization concept for stability analysis of ring reinforced cylindrical shells under external pressure. A

monograph is introduced based on the stability equation to determine the local and global buckling pressures of ring stiffened cylindrical shells under external pressure based on Flugge's strain displacement relations.

The scope of the classical methods is limited to simple boundary conditions, uniform shell thickness, regular stiffeners and uniform spacing.

2.3 AXISYMMETRIC CYLINDRICAL SHELL FINITE ELEMENTS

Axisymmetric cylindrical shell elements are singly curved, straight meridian elements. A few relevant papers on axisymmetric shell elements have been reviewed and presented. Review of literature on finite element modeling of unstiffened and stiffened cylindrical shells is described subsequently.

2.3.1 Unstiffened Shells

Grafton and Strome (1963) have presented the conical segment elements for the analysis of shells of revolution. Improvements in the derivation of element stiffness matrix are presented by Popov et al (1964). Percy et al (1965) have extended these formulations for orthotropic and laminated materials.

Navaratna et al (1968) have made a linear bifurcation buckling analysis of unstiffened shells using an axisymmetric rotational finite element in which the membrane displacements are approximated by linear polynomials and the radial displacement by cubic polynomial. Trigonometric functions are used to characterize the buckling waves in circumferential direction. Later this element has been used to study the influence of out of roundness on buckling theory of unstiffened shells. A systematic procedure to obtain the geometric stiffness matrix and subsequently the buckling load through variational approach is presented. Mc Donald and White (1973) have studied the effect of out of roundness in buckling strength of unstiffened shells. Ross (1974) has carried out lobar bifurcation buckling analysis of thin walled cylindrical shells under external pressure using axisymmetric finite element based linear-linear-cubic shape functions. Venkiteswara Rao et al (1974) have reported a rigorous linear buckling analysis using axisymmetric finite element based all-cubic shape functions. Surana (1982) has developed a nonlinear formulation for

axisymmetric shell elements. Cook has (1982) developed a finite element model for nonlinear analysis of shell of revolution. Rajagopalan and Ganapathy Chettiar (1983) have developed an all-cubic axisymmetric rotational shell element for modeling the cylindrical shell in the interstiffener buckling analysis. Ross and Mackeny (1983) have carried out deformation and stability studies of axisymmetric shells under external hydrostatic pressure using linear-linear–cubic axisymmetric finite elements. Gould (1985) has formulated and used axisymmetric shell elements for linear and nonlinear analysis.

Rajagopalan (1993) has developed a reduced cubic element based on condensation concept for stability problems. Internal nodes are introduced in the axisymmetric cylindrical shell element so as to permit cubic polynomial to be taken for modeling the membrane displacement in the meridional direction. The internal nodes are eliminated by geometric condensation procedure so that the condensed element will have only fewer degrees of freedom and hence computationally efficient.

Ross et al (1994) have carried out vibration analysis of axisymmetric shells under external hydrostatic pressure. Both shell and surrounding fluid are discretized as finite elements. It is reported that dynamic buckling can take place at a pressure less than that of static buckling pressure.

Koiter et al (1994) have investigated the influence of axisymmetric thickness variation on the buckling load of an axially compressed shell. Mutoh et al (1996) have presented an alternate lower bound analysis to elastic buckling collapse of thin shells of revolution. Axisymmetric rotational shell elements whose strain displacement relations are described by Koiter's small finite deflection theory have been used for the analysis. In this element the displacements are expanded circumferentially using a Fourier series.

Sridharan and Kasagi (1997) have presented a summary of the work carried out in Washington University on buckling and associated non-linear responds and collapse of moderately thick composite cylindrical shells.

Ross et al (2000) have carried out the inelastic buckling analysis of circular cylinders of varying thickness under external hydrostatic pressure. Analytical results are verified by experimental investigations. Gusic et al (2000) have analysed the influence of circumferential thickness variation on the buckling of cylindrical shells under external pressure by means of finite element bifurcation analysis. Two different finite element codes, one with quasi-axisymmetrical multimode Fourier analysis and the other with 3D shell element are used. Numerical integration of Fourier series permits the introduction of geometric and thickness imperfections at the integration points.

Correia et al (2000) have used higher order displacement fields with longitudinal and circumferential components of displacements as power series and the condition of zero stress at top and bottom surfaces of the shell are imposed. Combescure and Gusic (2001) have carried out nonlinear buckling analysis of cylinders under external pressure with nonaxisymmetric thickness imperfections using axisymmetric shell elements. Gould and Hara (2002) have reported recent advances in the finite element analysis of shell of revolution. Sze et al (2004) have discussed about popular benchmark problems for geometric nonlinear shell analysis.

2.3.2 Stiffened Shells

Ross (1976) has carried out stability analysis of ring reinforced circular cylindrical shells under external hydrostatic pressure. Subbiah and Natarajan (1981) have carried out a finite element analysis for general instability of ring-stiffened shells of revolution using axisymmetric shell elements. They have used linear-linear-cubic element for the finite element modeling of the shells. This smeared model analysis predicted a lower bound buckling pressure. Influence of various boundary conditions on buckling pressure has been investigated and reported. A rigorous derivation for potential due to hydrostatic loading as follower force and subsequent reduction in buckling pressure has been reported.

Subbiah (1988) has made a nonlinear analysis of geometrically imperfect stiffened shells of revolution. A nonlinear large deformation finite element analysis has been carried out for the general instability of ring stiffened cylindrical shells

subjected to end compression and circumferential pressure. Smeared model technique is adopted. A combined nonlinear and eigen value analysis is presented to determine the critical pressure for initially imperfect stiffened cylinders. The buckling pressures of thin shell structures are very much sensitive to initial imperfections. This is one of the major reasons for poor correlation between theoretically predicted and experimentally obtained buckling loads. The only way to overcome this discrepancy is to analyse the shell as a nonlinear large deformation problem with initial imperfections.

Rajagopalan (1993) has used a discrete ring stiffener element and axisymmetric cylindrical shell element to model the stiffened cylindrical shell. General buckling analysis has been carried out by rigorous stiffener modeling using annular plate bending elements and shell elements. The superelement modeling of stiffeners introduces off shell nodes, which are eliminated by geometric condensation procedure. Ross (1995) has carried out plastic buckling analysis of ring stiffened cylindrical shells under external hydrostatic pressure.

Kasagi and Sridharan (1995) have investigated the imperfection sensitivity of ring stiffened anisotropic composite cylindrical shells under hydrostatic pressure using an asymptotic procedure. The displacement function takes the form of exact trigonometric function along the circumferential direction and p-version in other two directions. Sridharan (1995) has extended an analysis of stiffened cylindrical shells under interactive buckling. Effects of interaction of local and overall buckling is analysed using finite elements, in which the local buckling information is embedded. Schokker et al (1996) have carried out dynamic instability analysis of ring stiffened composite shells under hydrostatic pressure.

Stanley and Ganesan (1997) have investigated the natural frequencies of stiffened cylindrical shell (both short and long) with clamped boundary condition. Two nodded cylindrical shell element with four degrees of freedom per node is used.

2.4 RING STIFFENED CYLINDRICAL SHELLS WITH OTHER TYPES OF FINITE ELEMENTS

Kohnke et al (1972) have made a finite element analysis for eccentrically stiffened cylindrical shells using 48 degree of freedom shell elements. Giacofci (1981) has developed modeling techniques for the analysis of stiffened shell structures. Tsang and Harding (1987) have made plastic and elastic analysis of ring stiffened cylindrical shells by using finite element program FINAS. Zhen and Yeh (1990) have developed a new method of analysis capable of predicting nonlinear buckling load for stiffened cylindrical shells. Pegg (1992) has made a numerical study of dynamic buckling of ring-stiffened cylinders using general shell elements. Omurtag and Akoz (1993) have developed mixed finite element formulation for eccentrically stiffened cylindrical shells. A rectangular four nodded shell element and a two nodded circular bar element are used for the analysis. Chen et al (1994) have carried out buckling analysis of ring stiffened cylindrical shells with cutouts by mixed method of finite strip and finite elements. Finite strip and finite elements are connected together by specially developed transition elements. Goswami and Mukopadhyay (1995) have carried out geometrically nonlinear analysis of laminated stiffened shells. Li et al (1997) have made an adaptive finite element analysis method for shells with stiffeners.

2.5 FOLLOWER FORCE EFFECT

Bodner (1958) has described the buckling of infinitely long cylindrical shell under various distributed load systems with and without considering the follower force effect. The buckling load for hydrostatic pressure is found to be lower than that for the uniformly distributed conservative load system.

Herrman and Bungay (1964) have studied the stability of elastic system subjected to nonconservative forces. Oden (1970) has developed an approximate method for computing nonconservative generalized forces on large deformation problems.

Hibbit (1979) has discussed about the importance of coupling of the follower force effect with the tangent stiffness matrix of the structure for the accurate solution of the problems. In presence of free loaded ends, the system become nonconservative, hence leads to an unsymmetric matrix. Loganathan et al (1979) have carried out a study of effect of pressure stiffness in shell stability analysis. The analysis is carried out in deep and shallow shell situations with and without pressure stiffness matrix. The analysis without follower force effect leads to bifurcation buckling modes and with pressure stiffness matrix, the mode of instability changes to a limit point phenomenon. In general, the inclusion of pressure rotation effect will introduce unsymmetric stiffness matrices into the finite element equations. Under such circumstances, the classical bifurcation concept is no longer valid. The solution of unsymmetric simultaneous system of algebraic equations is very tedious. But in some cases, such as uniform external pressure on cylindrical shells, the pressure stiffness matrix is symmetric. Although the problem of follower forces is in general a noncoservative-loading problem, the symmetric matrix is conservative in character. Mang (1980) has derived techniques to impose symmetricability to pressure stiffness matrix. According to him the buckling pressure derived for a cylindrical shell with unsymmetric pressure stiffness matrix differs very little from the buckling pressure, resulting from an alternative symmetric pressure stiffness matrix.

Subbiah and Natarajan (1981) have analysed the follower force effect of hydrostatic pressure in the finite element analysis for general instability of ring-stiffened shells of revolution using axisymmetric shell elements. A rigorous derivation for potential due to hydrostatic loading including follower force effect has been presented. Substantial reduction in buckling pressure due to follower force effect has been reported. Carnoy et al (1984) have carried out static buckling analysis of shells subjected to follower pressure by finite element method. Tomski and Przybyski (1987) have studied the behaviour of a clamped, elastically supported planar structure under follower force.

Hasegawa et al (1988) have investigated the elastic instability and nonlinear finite displacement behaviour of special thin walled members under displacement dependant loadings. When the load stiffness matrix is unsymmetric indicating the nonconservativeness of the load, the dynamic stability becomes a matter of great

concern and hence the mass matrices of the special thin walled members are derived in the study to examine its possibility. The methods of analysis presented in the paper have been of four types, static instability analysis called divergence, dynamic instability analysis called flutter, static nonlinear finite displacement analysis and static linearised finite displacement analysis.

2.6 DESIGN ASPECTS OF SUBMARINE HULLS

Faulkner (1983) has made a discussion about the design practices used in BS 5500 (1976). According to him the interframe shell collapse determines the main weight and cost and safety factors should be chosen by ensuring this as the prime mode of failure. This paper is not meant to provide a comprehensive coverage of structural design but concentrated on the philosophy and underlying essentials of strength formulations and design.

Gorman and Louie (1991) have developed an optimization methodology, which explicitly considers shell yielding, lobar buckling, general instability and local frame instability failure modes. Quantitative results on the effects of hull circularity is also presented. Some novel results for the buckling performance of nonaxisymmetric rings are further presented to identify the design payoff of new software tools. Empirical relations are used to get the principal characteristics desired of pressure hull material from weight displacement ratio. The hull wall architecture has also been commented.

Jackson (1992) describes the concepts of design that has been developed over a number of years. The optimum length to diameter ratio is 4 to 6. Neto et al (1996) have determined the collapse pressures of ring stiffened cylindrical shells under hydrostatic pressure using code formulations and elastic plastic finite element analysis.

Bushnell and Bushnell (1996) have developed an approximate method for the optimum design of ring and stringer stiffened cylindrical shell panels and shells with imperfections. The PANDA.2 computer program for minimum weight design of stiffened composite panel is expanded to handle optimization of ring and stringer stiffened cylindrical panels and shells with three types of initial imperfections in

the form of buckling modes, any combination of which may be present; local, inter-ring and general.

Das et al (1997) have made a reliability based design procedure of stiffened cylinder using multiple criteria of optimization techniques. The various limit states of orthogonaly stiffened cylindrical shells have been used and they include bay instability, frame bending and frame tripping. A rational comprehensive analysis is required for a safe effective design.

2.7 SCOPE AND OBJECTIVES

For the linear analysis of ring stiffened cylindrical shell with simple boundary conditions, closed form solutions are available. However, a definite necessity is felt for the solution of the problem for various practical configurations and boundary conditions. Finite element method can be adopted for the analysis of stiffened cylindrical shells owing to its versatility. Finite element modeling of stiffened cylindrical shell can be done either using a stiffener shell model or a smeared model. The hydrostatic pressure acting at a considerable depth can be treated as uniformly distributed pressure loading and consistent load vector can be formulated. Efficient cylindrical shell elements and circular stiffener elements are available in the literature, which can be employed for the analysis of subsea stiffened cylindrical shells. The analytical investigations of cylindrical shells constituting the submarine hull are classified documents and are rarely found in literature; hence it is found apt to carryout such investigations to provide design recommendations. A definite need is felt to have a software based on an efficient finite element to analyse the stiffened cylindrical shell for various boundary conditions, incorporating the follower force effect.

Scope of the work is to conduct linear elastic, linear buckling and geometric nonlinear analysis of stiffened cylindrical submarine shells incorporating the follower force effect of hydrostatic pressure.

The objectives of the thesis are listed below.

- To develop a software based on all-cubic axisymmetric cylindrical shell finite element and discrete ring stiffener element for linear elastic, linear buckling and geometric nonlinear analysis of stiffened cylindrical shells.
- To implement the software in pc environment and use it to predict the stress resultants, linear buckling pressures and collapse pressures for various boundary conditions and configurations of the shell and stiffener.
- To study the influence of follower force effect due to hydrostatic pressure on the collapse pressure of stiffened cylindrical submarine shells.

CHAPTER 3
LINEAR STATIC ANALYSIS

3.1 GENERAL

Axisymmetric shell finite elements can effectively be used for analysis of stiffened cylindrical shell under axisymmetric loading. In the present study discrete stiffener cylindrical shell model of the submarine hull is proposed, in which the shell is modeled using all-cubic axisymmetric shell finite element and the stiffeners, using discrete ring stiffener finite element presented by Rajagopalan (1993).

3.2 FINITE ELEMENT MODELING OF CYLINDRICAL SHELL

An all-cubic axisymmetric cylindrical shell finite element has been used in the finite element analyis of cylindrical shells.

3.2.1 Geometry, Displacement Field and Shape Functions

The all-cubic axisymmetric thin cylindrical shell finite element represents meridian of a cylindrical shell it models. The geometric features of the cylindrical shell segment are radius, thickness and length(R,t,L).

Displacement field of the all-cubic element used in the present study consists of meridional, tangential and radial displacements (u, v, w).

The element is bound by two end nodal circles with six degrees of freedom per each and the degrees of freedom at nodal circle 1 are meridional, tangential and radial translations (u_1, v_1, w_1), u_{x1},v_{x1} and the meridional rotation φ_1(w_{x1}).

The corresponding values at nodal circle 2 are u_2, v_2, w_2, u_{x2}, v_{x2} and φ_2. Nodal degrees of freedom u, v, w and φ are shown in fig. 3.1

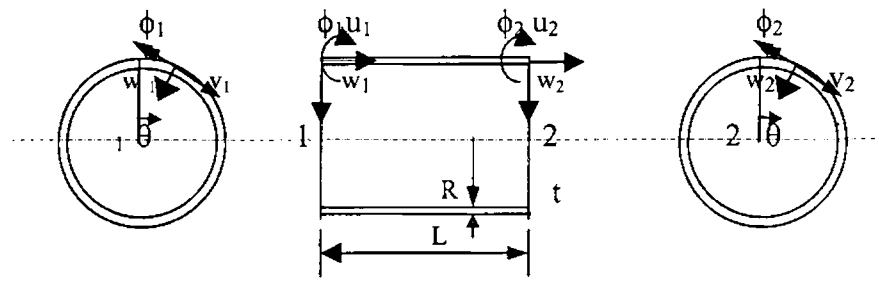

Fig. 3. 1 All- cubic cylindrical shell finite element

Finite element representation of the displacement field and the meridional rotation are given below, in which the polynomial and the trigonometric terms represent the meridional field and the sinusoidal variation in the circumferential direction.

$$\left.\begin{aligned} u &= [N_1 u_1 + N_2 u_{x1} + N_3 u_2 + N_4 u_{x2}] \cos n\theta \\ v &= [N_1 v_1 + N_2 v_{x1} + N_3 v_2 + N_4 v_{x2}] \sin n\theta \\ w &= [N_1 w_1 + N_2 \varphi_1 + N_3 w_2 + N_4 \varphi_2] \cos n\theta \end{aligned}\right\} \quad \text{.....} (3.1)$$

The meridional rotation φ at the interior nodal circle is given by

$$\varphi = \partial w/\partial x = [N_{\xi 1} w_1 + N_{\xi 2} \varphi_1 + N_{\xi 3} w_2 + N_{\xi 4} \varphi_2] \cos n\theta$$

where

$$\left.\begin{aligned} N_1 &= 1-3\xi^2 + 2\xi^3;\ N_2 = L(\xi - 2\xi^2 + \xi^3);\ N_3 = 3\xi^2 - 2\xi^3;\ N_4 = L(-\xi^2 + \xi^3); \\ N_{\xi 1} &= {}^1/_L(-6\xi + 6\xi^2);\ N_{\xi 2} = (1-4\xi+3\xi^2);\ N_{\xi 3} = {}^1/_L(6\xi - 6\xi^2);\ N_{\xi 4} = (-2\xi + 3\xi^2); \end{aligned}\right\} (3.2)$$

where $\xi = x/L$

3.2.2 Strain Matrix

Strain displacement relations are adopted from Sander's theory [1963]. The total strain $\in$ is composed of linear component $\in_L$ and nonlinear component $\in_{nL}$. Thus the strain vector can be written as

$$\{\in\} = \{\in\}_L + \{\in\}_{nL} \quad \text{.....} (3.3)$$

where $\{\in\}$ is the vector of generalized strains containing the in-surface strains $\in_x$, $\in_\theta$ and $\in_{x\theta}$ and curvatures ψ_x, ψ_θ and $\psi_{x\theta}$.

The strain field can be expressed as

$$\begin{Bmatrix} \epsilon_x \\ \epsilon_\theta \\ \epsilon_{x\theta} \\ \psi_x \\ \psi_\theta \\ \psi_{x\theta} \end{Bmatrix} = \begin{Bmatrix} u_x \\ 1/R\,(v_\theta - w) \\ (v_x + u_\theta/R) \\ w_{xx} \\ 1/R^2\,(w_{\theta\theta} + v_\theta) \\ 2/R\,(w_{x\theta} + v_x) \end{Bmatrix} + \begin{Bmatrix} \tfrac{1}{2} w_x^2 \\ \tfrac{1}{2}\,(v/R + w_\theta/R)^2 \\ w_x w_\theta / R \\ 0 \\ 0 \\ 0 \end{Bmatrix} \quad \ldots(3.4)$$

The linear elastic generalized strains are expressed as eqn. 3.5

$$\begin{Bmatrix} \epsilon_x \\ \epsilon_\theta \\ \epsilon_{x\theta} \\ \psi_x \\ \psi_\theta \\ \psi_{x\theta} \end{Bmatrix} = [B] \begin{Bmatrix} u_{x1} \\ v_1 \\ v_{x1} \\ w_1 \\ \varphi_1 \\ u_2 \\ u_{x2} \\ v_2 \\ v_{x2} \\ w_2 \\ \varphi_2 \end{Bmatrix} \quad \ldots\ldots\ldots\ldots\ldots\ldots(3.5)$$

where [B] is the small strain displacement matrix

$$\epsilon_L = [B]\,\{\delta\} = [C]\,[B^1]\,\{\delta\} \quad \ldots\ldots\ldots\ldots\ldots\ldots(3.6)$$

where [C] is the diagonal matrix of size 6 x 6.

$$[C] = \begin{bmatrix} \cos n\theta & & & & & \\ & \cos n\theta & & & & \\ & & \sin n\theta & & & \\ & & & \cos n\theta & & \\ & & & & \cos n\theta & \\ & & & & & \sin n\theta \end{bmatrix} \quad \ldots\ldots\ldots\ldots\ldots\ldots\ldots\ldots (3.7)$$

and $[B^1]$ is a matrix of order 6 x 12 whose elements are functions of non dimensional meridional co-ordinate ξ.

3.2.3 Constitutive Matrix

Constitutive matrix [D] for elastic shell problems is shown in eqn. 3.8

$$[D] = Et/(1-\nu^2) \begin{pmatrix} 1 & \nu & 0 & 0 & 0 & 0 \\ \nu & 1 & 0 & 0 & 0 & 0 \\ 0 & 0 & (1-\nu)/2 & 0 & 0 & 0 \\ 0 & 0 & 0 & t^2/12 & \nu t^2/12 & 0 \\ 0 & 0 & 0 & \nu t^2/12 & t^2/12 & 0 \\ 0 & 0 & 0 & 0 & 0 & (1-\nu)t^2/24 \end{pmatrix} \quad \text{.....(3.8)}$$

3.2.4 Linear Elastic Stiffness Matrix

The linear elastic stiffness matrix can be obtained using the eqn.3.9 (Zienkiewicz, 1979) given below.

$$[k] = \int_0^{2\pi} \int_0^{L} [B]^T [D] [B] R \, d\theta \, dx \quad \text{.....(3.9)}$$

which can be expressed using the eqn.3.6 as

$$[k] = RL \int_0^{2\pi} \int_0^{1} [B^1]^T [C] [D] [C] [B^1] \, d\theta \, d\xi \quad \text{..... (3.10)}$$

Substituting for the integrants and performing the circumferential integration, [k] can be obtained as

$$[k] = (\pi RL \, Et/(1-\nu^2)) \int_0^1 [B^1]^T \begin{pmatrix} 1 & \nu & 0 & 0 & 0 & 0 \\ \nu & 1 & 0 & 0 & 0 & 0 \\ 0 & 0 & (1-\nu)/2 & 0 & 0 & 0 \\ 0 & 0 & 0 & t^2/12 & \nu t^2/12 & 0 \\ 0 & 0 & 0 & \nu t^2/12 & t^2/12 & 0 \\ 0 & 0 & 0 & 0 & 0 & (1-\nu)t^2/24 \end{pmatrix} [B^1] \, d\xi \quad (3.11)$$

The present study is based on the linear elastic stiffness matrix given vide eqn.3.11 and the complete coefficients of stiffness matrix is available elsewhere (Rajagopalan, 1993) and is given in clause A.1 of Appendix A.

3.2.5 Load Vector

Hydrostatic pressure is treated as uniform pressure of intensity p acting normal to the element face. The consistent load vector due to surface pressure is given by

$$\{Q\} = \int\int [N]^T \, p \, dA = 2 \, p \, \pi RL \int_0^1 [N]^T \, d\xi \qquad \text{.....(3.12)}$$

3.2.6 Evaluation of Displacement

Displacements are calculated from the equilibrium equation in the form $[K] \{\delta\} = \{Q\}$ using Gauss elimination procedure.

3.2.7 Recovery of Stress Resultants and Principal stresses

The membrane stress resultants, N_x, N_θ and $N_{x\theta}$ and the bending moments M_x, M_θ and $M_{x\theta}$ are evaluated using the relation given in the eqn.3.13.

$$\text{Stress resultant} = \begin{Bmatrix} N_x \\ N_\theta \\ N_{x\theta} \\ M_x \\ M_\theta \\ M_{x\theta} \end{Bmatrix} = [D]\,[B]\,\{\delta\} = [S]\,\{\delta\} \qquad \text{.....(3.13)}$$

The elements of [S] matrix are developed and are given in clause A.2 of Appendix A.

Principal stresses σ_1 and σ_2 are evaluated at the middle layer from the membrane stress resultants and at the outer layers from the combined effect of membrane and bending stress resultants.

$$\left.\begin{array}{l} \sigma_1 = 1/2(\sigma_x + \sigma_\theta) + 1/2\sqrt{((\sigma_x - \sigma_\theta)^2 + 4\tau_{x\theta}^2)} \\ \sigma_2 = 1/2(\sigma_x + \sigma_\theta) - 1/2\sqrt{((\sigma_x - \sigma_\theta)^2 + 4\tau_{x\theta}^2)} \\ \text{where } \sigma_x = N_x/t,\ \sigma_\theta = N_\theta/t \text{ and } \tau_{x\theta} = N_{x\theta}/t \text{ at the middle layer and} \\ \sigma_x = N_x/t + 6\,M_x/t^2,\ \sigma_\theta = N_\theta/t + 6\,M_\theta/t^2 \text{ and } \tau_{x\theta} = N_{x\theta}/t + 6\,M_{x\theta}/t^2 \\ \text{at the outer layer} \end{array}\right\} \quad (3.14)$$

3.3 FINITE ELEMENT MODELING OF STIFFENED CYLINDRICAL SHELL

It is proposed to model the shell with all-cubic axisymmetric shell finite elements and stiffeners using discrete finite elements. All-cubic axisymmertic shell element has been described in section 3.2. The description of geometry and relevant matrices of the discrete stiffener finite elements are described subsequently.

3.3.1 Discrete Ring Stiffener Element

The ring stiffener of the submarine cylindrical shell is modeled as a discrete ring defined by cross sectional area and eccentricity of the cross section of the ring from the shell middle surface. The stiffeners are attached to end nodal circles of all-cubic axisymmetric shell finite elements and hence introduce no additional nodes. The stiffness matrix of the ring stiffener element is calculated and is transformed to shell node, at which the particular ring stiffener is attached. The stiffener element is built on the assumption that its behaviour can be completely described by centroidal degrees of freedom, which are u_r, v_r, w_r and φ_r. Geometry and degrees of freedom of the discrete ring stiffener element are shown in the fig. 3.2.

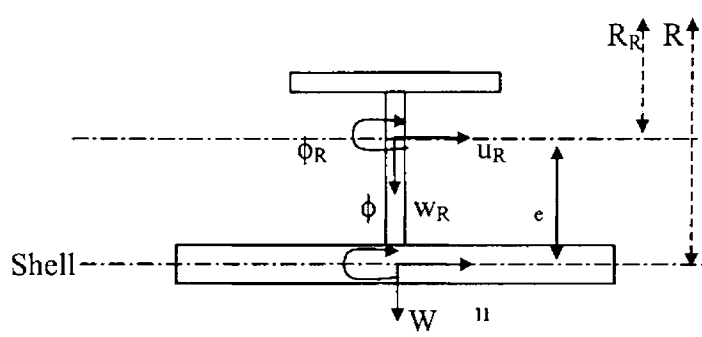

Fig. 3.2 Discrete ring stiffener element

The stiffener and the shell middle surface displacements are related by the eqn.3.15. The stiffener is rigidly attached to the shell and hence the displacements

$$u_r = u - e\,\varphi;\quad v_r = 1/R\,(R_r\,v - e(\partial w / \partial\theta));\quad w_r = w \text{ and } \varphi_r = \varphi \quad \text{..... (3.15)}$$

3.3.2 Elastic Stiffness Matrix of Ring Stiffener Element

Elastic stiffness matrix of the ring stiffener element corresponding to its centroidal degrees of freedom is derived by considering the strain energy of the ring stiffener. The axial, in-plane bending and St. Venant torsional energies are considered.

The present study is based on the linear elastic stiffness matrix and the complete coefficients of stiffness matrix are available elsewhere (Rajagopalan, 1993) and are given in clause A.3 of Appendix A.

3.3.3 Transformation Matrix for Stiffener

The transformation between the stiffeners centroidal degrees of freedom and the shell degrees of freedom can be expressed by the following matrix equation.

$$\{\delta_r\} = [T]\,\{\delta\} \qquad (3.16)$$

where [T] is the transformation matrix.

$$\begin{Bmatrix} u_r \\ 0 \\ v_r \\ 0 \\ w_r \\ \varphi_r \end{Bmatrix} = \begin{pmatrix} 1 & 0 & 0 & 0 & 0 & -e \\ 0 & 0 & 0 & 0 & 0 & 0 \\ 0 & 0 & R_r/R & 0 & ne/R & 0 \\ 0 & 0 & 0 & 0 & 0 & 0 \\ 0 & 0 & 0 & 0 & 1 & 0 \\ 0 & 0 & 0 & 0 & 0 & 1 \end{pmatrix} \begin{Bmatrix} u \\ u_x \\ v \\ v_x \\ w \\ \varphi \end{Bmatrix} \qquad \text{.....(3.17)}$$

3.3.4 Formulation of Stiffness Matrix of Stiffened Shell Element

In the discrete stiffener modeling, the properties of the stiffener are lumped to the corresponding nodal circle of the shell element. So the process of formulation of stiffness matrix for the stiffened shell element consists of the identification of the nodal circle to which the stiffener is attached and the algebraic addition of transformed stiffness matrix to the corresponding shell nodal degrees of freedom.

3.4 ASSEMBLY OF GLOBAL MATRIX

3.4.1 Stiffness Matrix

The global stiffness matrix of the stiffened cylindrical shell finite element model is obtained by computing the element stiffness matrix of each shell element and assembling them by posting them in appropriate global locations determined by node numbering and connectivity. The transformed stiffness matrix of the stiffener element are added to the relevant locations.

3.4.2 Load Vector

Consistent load vector is added algebraically at the junction of two stiffened shell elements. Since the load is the uniform radial pressure, equivalent joint moments gets cancelled at the joints and the equivalent joint loads get added up.

3.5 SOFTWARE DEVELOPMENT

Software has been developed in C language for the linear static analysis of stiffened cylindrical shells, which can be effectively used for, unstiffened ones also. The description of the program for the analysis of stiffened cylindrical shell is explained in subsequent sections.

3.5.1 Flow Chart

The schematic diagram is given in fig. 3.3a and the hierarchal order of operations is given in the flowchart (fig. 3.3b).

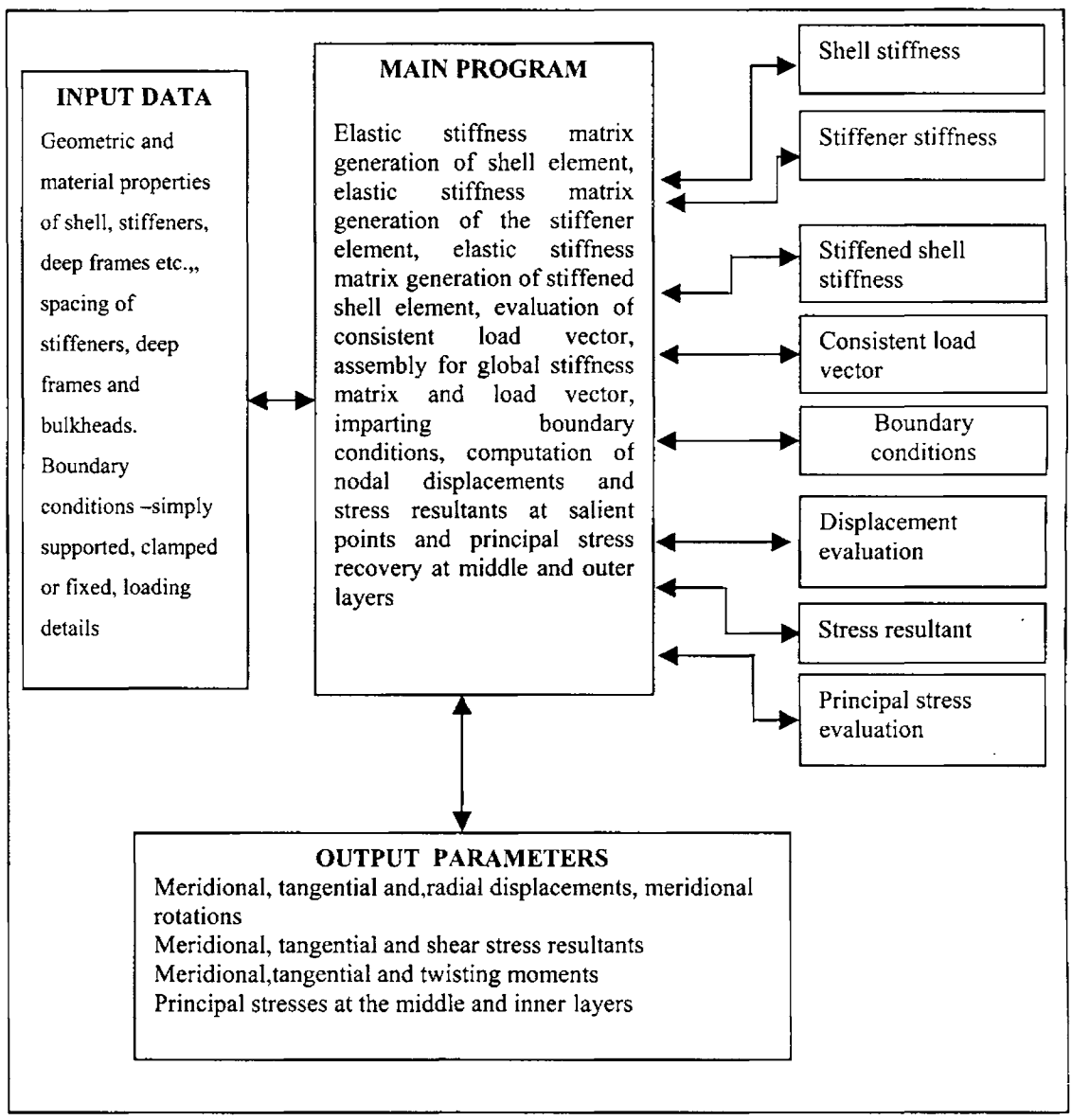

Fig. 3.3a Schematic diagram for linear static analysis

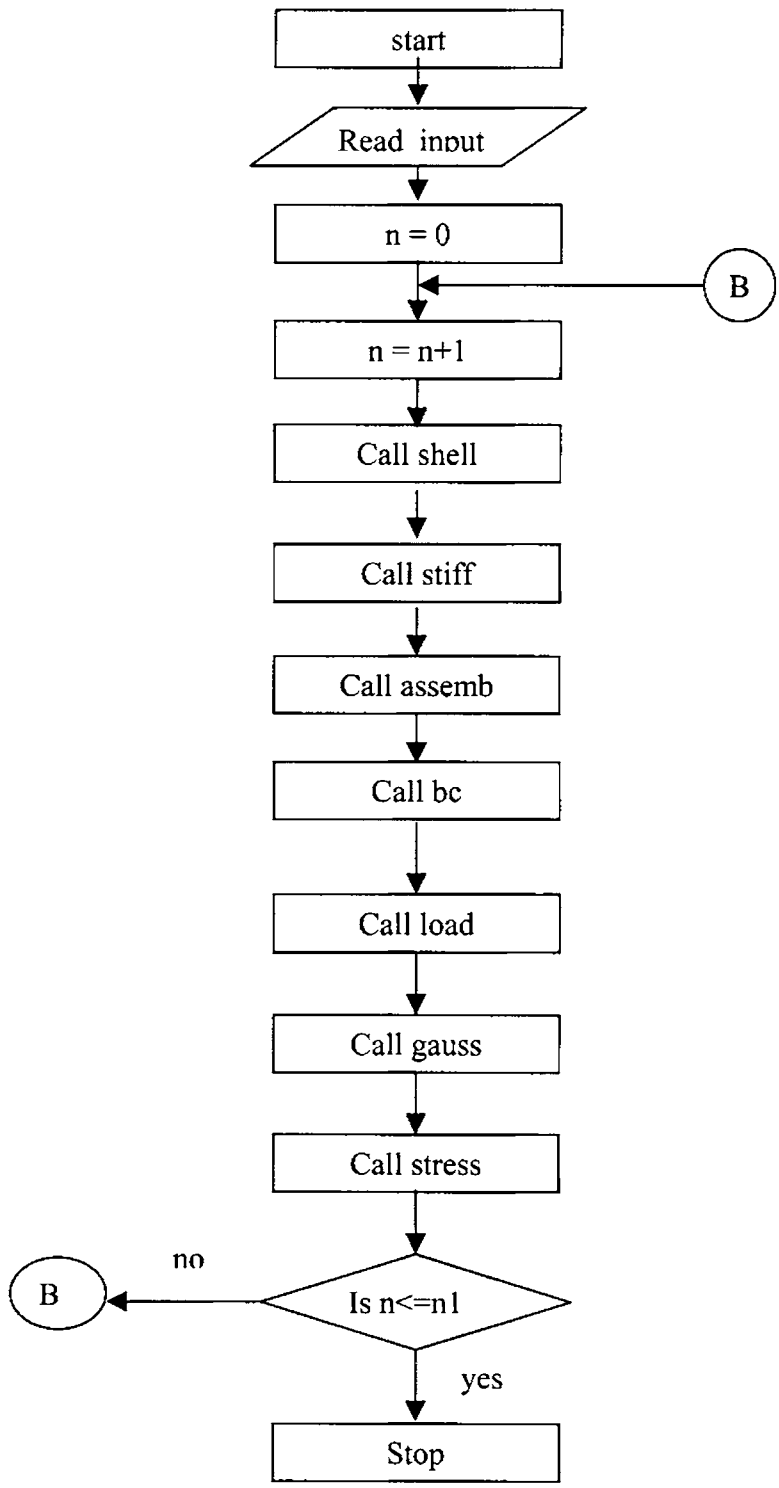

Fig. 3.3b Flowchart for linear static analysis

3.5.2 Program *MAIN*

The geometric data of the shell is obtained from the input file.

The execution of the program is as follows. The elastic stiffness matrix of the shell element is calculated by the function *shell* and that of the stiffener by the function *stiff*. These are assembled to form global stiffness matrix using the function *assemb*. Then the boundary conditions are imparted with function *bc*. The consistent load vector for the given pressure load is calculated and integrated by the function *load*. The displacements are evaluated using the function *gauss*. The function *stress* calculates the stress resultants and principal stresses.

3.5.3 Description of Functions

Function *shell*

This function is used to calculate the elastic stiffness matrix of the shell element, which is a 12x12 symmetric matrix described in section 3.2.4. The variables required for the evaluation of stiffness matrix are radius R, length L, thickness t, the modulus of elasticity E of the shell material and the number of shell elements required to model the hull.

Function *stiff*

Elastic stiffness matrix of the stiffener element is evaluated by the function *stiff*. The input details are the sectional properties of the stiffeners and the eccentricity of the centre of gravity of the stiffener from the shell middle surface.

Function *assemb*

The function *assemb* is used to assemble the stiffness matrices of the individual shell elements and the stiffeners to form the global stiffness matrix.

Function *bc*

This function incorporates the stipulated boundary condition for the stiffened shell. Four types of boundary conditions have been incorporated which are used in the stiffened cylindrical shell analysis. Fixed boundary condition is

implemented by arresting all six degrees of freedom. For clamped boundary condition, all degrees of freedom are arrested except the axial membrane displacement u. For simply supported boundary condition the axial membrane displacement u and the meridional rotation φ are kept unrestrained. Axisymmetric boundary condition is incorporated by arresting all translations normal to the plane of symmetry (u) and all rotations in the plane of symmetry (u_x and v_x).

Function *load*

It calculates the consistent load vector for the individual element using the eqn.3.12 and assembles to form the total load vector. The input data required for the function is the pressure intensity p.

Function *gauss*

The function *gauss* is the standard subroutine for Gauss elimination procedure and evaluates the nodal displacements. The results are delivered through the output file.

Function *stress*

The function *stress* is used to evaluate the stress resultants described in eqn.3.13. From the stress resultants stresses are evaluated. Principal stresses are evaluated using the eqn.3.14.

3.6 NUMERICAL INVESTIGATIONS

Validation of the program and the analytical investigations of submarine cylindrical shell models are explained in subsequent sections.

3.6.1 Validation

Validation of the program is done using the example from Flugge (1962) designated as BMP1 in this study. The geometric features of ring stiffened cylindrical shell are shown in fig. 3.4.

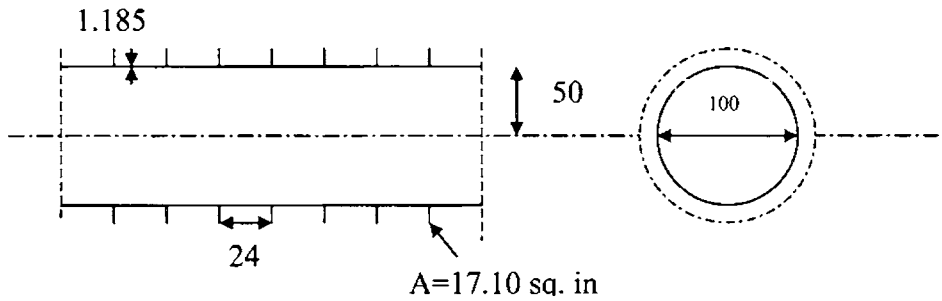

Fig. 3.4 Geometric features of ring stiffened cylindrical shell BMP1 (Flugge, page 286,1962) (all dimensions are in inches)

Uniform external pressure is 420 psi, modulus of elasticity of the material of the cylinder is $3x10^7$ psi and Poisson's ratio is 0.3. The finite element model of stiffened shell is given in fig. 3.5.

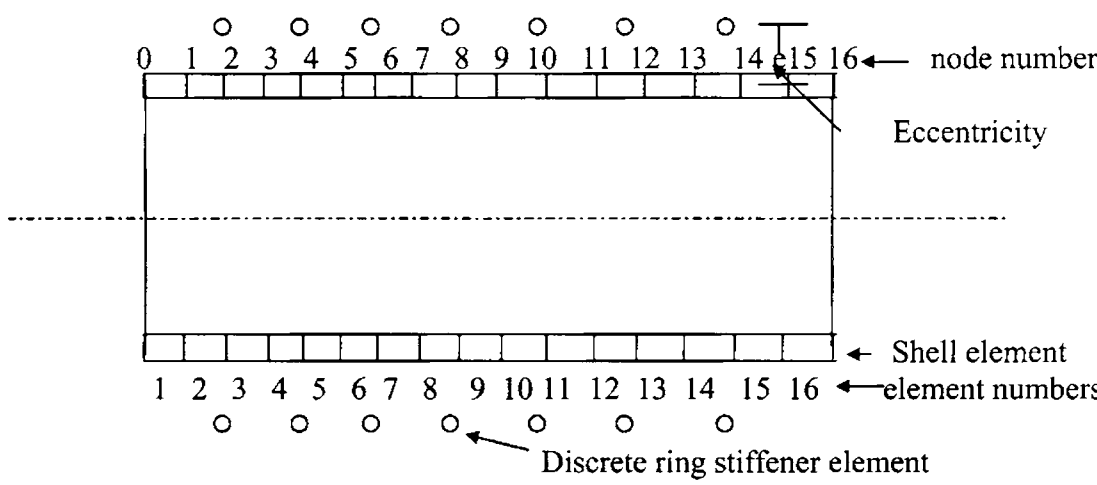

Fig. 3.5 Finite element model of ring stiffened cylindrical shell BMP1

The linear static analysis has been conducted using the software developed to predict radial deflection, circumferential stress and the meridional moment for fixed-fixed boundary conditions.

3.6.2 Linear Static Analysis of Submarine Models

Analytical investigations are carried out on submarine stiffened cylindrical shells models designated as M1 and M2. The submarine cylindrical shell models are taken from Pradeepkumar (1988) and Jacob (1989). These are hull models of attack

submarine designed as per BS 5500. The design specifications of M1 and M2 are given in table 3.1.

Table 3.1 Design specifications of submarine models M1 & M2

Description	MI	M2
Type of ship	Attack Submarine	Attack Submarine
Submerged displacement (t)	2400	3000
Diving depth (m)	300	300
Submerged speed (Kn)	25	22
Surface speed (Kn)	20	11
Material of construction	Hy 100 USA	Hy 110 USA
Yield strength (N/mm^2)	700	780
Total pressure hull length (m)	52.4	46.1
Hull diameter (m)	7.7	8.7
Overall height (m)	14.0	14.0
Modulus of elasticity (N/mm^2)	210000	210000
Poisson's ratio	0.3	0.3

The cylindrical shell is properly stiffened with stiffeners, deepframes and bulkheads. Geometric features of stiffened cylindrical shells of M1 and M2 are given in table 3.2 and shown in figs. 3.6a, 3.6b, 3.7a and 3.7b.

Table 3.2 Geometric features of submarine models M1 & M2

Description	M1 (mm)	M2 (mm)
Length of the shell between compartments	13200.00	20000.00
Radius of the shell	3850.00	4350.00
Thickness of the shell	34.00	34.00
Length of the shell between stiffeners	550.00	833.33
Length of the shell between deepframes	1650.00	2500.00

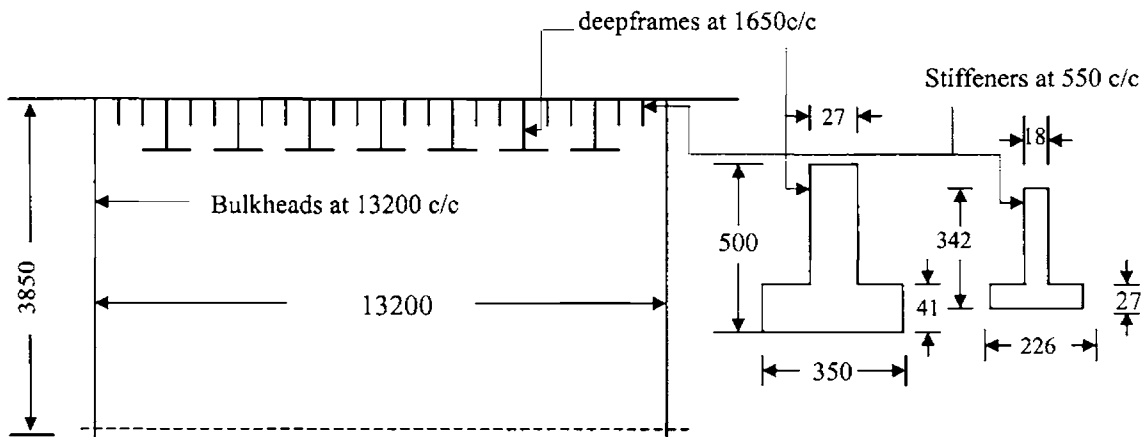

Fig. 3.6a Stiffened cylindrical shell of M1 between two bulkheads (all dimensions in mm)

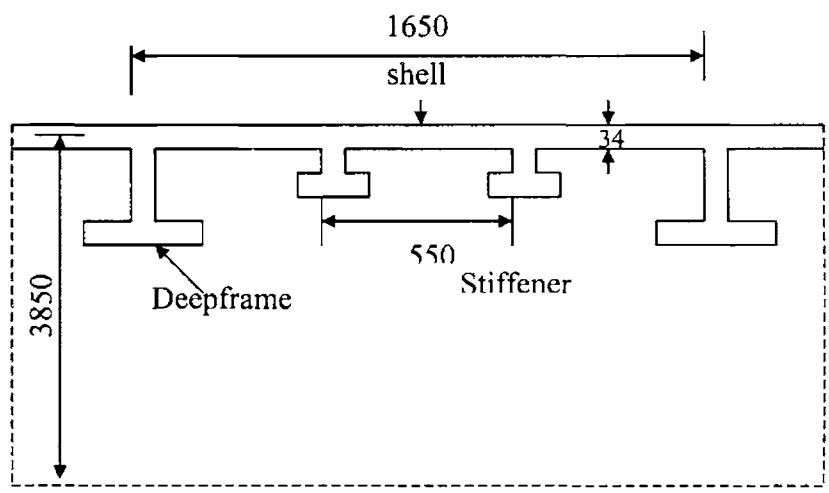

Fig. 3.6b Stiffened cylindrical shell of M1 with deepframes (all dimensions in mm)

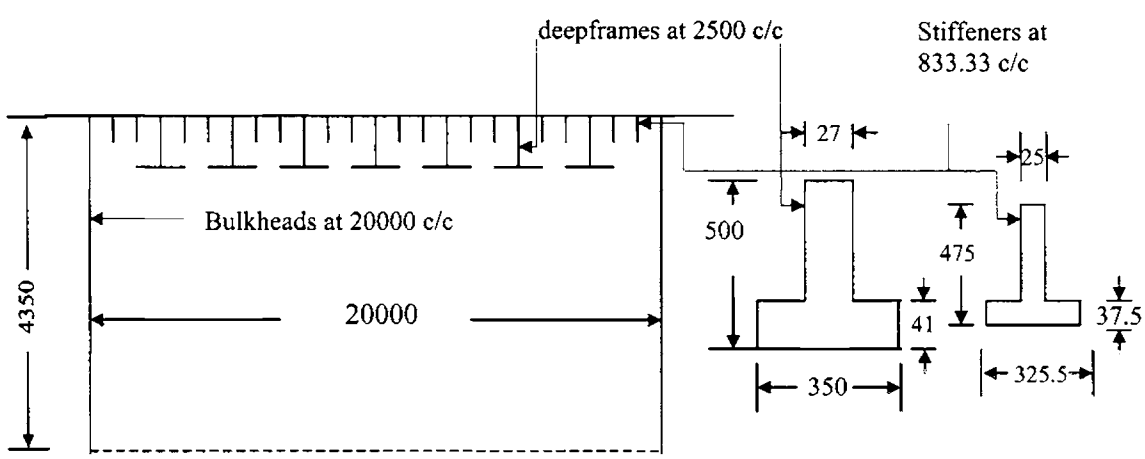

Fig.3.7a Stiffened cylindrical shell of M2 between two bulkheads (all dimensions in mm)

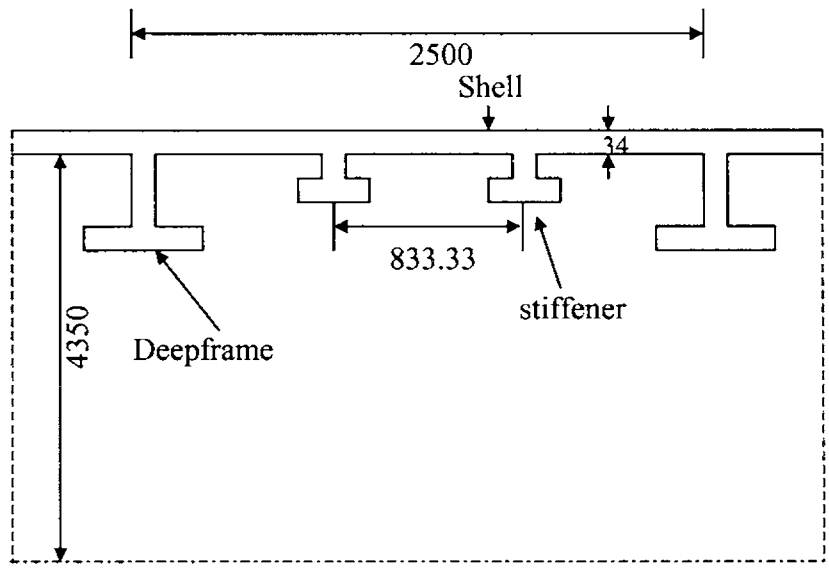

Fig. 3.7b Stiffened cylindrical shell of M2 with deepframes (all dimensions are in mm)

The L/R values for three configurations, viz., (a) cylindrical shell between stiffeners (interstiffener), (b) stiffened cylindrical shell between deepframes (interdeepframe) and (c) stiffened cylindrical shell between bulkheads (interbulkhead) and R/t values for M1 and M2 are given in table 3.3.

Table 3.3 The L/R values for three configurations and R/t values for M1 and M2

Ratio	Shell configuration	M1	M2
L/R	Interbulkhead	3.429	4.598
	Interdeepframe	0.428	0.57
	Interstiffener	0.14	0.19
R/t	Interbulkhead, interdeepframe & interstiffener	113.24	127.9

From the values given in the table 3.3, it is observed that M1 is shorter and thinner than M2. The analysis has been carried out for uniform external pressure of 3.016 N/mm^2, which is the hydrostatic pressure at the designed depth of 300m for M1 and M2.

The submarine cylindrical hull has been analysed for three configurations, viz., (a) cylindrical shell between stiffeners, (b) stiffened cylindrical shell between

deepframes and (c) stiffened cylindrical shell between bulkheads. In each case the ends of the shell are treated as fixed. Linear static analysis has been carried out to predict deformations, stress resultants and principal stresses in the above-mentioned configurations.

Analytical investigations are carried out for interbulkhead portions of M1 and M2 without attaching stiffeners. Finite element deflection and stresses of long unstiffened shell is compared with classical solutions.

3.7 RESULTS AND DISCUSSION

Software based on all-cubic axisymmetric cylindrical shell element and discrete ring stiffener element for linear static analysis is developed and operational in pc environment. The program is validated with Flugge's problem (BMP1). The variation of radial deflection, circumferential stress resultant and the radial moments are presented in figs.3.8, 3.9 and 3.10 respectively. Flugge's classical solution and authoress' solution are given in table 3.4.

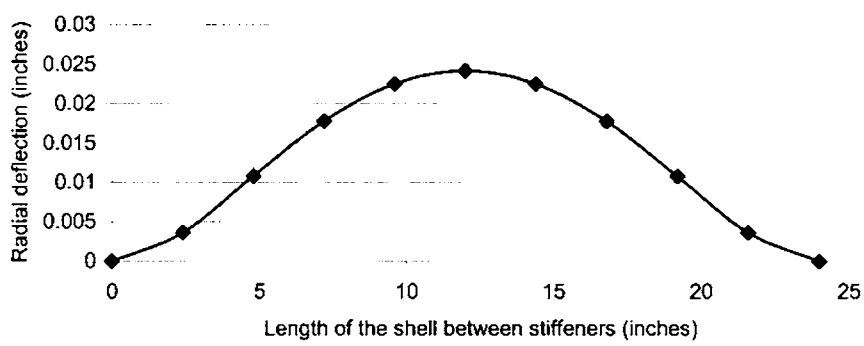

Fig. 3.8 Variation of radial deflection for BMP1

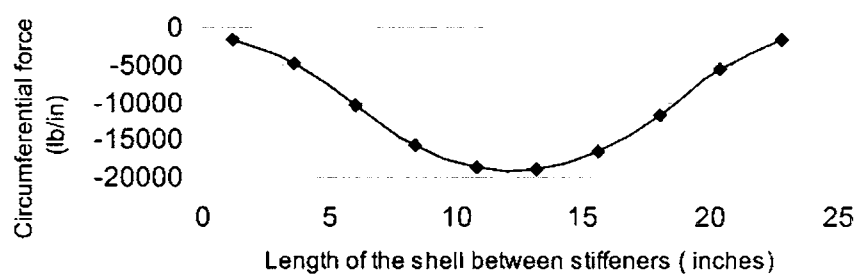

Fig. 3.9 Variation of circumferential stress for BMP1

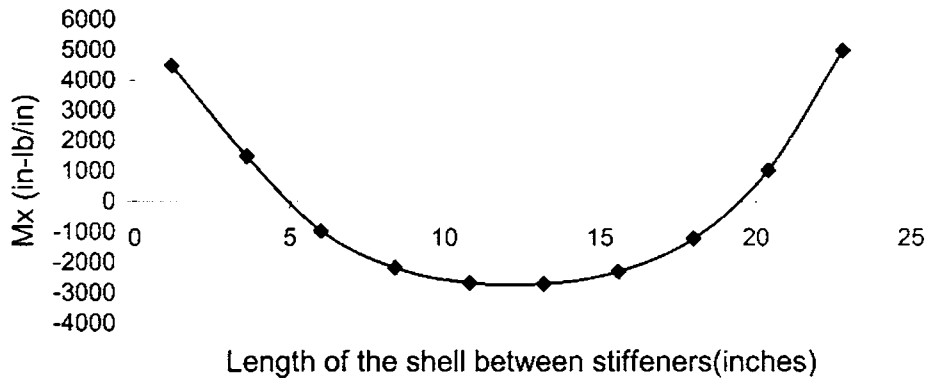

Fig. 3.10 Variation of meridional moment for BMP1

Table 3.4 Comparison with Flugge's results

Description	Flugge's closed form solution	Obtained values	% variation (upper bound)
Radial deflection at centre (in)	0.0233	0.024	3.0
Meridional moment Mx at centre (in-lb/in)	4223	4295	1.70
Circumferential stress resultants at centre N_Q (lb/in)	19200	19255	0.28

From the table 3.4 it can be seen that the obtained results are having upperbound values of 3.0% for radial deflection 1.7% for meridional moment and 0.28% for circumferential stress resultants.

Analysis has been carried out for interstiffener, interdeepframe and interbulkhead configurations for M1 and M2. The variation of radial deflection, major and minor principal stresses at middle and outer layers, meridional and circumferential stress resultants (Nx, N_Q), meridional and circumferential moments (Mx, M_Q) are graphically presented through figs. 3.11 to 3.18 for interstiffener configurations. Respective values for interdeepframe configuration and interbulkhead configuration are shown in figs. 3.19 to 3.26 and figs. 3.27 to 3.34 respectively.

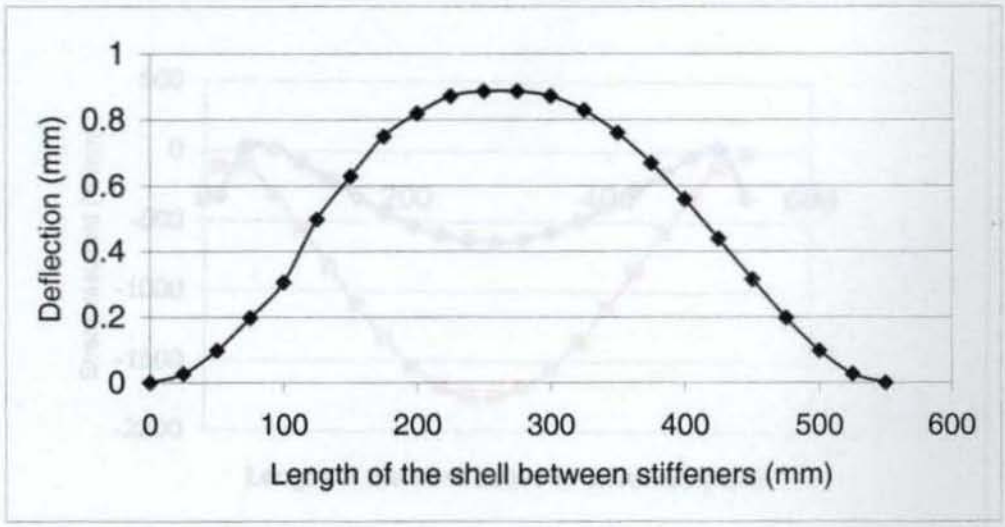

Fig. 3.11 Variation of radial deflection for M1 for interstiffener configuration

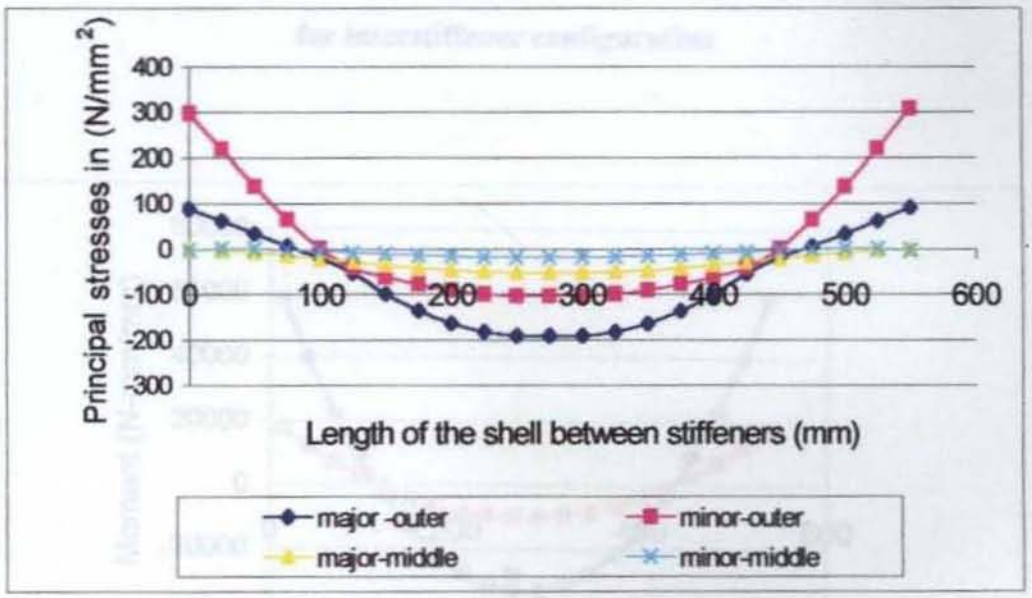

Fig. 3.12 Variation of major and minor principal stresses in the outer and the middle layers for M1 for interstiffener configuration

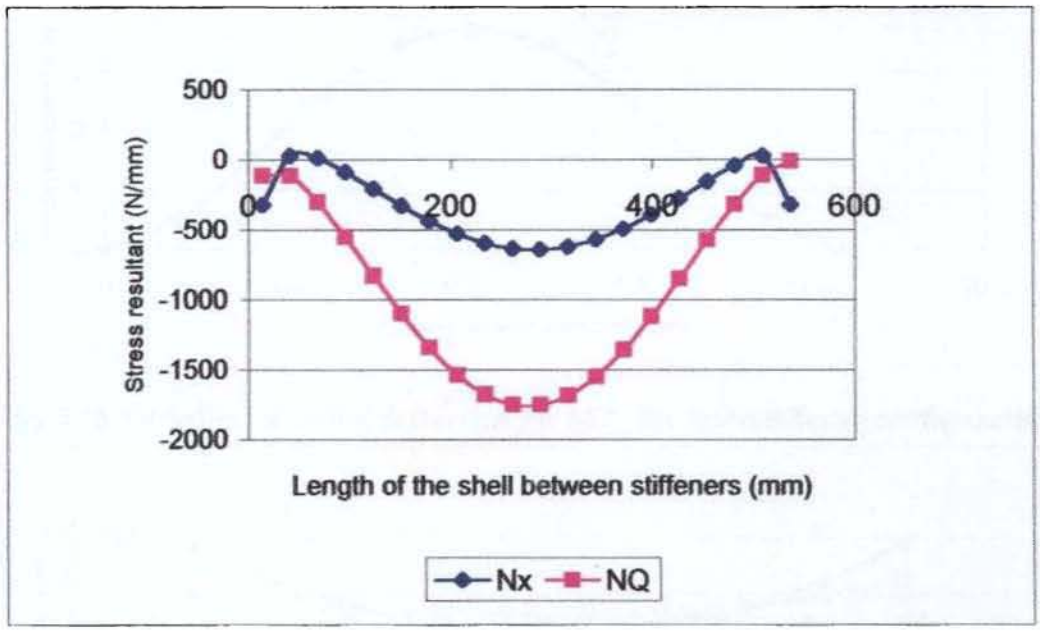

Fig. 3.13 Variation of longitudinal and circumferential stress resultants for M1 for interstiffener configuration

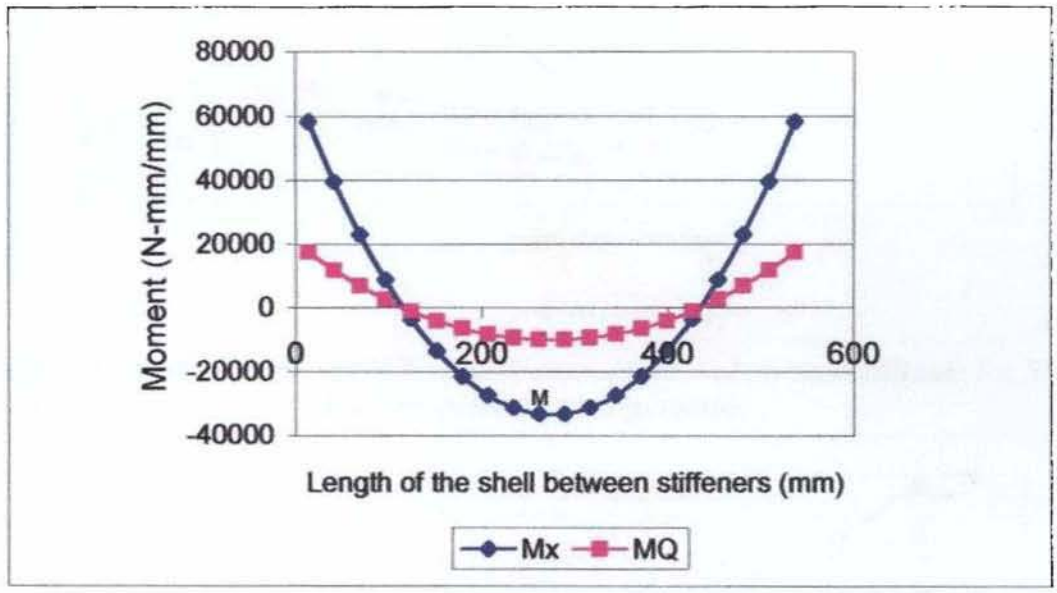

Fig. 3.14 Variation of longitudinal and circumferential moments for M1 for interstiffener configuration

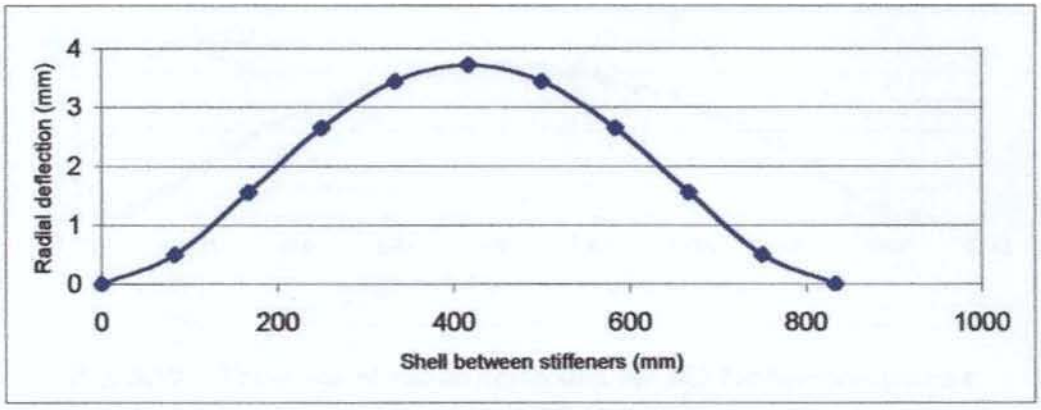

Fig. 3.15 Variation of radial deflection for M2 for interstiffener configuration

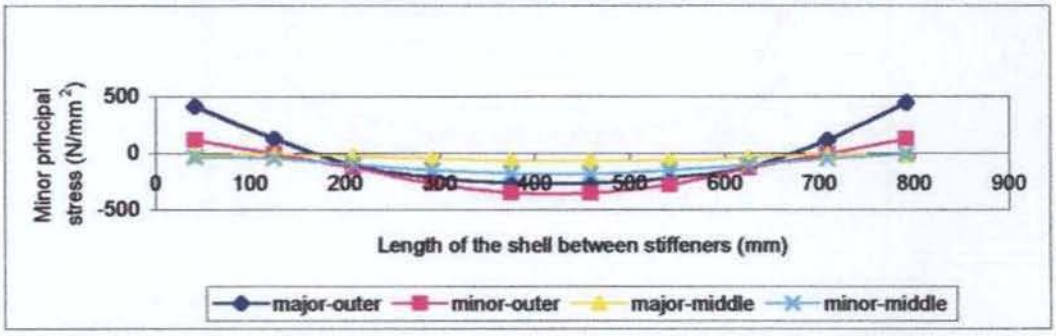

Fig. 3.16 Variation of major and minor principal stresses in the outer and the middle layers for M2 for interstiffener configuration

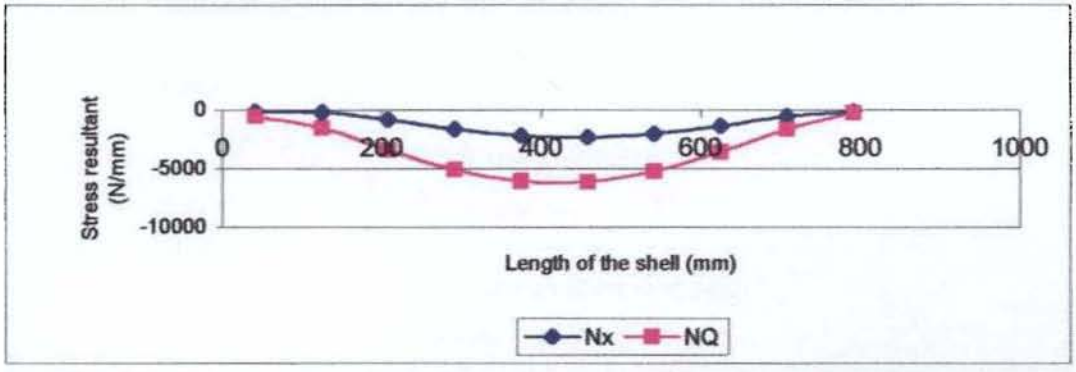

Fig. 3.17 Variation of longitudinal and circumferential stress resultants for M2 for interstiffener configuration

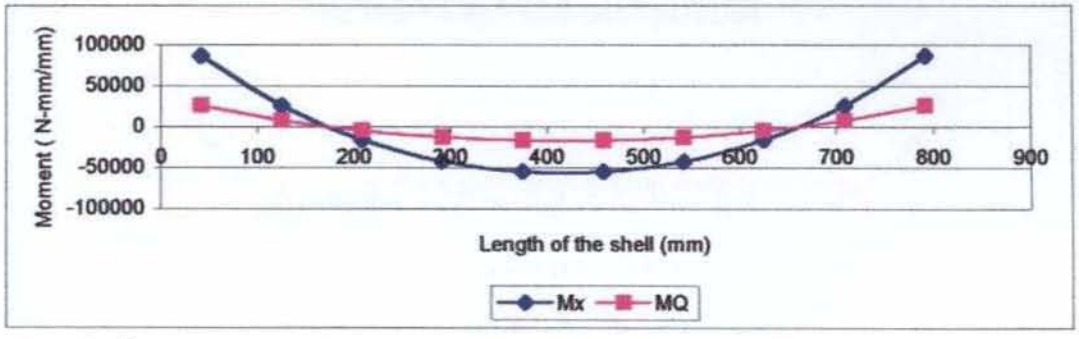

Fig. 3.18 Variation of longitudinal and circumferential moments for M2 for interstiffener configuration

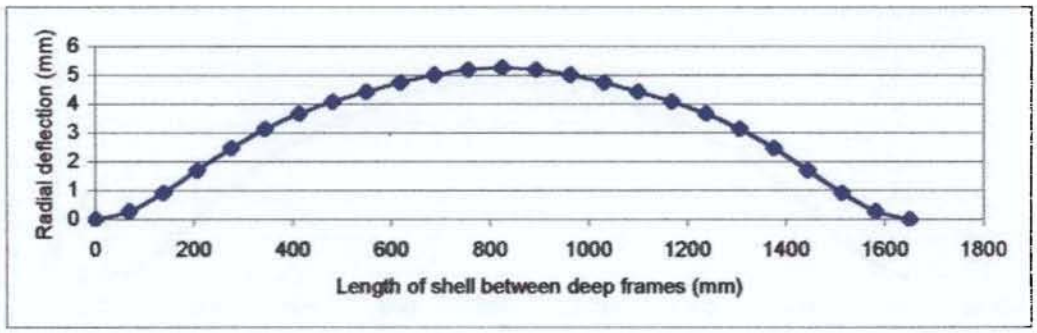

Fig. 3.19 Variation of radial deflection for M1 for interdeepframe configuration

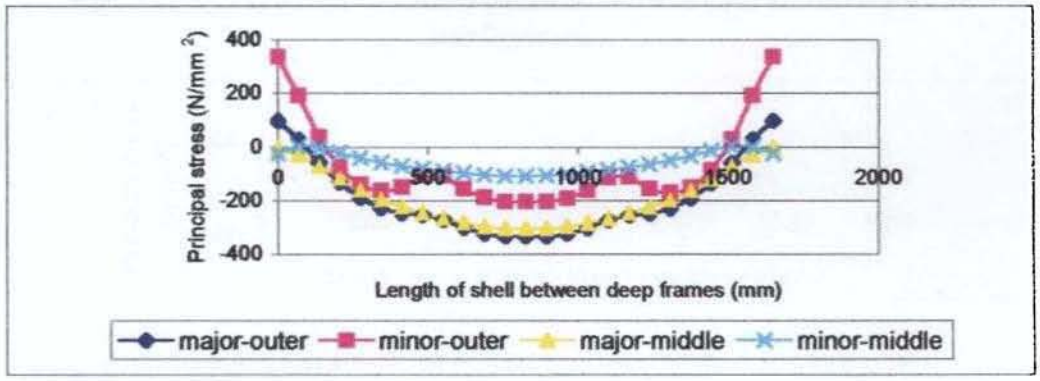

Fig. 3.20 Variation of major and minor principal stresses in the outer and the middle layers for M1 for interdeepframe configuration

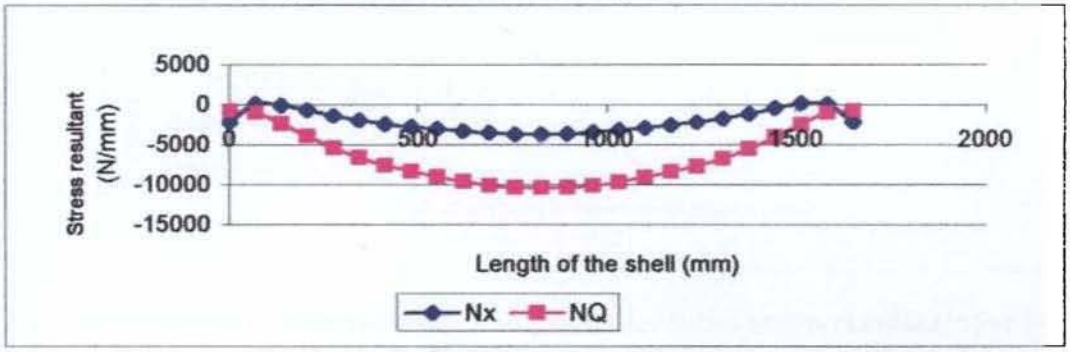

Fig. 3.21 Variation of longitudinal and circumferential stress resultants for M1 for interdeepframe configuration

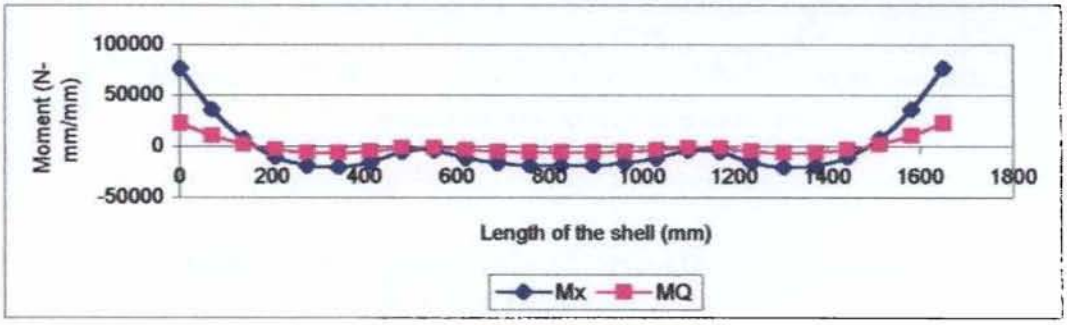

Fig. 3.22 Variation of longitudinal and circumferential moments for M1 for interdeepframe configuration

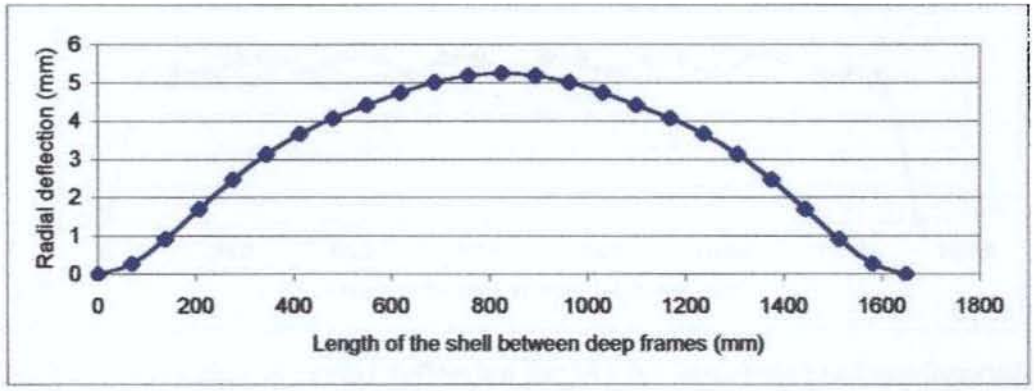

Fig. 3.23 Variation of radial deflection for M2 for interdeepframe configuration

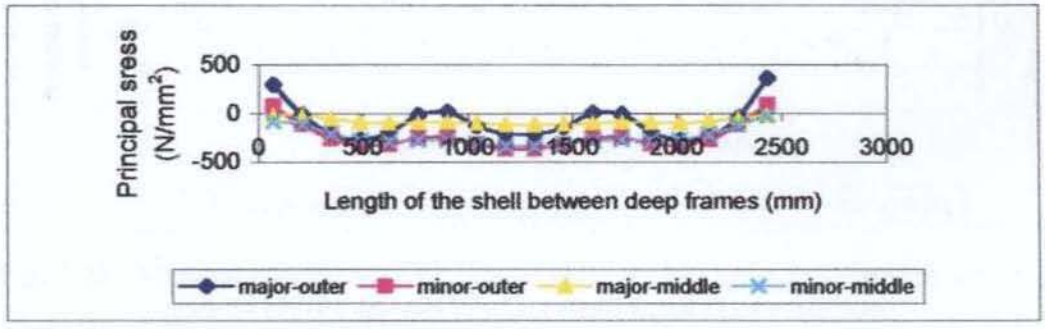

Fig. 3.24 Variation of major and minor principal stresses in the outer and the middle layers for M2 for interdeepframe configuration

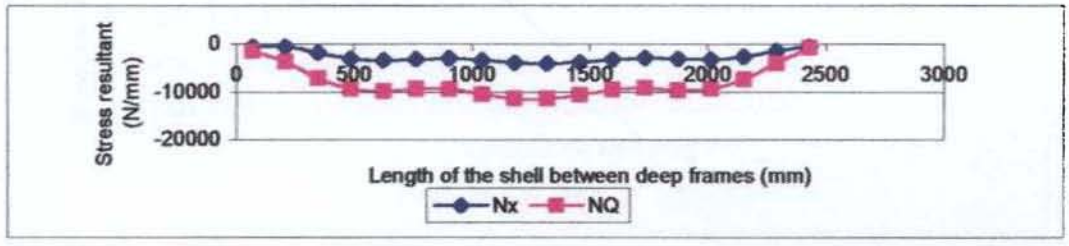

Fig. 3.25 Variation of longitudinal and circumferential stress resultants for M2 for interdeepframe configuration

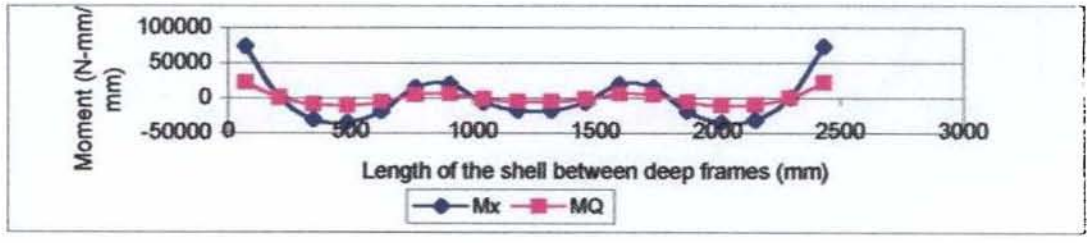

Fig. 3.26 Variation of longitudinal and circumferential moments for M2 for interdeepframe configuration

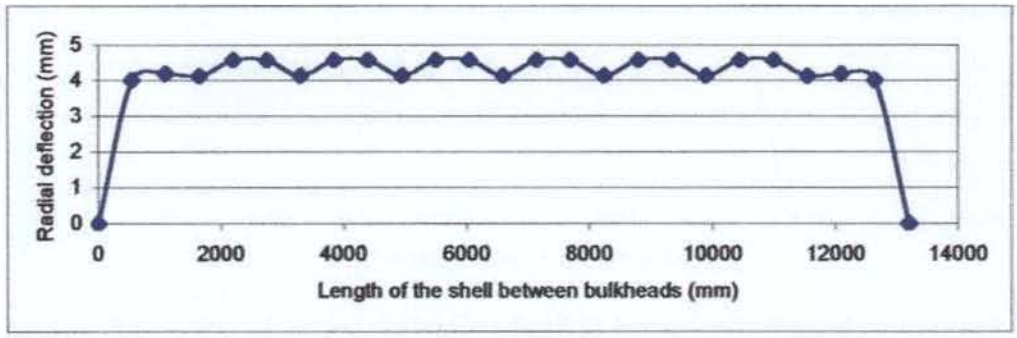

Fig. 3.27 Variation of radial deflection for M1 for interbulkhead configuration

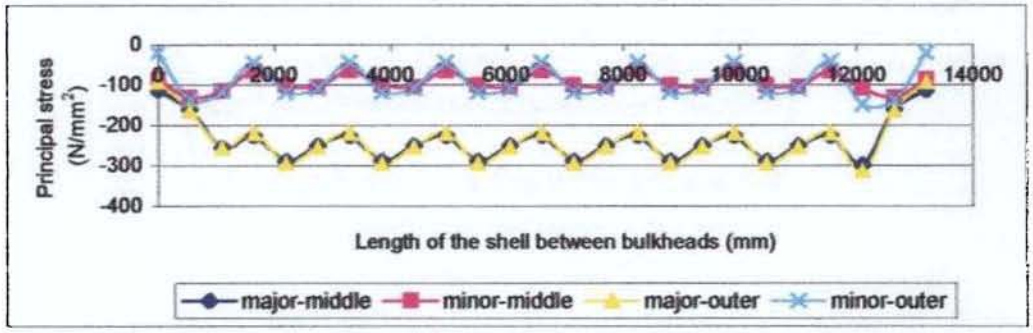

Fig. 3.28 Variation of major and minor principal stresses in the outer and the middle layers for M1 for interbulkhead configuration

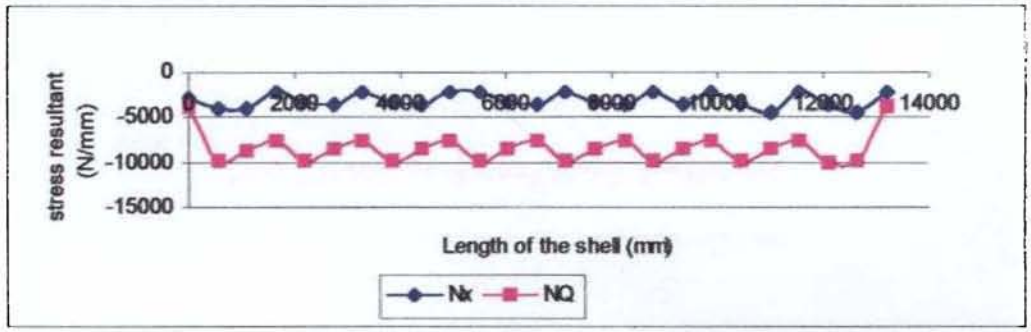

Fig. 3.29 Variation of longitudinal and circumferential stress resultants for M1 for interbulkhead configuration

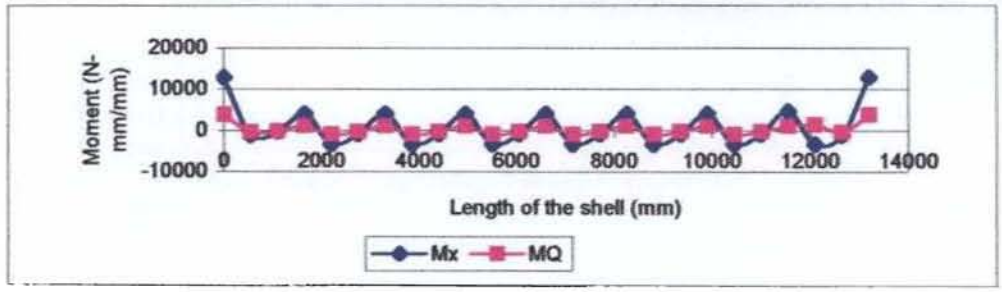

Fig. 3.30 Variation of longitudinal and circumferential moments for M1 for interbulkhead configuration

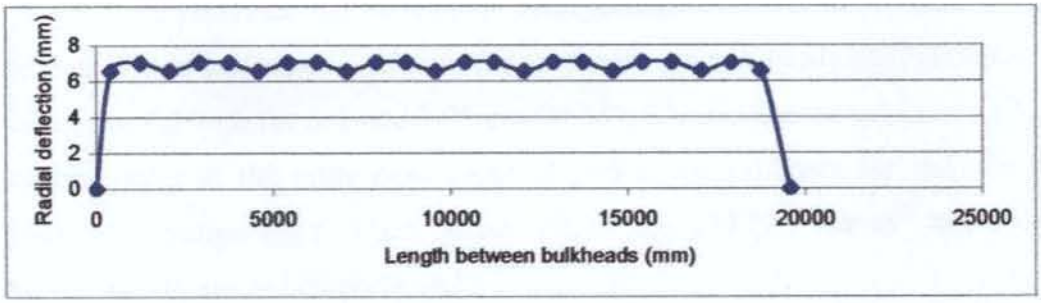

Fig. 3.31 Variation of radial deflection for M2 for interbulkhead configuration

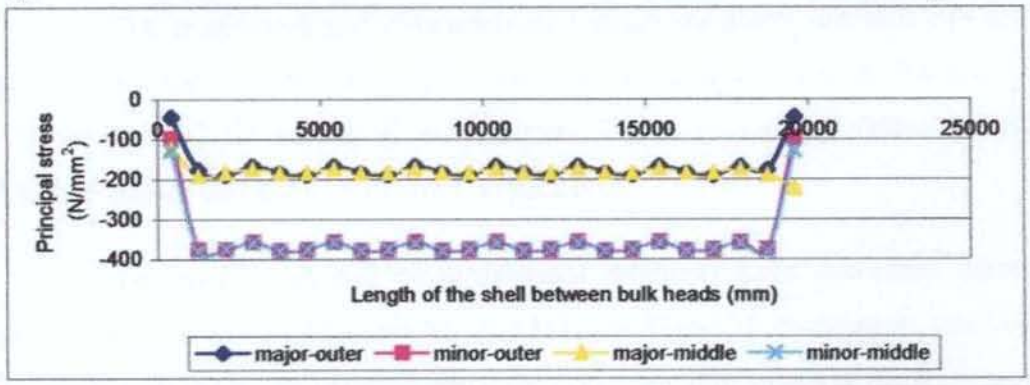

Fig. 3.32 Variation of major and minor principal stresses in the outer and the middle layers for M2 for interbulkhead configuration

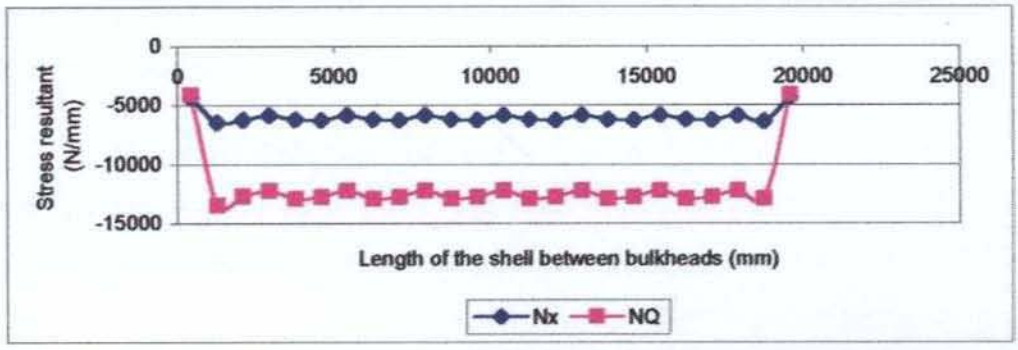

Fig. 3.33 Variation of longitudinal and circumferential stress resultants for M2 for interbulkhead configuration.

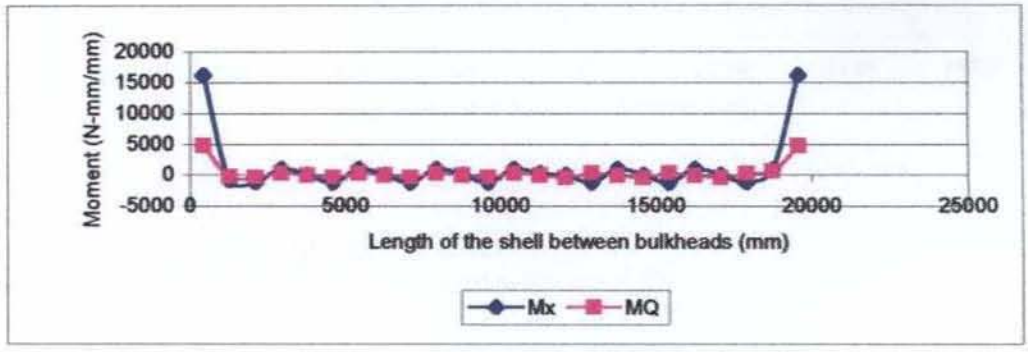

Fig. 3.34 Variation of longitudinal and circumferential moments for M2 for interbulkhead configuration

It is observed that for various configurations the maximum value of radial deflection is at midbay of stiffeners for shell between bulkheads configuration. The values are 4.57mm for M1 and 7.05mm for M2. The maximum values of principal stresses occur at the outer most layer of midbay of stiffeners for shell between bulkheads configuration. These stress values are 284.723 N/mm^2 and 378.410 N/mm^2 for M1 and M2 respectively.

The meridional and circumferential stress resultants are also having their peak values for shell between bulkheads. The maximum values for Nx and N_Q for M1 are 4445.62 N/mm and 9786.81 N/mm. The corresponding values for M2 are 6253.27 N/mm and 12685.95 N/mm respectively.

The meridional and circumferential moments have maximum values for interstiffener analysis. Mx and M_Q for M1 are 33162.72 N-mm/mm and 9948.81 N-mm/mm in the middle portion while the corresponding values at the fixed ends are 58315.69 N-mm/mm and 17494.0 N-mm/mm. The Mx and M_Q for M2 are 6253.27 N-mm/mm and 12685.95 N-mm/mm at the middle and 86621.43 N-mm/mm and 25995.71 N-mm/mm at the ends respectively.

The radial deflection with and without stiffeners is plotted in figs.3.35 and 3.36 for M1 and M2 respectively. The results of radial deflection without stiffeners are compared with that of the classical solution for long shells and is given table 3.5.

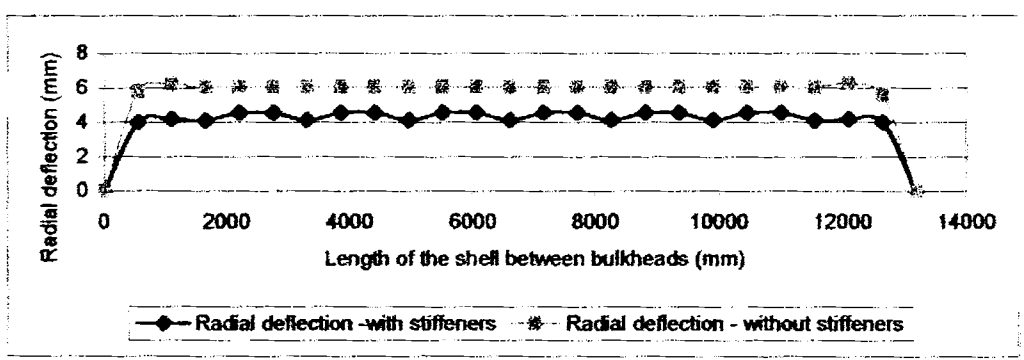

Fig. 3.35 Variation of radial deflection for interbulkhead configuration of M1 with and without stiffeners

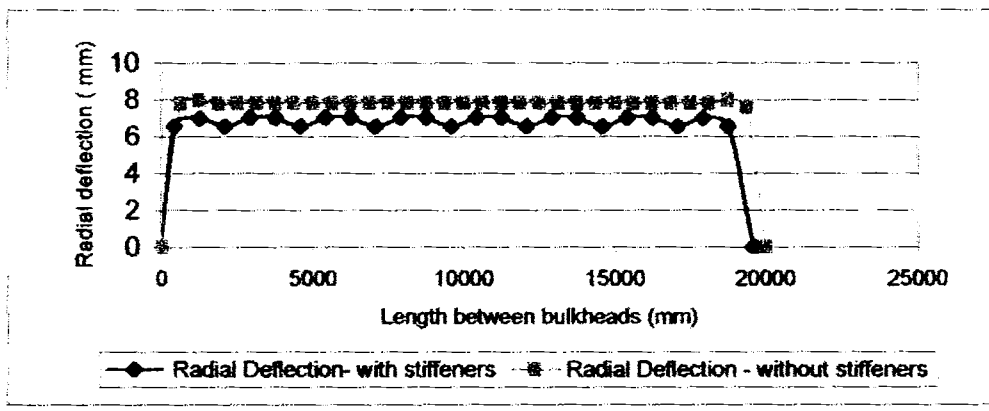

Fig. 3.36 Variation of radial deflection for interbulkhead configuration of M2 with and without stiffeners

Table 3.5 Comparison with classical solutions for radial deflection for long shells

Model	Radial deflection (mm)		% variation
	Finite element	Classical solution	
M1	6.06	6.26	3.19
M2	7.83	7.99	2.00

For long unstiffened shells between bulkheads analysis using all-cubic axisymmetric shell element gives lowerbound values of 3.19% and 2% for models M1 and M2 for radial deflection.

CHAPTER 4
LINEAR BUCKLING ANALYSIS

4.1 INTRODUCTION

The linear buckling analysis of the stiffened cylindrical shell has been described in this chapter for two load cases, treating hydrostatic pressure as a radial load as well as a follower force.

4.2 HYDROSTATIC PRESSURE AS RADIAL PRESSURE LOAD

Determination of bifurcation buckling pressure involves the formulation of linear elastic stiffness matrix and the geometric stiffness matrix (eqn.1.4). Linear elastic stiffness matrix has been described in the section 3.3 and 3.4. Formulation for geometric stiffness matrix is explained subsequently.

4.2.1 Development of Geometric Stiffness Matrix

The basic expression for geometric stiffness matrix is given by Zienkiewicz (1979) based on the principle of virtual work.

For large displacements problems the strain matrix $[\overline{B}]$ can be represented as

$$[\overline{B}] = [B] + [B_{nl}] \qquad \text{.....} (4.1)$$

where [B] is the usual small displacement matrix encountered in the linear infinitesimal strain analysis. In general $[B_{nl}]$ is linear function of nodal displacement $\{\delta\}$. Using that $[\overline{B}]$, the total large displacement stiffness matrix $[K_{nl}]$ is derived

$$[K_{nl}] = {}_v\{[B]^T[D][B_{nl}] + [B_{nl}]^T[D][B_{nl}] + [B_{nl}]^T[D][B]\}\, dv \text{.....} (4.2)$$

This expression contains the terms, which are linear and quadratic in $\{\delta\}$. The total tangent stiffness matrix can be rewritten as

$$[K_T] = [K] + [K_G] + [K_{nl}] \qquad \text{.....} (4.3)$$

where [K] is the linear elastic stiffness matrix, $[K_G]$ is the geometric stiffness matrix and $[K_{nl}]$ is due to large displacement effect. In linear stability problems large displacement effect is less important and hence $[K_{nl}]$ has been neglected in the present study.

At the buckling stage stiffness matrix becomes singular, hence

$$\left| [K] + [K_G] \right| = 0 \qquad \text{..... (4.4)}$$

In linear buckling analysis, this relation can be rewritten in terms of prebuckling stress resultant as

$$\left| [K] + \lambda [K_g] \right| = 0 \qquad \text{..... (4.5)}$$

where λ is the nondimensional buckling load and $[K_g]$ is the geometric stiffness matrix derived in the initial configuration.

Geometric stiffness matrix has been derived from the expression (Zienkiewicz, 1979) given below.

$$[K_g]\, d\{\delta\} = \int_v d[B_{nl}]^T \{\sigma\} dv \qquad \text{..... (4.6)}$$

According to Sander's (1963) theory the nonlinear generalized strains for stiffened cylindrical shell consist of linear and nonlinear membrane strains and linear bending strains. This assumption will lead to the prebuckling stress resultants as given in eqn.4.7.

The basic expression for geometric stiffness matrix is given as

$$[K_g] = \int_v [G]^T \begin{pmatrix} \sigma_x & 0 \\ 0 & \sigma_\theta \end{pmatrix} [G] \quad dv \qquad \text{..... (4.7)}$$

where σ_x and σ_θ are the prebuckling stresses and [G] is constructed from derivatives of shape functions.

4.2.2 Geometric Stiffness Matrix of the Shell Element

Geometric stiffness matrix $[k_g]$ of the all-cubic cylindrical shell element already derived in section 3.2 is obtained from eqn.4.7.

The general expression is

$$[k_g]=\Pi R^2 L/2 \quad \begin{Bmatrix} k_{g1,1} & k_{g1,2} & k_{g1,3} \ldots\ldots\ldots\ldots & k_{g1,12} \\ \ldots\ldots\ldots\ldots & \ldots\ldots\ldots\ldots & \ldots\ldots\ldots\ldots & \\ \ldots\ldots\ldots\ldots & \ldots\ldots\ldots\ldots & \ldots\ldots\ldots\ldots & k_{g2,12} \end{Bmatrix} \qquad (4.8)$$

The geometric stiffness matrix proposed by Rajagopalan (1993) is used in the present study and is given in clauseA.4 of Appendix A.

4.2.3 Geometric Stiffness Matrix of the Discrete Stiffener Element

The geometric stiffness of the discrete ring stiffener element already described in section 3.3 is obtained from the following expression.

$$W = \int_v \sigma \{\epsilon_\theta\}_{nL} \, dv \qquad \ldots\ldots\ldots\ldots\ldots\ldots\ldots (4.9)$$

where σ is the prebuckling axial stress and $\{\epsilon_\theta\}_{nL}$ is the nonlinear buckling strain. The expression for 4x4 geometric stiffness matrix of the discrete ring stiffener element is obtained as

$$k_{gSij} = \partial^2 W/\partial q_i \partial q_j \qquad \ldots\ldots\ldots\ldots\ldots\ldots (4.10)$$

where $\partial qi, \partial qj$ be the displacement vectors. The matrix obtained is transformed into 6x6 in global coordinate using the transformation matrix given in eqn.3.17

The geometric stiffness matrix proposed by Rajagopalan (1993) is used in the analysis and is given in clause A.5 of Appendix A.

The transformed geometric stiffness matrix of the stiffener element is added to the relevant locations of the global geometric stiffness matrix of the shell.

4.2.4 Prediction of Linear Buckling Pressure

The finite element model of the stiffened cylindrical shell for linear buckling analysis is same as that of linear static analysis. The elements of [k] and $[k_g]$ are derived in terms of circumferential wave numbers.

The solution procedure adopted for obtaining the linear buckling pressure is the determinant search procedure. A value of λ is assumed and the determinant of the matrix is calculated. The process is repeated by changing the value of λ until the determinant changes its sign. The value of λ for zero determinant is the buckling pressure. This procedure is repeated for possible values of circumferential wave number. The minimum of these buckling pressures defines the buckling pressure of the shell.

4.3 FOLLOWER FORCE EFFECT DUE TO HYDROSTATIC PRESSURE

Hydrostatic pressure is considered as follower force in the second phase of analysis. The development of pressure stiffness matrix for the stiffened cylindrical shell from the virtual work principle is explained in the subsequent sections.

4.3.1 Development of Pressure Stiffness Matrix

Expression for the work done by hydrostatic pressure during pressure-rotation phase derived by Mc Donald and White [1973] has been used to derive the basic expression for pressure stiffness. Deformation of infinitesimal area $dx\ Rd\theta$ of shell surface is considered and the pressure vector will be acting in the direction of the normal vector of that deformed surface.

In a cylindrical shell, the displacement vector $d\overline{\delta}$ can be represented as

$$d\overline{\delta} = ui + vj + wk \qquad \text{..... (4.11)}$$

where u,v and w are the axial circumferential and normal displacements respectively and i,j and k are unit vectors in these directions. The infinitesimal area on the shell surface $R\ d\theta\ dx$ deforms into $(1+\varepsilon\theta)\ Rd\theta(1+\varepsilon x)\ dx$

$$\text{where } \varepsilon x = \partial u/\partial x \text{ and } \varepsilon\theta = 1/R\ (w+\partial v/\partial\theta) \qquad \text{..... (4.12)}$$

The unit vector in the direction normal to the deformed surface becomes k^l.

$$k^l = \frac{-\partial w}{\partial x}\ i + \frac{1}{R}(v - \frac{\partial w}{\partial \theta})\ j + k \qquad \text{..... (4.13)}$$

where $\partial w/\partial x$ *and* $(v-\partial w/\partial\theta)/R$ are the meridional and circumferential rotations respectively.

The hydrostatic buckling pressure now acts on the new area in the direction of k^l

$$pI = p(1+\varepsilon x)(1+\varepsilon\theta)R\, d\theta\, dx\ k^l \qquad \text{.....} (4.14)$$

where pI is the modified pressure.

Substituting k^l from eqn.4.13 in eqn.4.14 and on neglecting the higher powers

$$pI = (-\partial w/\partial x\, i + 1/R(v-\partial w/\partial\theta)\, j + (\partial u/\partial x + 1/R\,(w+\partial v/\partial\theta))\, k)\, R\, d\theta\, dx \text{.....} (4.15)$$

The dot product of the pressure force vector and the buckling displacement vector will be the work done by the hydrostatic pressure on the pressure rotation phase.

The work done is given by

$$\Omega = \frac{1}{2} \int\int pI.d\{\overline{\delta}\} \qquad \text{.....} (4.16)$$

Substituting the eqn.4.11 and 4.15 in eqn.4.16

$$\Omega = p/2 \int\int [\{(-\partial w/\partial x)u + 1/R(v-\partial w/\partial\theta)v + (\partial u/\partial x + 1/R\,(w+\partial v/\partial\theta))w\}\, R\, d\theta\, dx \text{.....} (4.17)$$

The eqn.4.17 can be elaborated and can be written in a matricised form for a particular finite element as

$$\Omega = 1/2\{\delta\}\,[k_p]\,\{\delta\} \qquad \text{.....} (4.18)$$

where $\{\delta\}$ be the nodal degrees of freedom which is related to the displacement by means of shape functions and $[k_p]$ the pressure stiffness matrix.

Comparing the eqn.4.17 and 4.18, $[k_p]$ can be arrived at. The finite element substitution of $[k_p]$ with all-cubic axisymmetric shell element will be a 12x12 matrix in the form

$$[k_p] = \begin{Bmatrix} k_{p1,1} & k_{p1,2} & k_{p1,3} \ldots & \ldots\ldots k_{p1,12} \\ \ldots & \ldots & \ldots & \ldots \\ \ldots & \ldots & \ldots & \ldots k_{p12,12} \end{Bmatrix} \qquad \ldots\ldots\ldots\ldots\ldots\ldots (4.19)$$

All the terms in the pressure stiffness matrix proposed by Rajagopalan (1993), which are used in the present study, are given in clauseA.6, Appendix A.

4.3.2 Buckling Pressure Prediction

The linear buckling analysis with follower force effect is carried out using pressure stiffness matrix along with linear elastic and geometric stiffness matrices. $[K_g]$ and $[K_P]$ are added algebraically so as to form the matrix $[K_{gP}]$ and is used in the general expression for linear buckling as

$$\left| [K] - \lambda [K_{gP}] \right| = 0 \qquad \ldots\ldots\ldots\ldots\ldots\ldots (4.20)$$

The nondimensional buckling load λ is evaluated using the procedure explained in section 4.2.4.

4.4 DEVELOPMENT OF SOFTWARE

A computer code has been developed to determine the interstiffener buckling pressure and overall buckling pressure of stiffened cylindrical shell. The program implementation and various functions that constitute the core of the program are explained in subsequent subsections.

4.4.1 Flow Chart

The schematic diagram for linear buckling analysis is given in fig. 4.1a and the hierarchal order of operations is given in the fig. 4.1b.

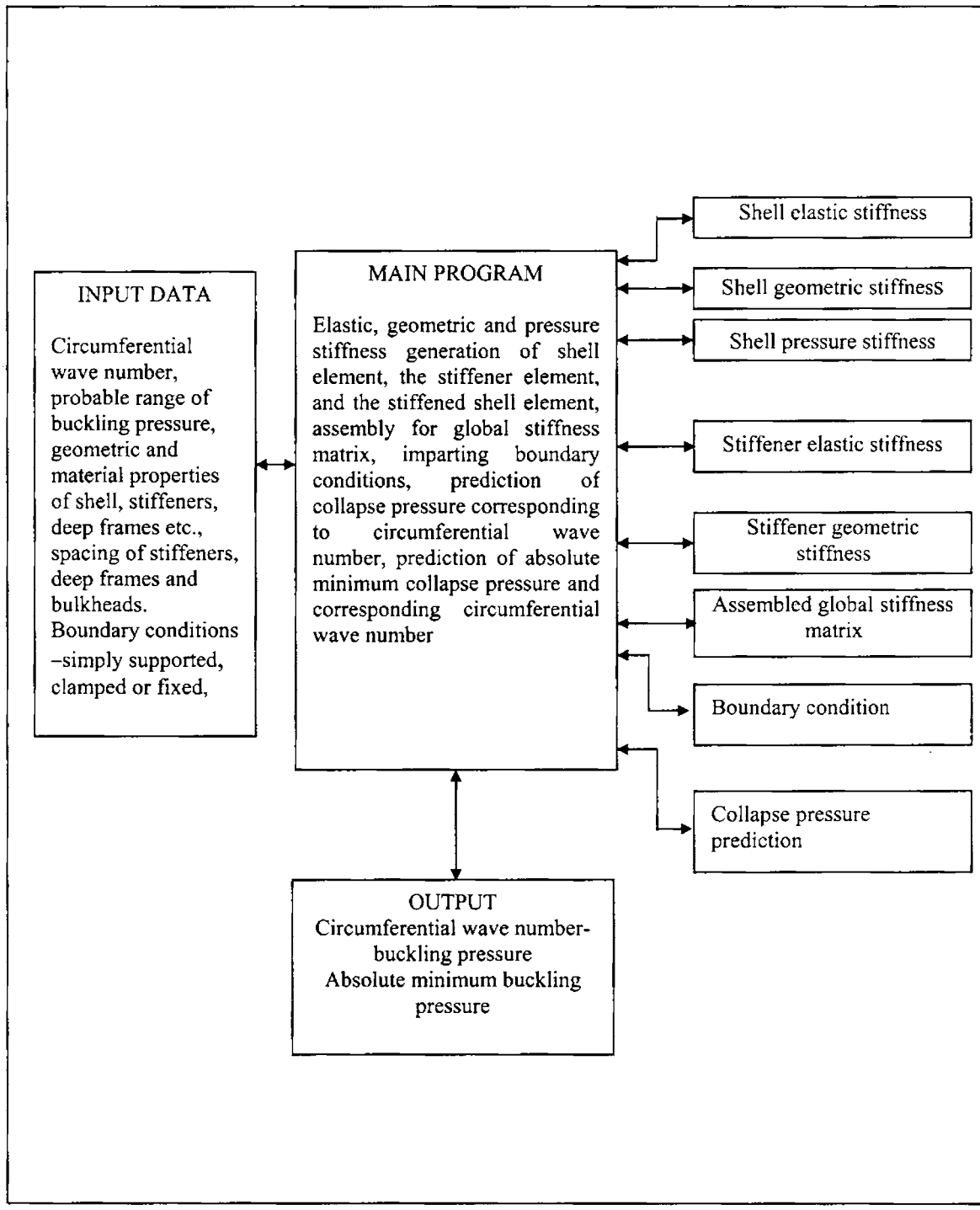

Fig. 4.1a Schematic diagram for linear buckling analysis

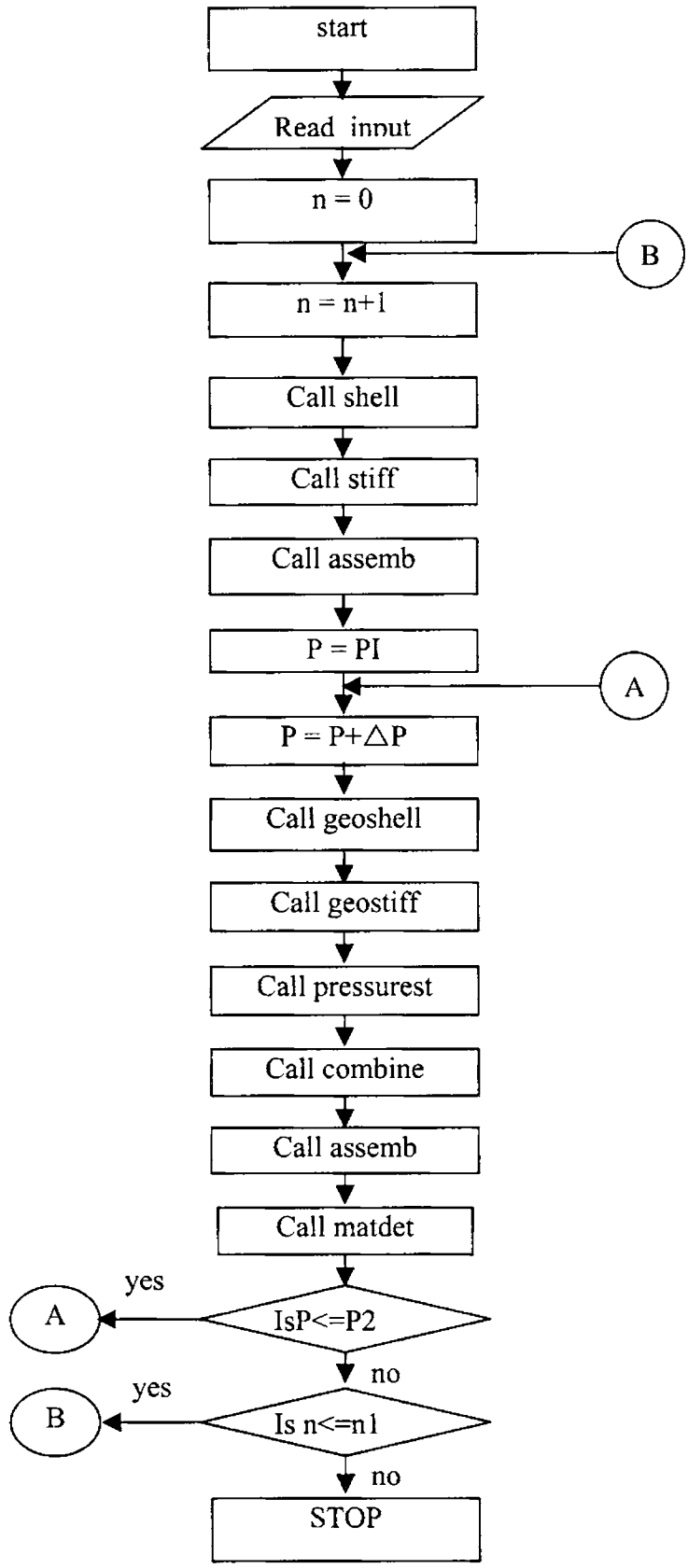

Fig. 4.1b Flowchart for linear buckling analysis

4.4.2 Program *MAIN*

The execution of the program is as follows. The elastic stiffness matrix of the finite shell element and the stiffener element are calculated for a given value of circuferntial wave number. These matrices are assembled to form global elastic stiffness matrix. For different values of pressure (p) starting from p1 to p2 with an increment of $\triangle$p, the geometric stiffness matrix of the shell and the stiffener element and the pressure stiffness matrix of the shell are calculated and the global stiffness matrices are formed by calling an assembly program. For each value of p the determinant of the sum of the global stiffness matrices of the shell and the stiffener is finally calculated. A plot is made with p Vs the determinant. The value of p corresponding to zero determinant is the linear buckling pressure corresponding to that value of n. The procedure is repeated for various values of n. Minimum of all these buckling pressures is the actual collapse pressure. The main program calls in turn a number of functions at appropriate stages to perform the above-mentioned operations. The functions *shell, stiff* and *assemb* are already explained in section 3.5.3. The remaining functions are described below.

4.4.3 Description of Functions

Function *geoshell*

The geometric stiffness matrix of the shell element is evaluated by the *geoshell* function as described in section 4.2.2 for each load increment.

Function *geostiff*

This function calculates the geometric stiffness matrix for the stiffener element as explained in section 4.2.3.

Function *pressurest*

This function calculates the pressure stiffness matrix of the shell element as explained in section 4.3.1.

Function *matdet*

This function is used to determine the value of the determinant of the sum of the global stiffness matrices [K], [Kg] and [K_P], as explained in section 4.2.4.

4.5 NUMERICAL INVESTIGATIONS

To validate the program developed for interstiffener buckling analysis using all-cubic element, a stiffened cylindrical shell suggested by Kendrick [1970] designated here as BMP2 has been attempted. The geometric features are shown in fig. 4.2a.

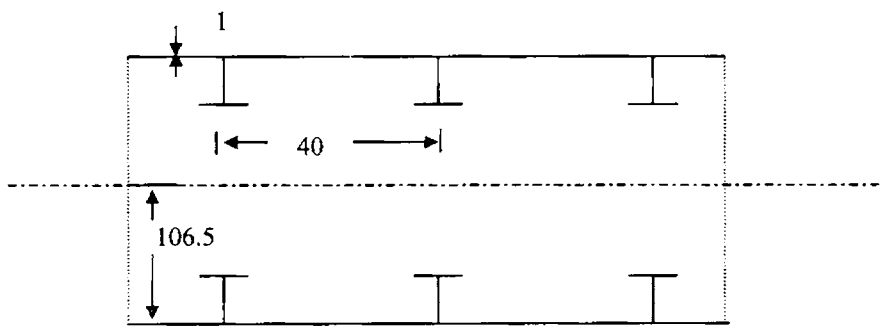

Fig. 4.2a Geometric features of BMP2 (all dimensions are in inches)

The finite element model is given in fig. 4.2b, in which the interstiffener region of the shell is divided into sixteen elements.

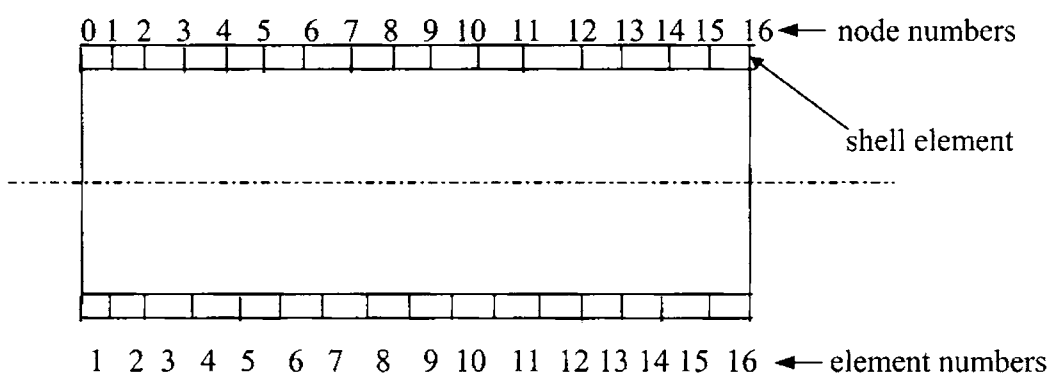

Fig. 4.2b Finite element model of interstiffener portion of BMP2

Influence of simply supported - simply supported (s.s-s.s), clamped – clamped (c-c) and fixed-fixed (f-f) boundary conditions on linear buckling pressure is

investigated. Influence of derivatives of degrees of freedom is also studied by arresting those degrees of freedom at end nodal circles for s.s-s.s boundary conditions.

General instability studies are conducted on stiffened cylindrical shell designated as BMP3 suggested by Kendrick (1970) is shown in figs. 4.3a and 4.3b.

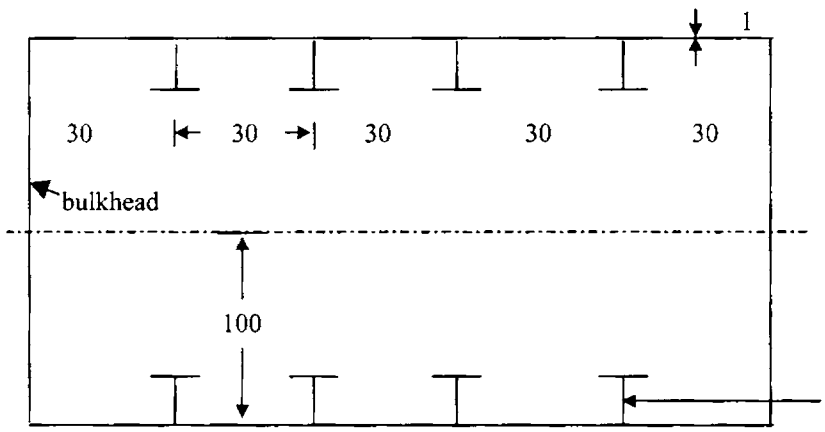

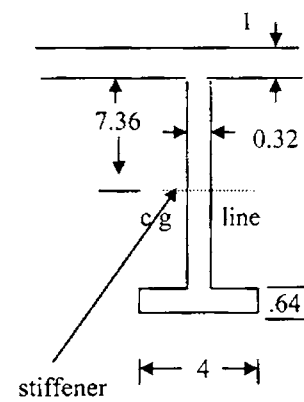

Fig. 4.3a Geometric features of BMP3 (All dimensions are in inches)

Fig.4.3bCross sectional details of stiffener (All dimensions are in inches)

The shell skin is modeled using all-cubic axisymmetric shell elements and stiffeners using discrete ring stiffener elements. The finite element model is given in fig. 4.3c in which the stiffened shell is divided into 30 elements with attachment of stiffeners at interval of six elements.

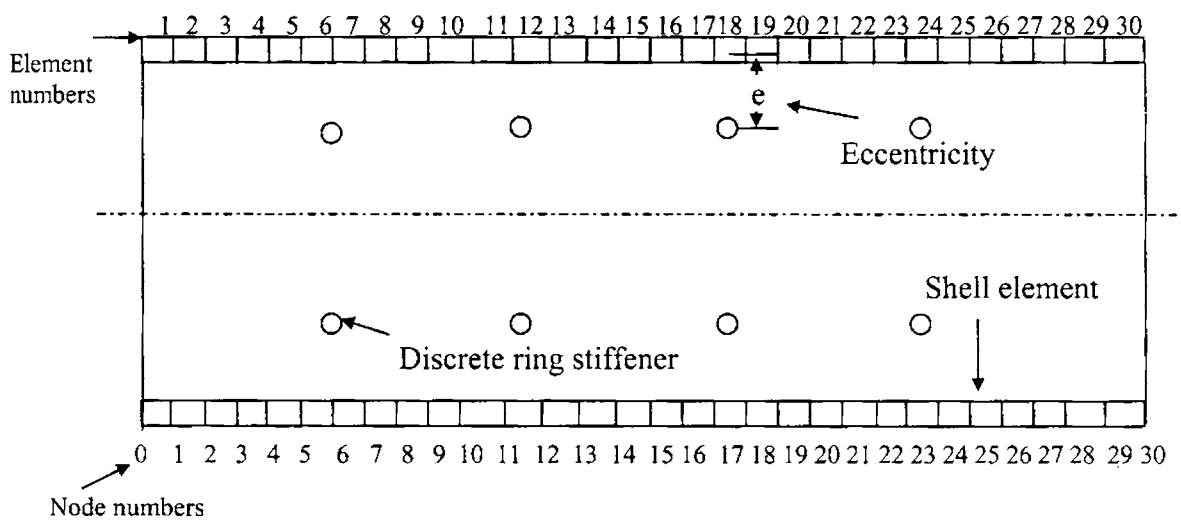

Fig. 4.3c Finite element model of BMP3

Linear buckling analysis has been carried out for stiffened cylindrical hull of attack submarines designated as M1 and M2. Design specifications, geometry etc., are described in tables 3.1 and 3.2 and in figs. 3.6a, 3.6b, 3.7a and 3.7b. Analysis has been carried out for the three configurations viz., cylindrical shell between stiffeners (interstiffener), stiffened cylindrical shell between deepframes (interdeepframe) and stiffened cylindrical shell between bulkheads (interbulkhead). The shell is considered to be attached to the stiffeners, deepframes or bulkheads as the case may be. The scope of the numerical investigation has been extended to realize the influence of possible boundary conditions. The follower force effect of hydrostatic pressure is also investigated for M1 and M2 for the three configurations and the three boundary conditions already considered for radial load case.

4.6 RESULTS AND DISCUSSION

4.6.1 Interstiffener Buckling Analysis of BMP2

The buckling pressure is evaluated from the linear buckling analysis of BMP2 using determinant search procedure explained in subsection 4.2.4. The determinant search procedure is carried out for various values of n for each case studied. A typical determinant Vs buckling pressure for s.s-s.s boundary condition for BMP2 with circumferential wave number 12 is shown in the fig. 4.4. The value of the pressure corresponding to zero determinant gives the buckling pressure (765 psi).

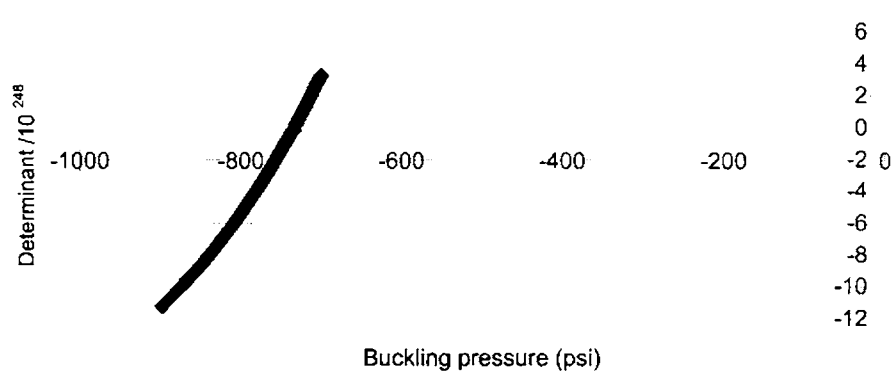

Fig. 4.4 Determinant Vs buckling pressure of BMP2 for interstiffener linear buckling analysis for s.s-s.s boundary condition for minimum buckling pressure with circumferential wave no. 12

The buckling pressure has been evaluated from the linear buckling analysis of BMP2 for s.s-s.s, c-c and f-f boundary conditions. The convergence study has been conducted by choosing finite element model with 6, 12,18 and 24 elements. Linear buckling pressure for three above mentioned boundary conditions and for finite element models are shown in table 4.1.

Table 4.1 Linear interstiffener buckling pressures of BMP2 for various boundary conditions and finite element models

Circumferential wave no. (n)	Buckling pressure (psi)							
	Boundary conditions							
	s.s-s.s				c-c		f-f	
	No. of elements				No. of elements		No. of elements	
	6	12	18	24	18	24	18	24
9	1292	1104	1048	1028	1598	1572	1682	1662
10	1044	928	892	879	1412	1397	1468	1456
11	900	833	808	799	1290	1280	1372	1362
12	828	789	**765**	**765**	1211	1210	1262	1262
13	804	781	766	766	1174	1174	1219	1219
14	812	799	788	788	**1163**	**1163**	**1202**	**1202**
15	844	835	828	826	1175	1173	1207	1205
16	892	883	876	876	1200	1199	1227	1225
17	952	942	932	932	1339	1237	1262	1260

The minimum buckling pressures and corresponding n values are given in bold. The minimum buckling pressures are 765 psi (n=12), 1163 psi (n=14) and 1202 psi (n=14) for s.s-s.s, c-c and f-f boundary conditions. For s.s-s.s boundary condition, the buckling pressure converges to 765 psi. The reference value for this case is 749 psi (table 4.2) as reported by Kendrick (1970). On analyzing the influence of end restraints it is observed that there is an increase in buckling pressure by 57% for f-f boundary condition and 52% for c-c boundary condition.

The variation of critical buckling pressure Pcr against circumferential wave number (n) for the three boundary conditions are shown in fig. 4.5.

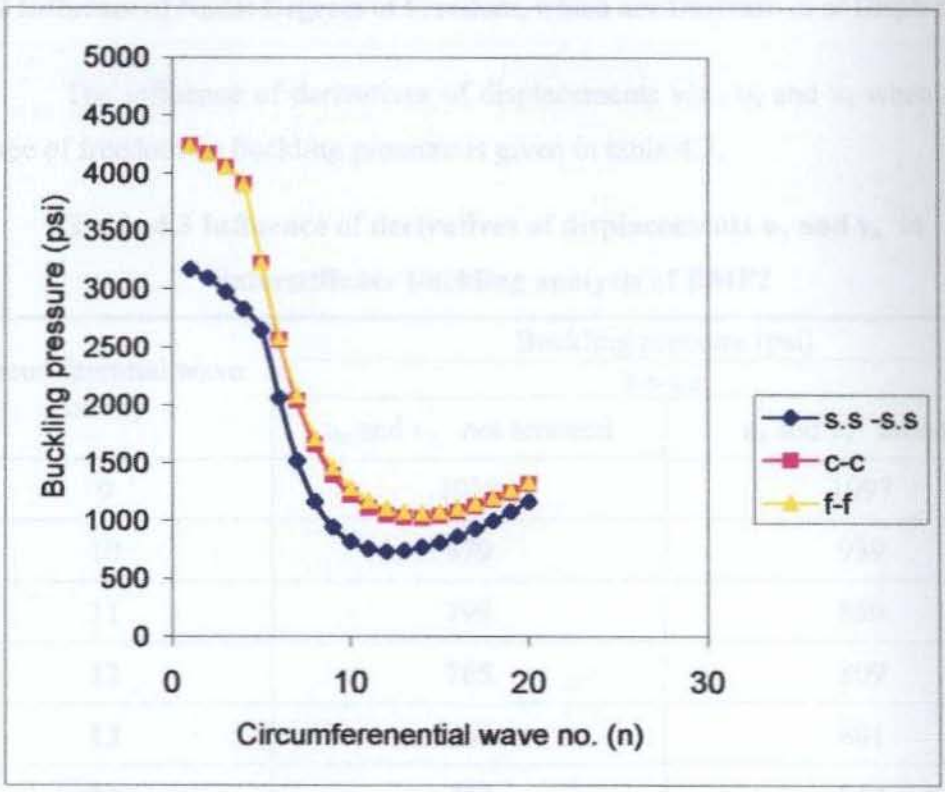

Fig. 4.5 Interstiffener linear buckling pressures of BMP2 for various boundary conditions

The comparison of the buckling pressure predicted by the authoress with those predicted by Kendrick and von Mises (1970) is shown in table 4.2.

Table 4.2 Comparison with Kendrick's and von Mises' results for BMP2

Circumferential wave no. (n)	Buckling pressure (psi)		
	Kendrick's results	von Mises' results	Obtained results
10	841	843	879
11			799
12	**749**	**751**	**765**
13	753	755	766

For s.s-s.s.s boundary condition the buckling pressure is higher by 2.1% than Kendrick's and 1.9% than von Mises' results. But in all cases the minimum buckling pressure occurs at a circumferential wave no.12. The results prove the adaptability of the program for linear buckling analysis.

4.6.2 Influence of Nodal Degrees of Freedom, which are Derivatives of Displacements

The influence of derivatives of displacements viz., u_x and v_x when used as degree of freedom on buckling pressure is given in table 4.3.

Table 4.3 Influence of derivatives of displacements u_x and v_x in interstiffener buckling analysis of BMP2

Circumferential wave no.(n)	Buckling pressure (psi)	
	s.s-s.s	
	u_x and v_x not arrested	u_x and v_x arrested
9	1028	1097
10	879	939
11	799	850
12	**765**	809
13	766	**801**
14	788	818
15	826	856
16	876	898
17	932	946

On arresting the derivatives u_x and v_x at the supports, the linear buckling pressure has increased from 765 psi (n=12) to 801 psi (n=13) showing 4.7% increase.

4.6.3 Analysis of Stiffened Cylindrical Shell of BMP3

Table 4.4 gives the variation of buckling pressure for general instability analysis of BMP3 for various circumferential wave numbers for s.s-s.s, c–c and f–f boundary conditions. The minimum buckling pressures and corresponding n values are given in bold. The variations of buckling pressure against n for three boundary conditions are given fig. 4.6.

Table 4.4 Linear buckling pressures of BMP3 for various boundary conditions

Circumferential waves no. (n)	Buckling pressure (psi)		
	s.s-s.s	c-c	f-f
1	3731	3791	3791
2	3645	3709	3709
3	3443	3505	3527
4	3255	3285	3329
5	2949	2987	3003
6	2525	2529	2529
7	2069	2091	2091
8	1729	1765	1765
9	1493	1535	1535
10	1339	1383	1383
11	1247	1291	1291
12	1203	1243	1245
13	**1193**	**1231**	**1233**
14	1211	1247	1247
15	1251	1281	1283
16	1305	1333	1335

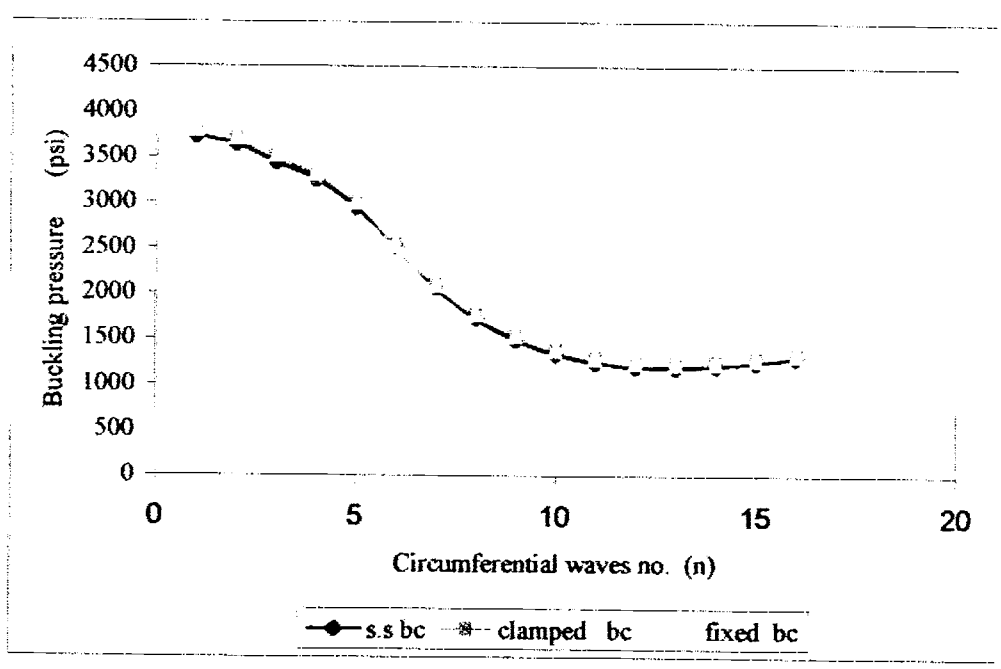

Fig. 4.6 Linear buckling pressures of BMP3 for various boundary conditions

The critical buckling pressures are obtained as 1193 psi, 1231 psi and 1233 psi for circumferential wave no. 13 for all the three boundary conditions studied.

The buckling pressure for f-f boundary condition is 3.2% and c-c boundary condition is 3.1% more than s.s-s.s boundary condition. These results are compared with the values published by Kendrick [1970] and with values obtained using Bryant's formula [Rajagopalan1993] in table 4.5.

Table 4.5 Comparison with Kendrick's and Bryant's results for BMP3

Circumferential wave no. (n)	Buckling pressure (psi)		
n	Bryant's formula	Kendrick's results	Obtained results
2	16399	4596	3645
3	4748	3996	3443
4	**3785**	**3401**	3255
5	5019	3518	2949
6	7043	3214	2525
7	9568	2924	2069
8	12524	2676	1819
9			1493
10			1339
11			1247
12			1203
13			**1193**
14			1211
15			1251
16			1305

Kendrick's and Bryant's results are having a local minimum at n=4 referring to the general instability mode i.e. one lobe in longitudinal direction. It implies that for a given L/R ratio there exists a value of n, which gives the minimum buckling pressure in the general instability mode. Kendrick's results has a tendency to decline after n=5. The results are available only up to n=8. The authoress' results are declining continuously and reaches the minimum value at n=13. The higher values of n refer to the interframe buckling mode with as many longitudinal lobes as frame spaces. There exists a value of n, for which the collapse pressure in the interframe mode is minimum.

4.6.4 Interstiffener Buckling Analysis of Submarine Models

Interstiffener buckling values for M1 for various n values are shown in table 4.6 and shown in fig. 4.7.

Table 4.6 Interstiffener linear buckling pressures for M1 for various boundary conditions

Circumferential wave no. (n)	Buckling pressure (N/mm^2)		
	f-f	c-c	s.s-s.s
1	65.962	65.660	20.540
2	65.562	65.260	20.240
3	64.881	64.640	19.980
4	63.971	63.780	19.640
5	62.723	62.720	19.240
6	61.622	61.500	18.820
7	60.282	60.140	18.360
8	58.764	58.701	17.960
9	57.231	57.181	17.540
10	55.682	55.642	17.100
11	54.162	54.121	16.880
12	52.622	52.602	16.640
13	51.211	51.160	16.470
14	49.799	49.760	16.400
15	48.499	48.460	16.380
16	47.261	47.220	**16.380**
17	46.142	46.100	16.460
18	45.122	45.081	16.620
19	44.201	44.165	16.840
20	43.381	43.344	17.120
21	42.780	42.736	17.412
22	42.060	42.011	18.288
23	41.661	41.601	18.764
24	41.261	41.201	
25	40.761	40.721	
26	40.522	40.482	
27	40.420	40.380	
28	40.366	40.300	
29	40.332	40.286	
30	**40.330**	**40.283**	
31	40.380	40.341	
32	40.622	40.460	
33	40.930	40.650	
34	41.300	40.990	
35	41.620	41.340	
35	42.102	41.830	
37	42.582	42.270	
38	43.122	42.770	
39	43.822	43.410	
40	44.38	43.970	

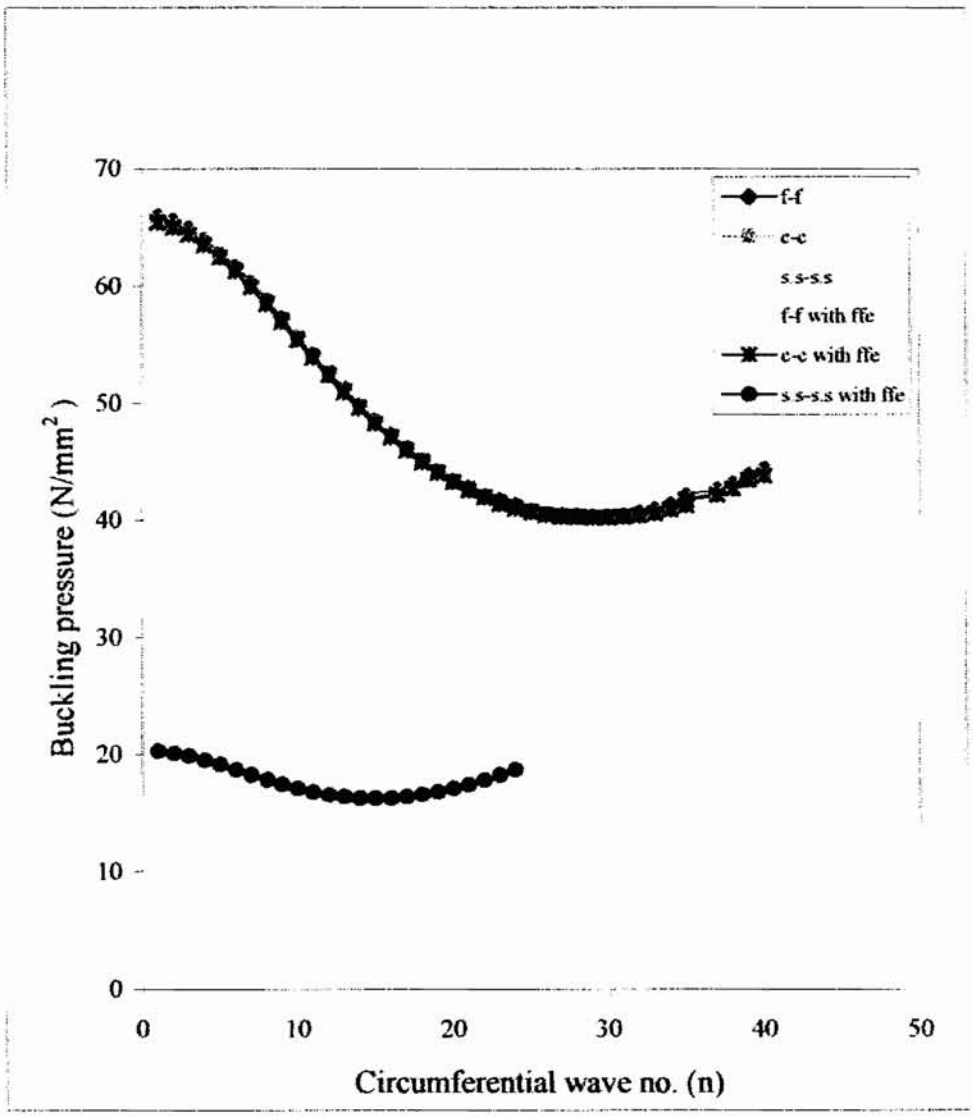

Fig. 4.7 Interstiffener linear buckling pressures for M1 for various boundary conditions with and without follower force effect

The buckling pressures for f-f, c-c and s.s-s.s boundary conditions have been obtained as 40.330 N/mm^2 (n = 30), 40.283 N/mm^2 (n=30) and 16.380 N/mm^2 (n= 16) respectively. The interstiffener buckling pressure values for M2 for various n values are shown in table 4.7. Variation of Pcr with n is shown in fig. 4.8.

Table 4.7 Interstiffener linear buckling pressures of M2 for various boundary conditions

Circumferential wave no. (n)	Buckling pressure (N/mm^2)		
	f-f	c-c	s.s-s.s
1	31.762	31.262	17.042
2	30.960	30.514	16.710
3	30.150	29.820	16.352
4	29.262	28.922	15.940
5	28.034	27.862	15.420
6	26.780	26.716	14.920
7	25.552	25.489	14.360
8	24.262	24.240	13.840
9	23.062	23.026	13.369
10	21.922	21.877	12.940
11	20.928	20.880	12.580
12	19.960	19.920	12.280
13	19.140	19.109	12.042
14	18.420	18.360	11.860
15	17.820	17.745	11.740
16	17.300	17.225	**11.660**
17	16.884	16.783	11.660
18	16.580	16.458	11.680
19	16.160	16.103	11.740
20	16.020	15.980	11.860
21	**15.980**	**15.880**	12.042
22	16.000	15.940	12.182
23	16.244	16.183	12.422
24	16.480	16.280	12.72

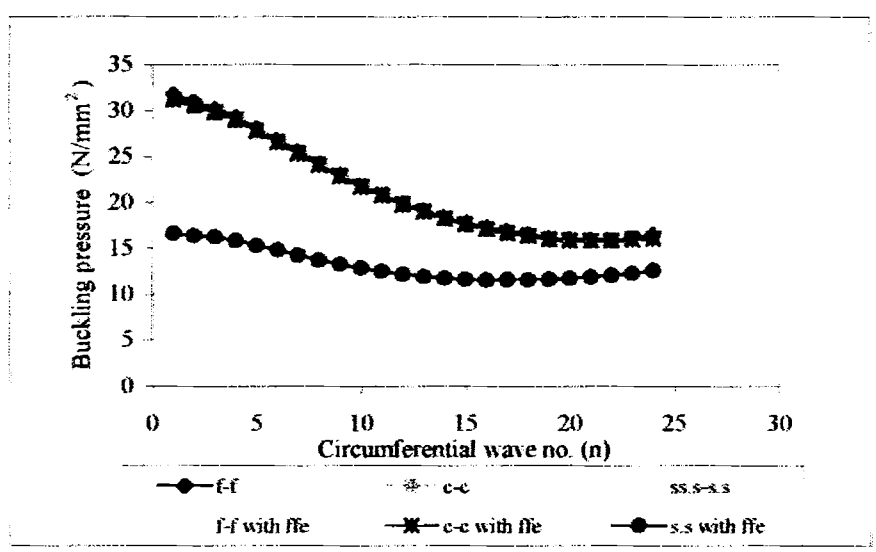

Fig. 4.8 Interstiffener buckling pressures for M2 for various boundary conditions with and without follower force effect

The buckling pressures for f-f, c-c and s.s-s.s boundary conditions have been obtained as 15.980 N/mm^2 (n=21), 15.880 N/mm^2 (n=21) and 11.660 N/mm^2 (n = 16) respectively.

Percentage reduction in linear buckling pressure value for change in end condition from rotation restraint (f-f and c-c) to s.s-s.s is 60 for M1 and 30 for M2. The influence of axial restraint (u) is negligible. The reduction in buckling pressure is less than 1% from f-f to c-c boundary condition for M1 and M2.

From the above observations it can be concluded that for s.s-s.s, the interstiffener buckling pressure is the lowest and collapse occurs at lower value of n compared to c-c and f-f boundary conditions. The collapse pressure predicted for fixed boundary condition is the highest and is at a higher value of n. Fixity at the ends reduces the effective length and the shell in effect becomes shorter and buckles at a higher pressure and at higher circumferential wave number.

The effect of L/R ratio on buckling pressure and on circumferential wave number is more pronounced with end restraints. Here L/R ratios for interstiffener portions for M1 and M2 are 0.14 and 0.19 respectively. The observation that the circumferential wave number is inversely proportional to L/R ratio (Windenburg and Trilling, 1934) is reflected in the results of the present study.

From M1 to M2, as L/R ratio changes from 0. 14 to 0.19 and R/t ratio from 113 to 128, there is a reduction in collapse pressure by 60% for rotation restraint and 30% for s.s-s.s cases.

Both M1 and M2 are designed for diving depth of 300m. Among M1 and M2, M1, which is shorter and thicker, buckles at a higher pressure compared to M2. These interstiffener buckling pressures indicate a factor of safety of 13.4 and 5.4 for end restraint and simply supported conditions for M1. The corresponding values are 5.3 and 3.8 for M2.

4.6.5 Interdeepframe Buckling Analysis of Submarine Models

Linear buckling analysis of stiffened cylindrical shell portion between deepframes is conducted for M1 and M2. The buckling pressure values for M1 for

various n values are given in table 4.8. The critical values are shown in bold. The variation of Pcr with n is shown in fig. 4.9.

Table 4.8 Interdeepframe linear buckling pressures for M1 for various boundary conditions

Circumferential wave no. (n)	Buckling pressure (N/mm^2)		
	f-f	c-c	s,s-s,s
1	28.280	28.260	22.540
2	27.520	27.506	22.400
3	27.020	27.060	22.380
4	26.820	26.810	22.260
5	26.660	26.642	22.040
6	26.360	26.340	22.000
7	26.060	25.988	21.866
8	25.640	25.630	21.762
9	25.310	25.302	21.664
10	24.980	24.972	21.604
11	24.730	24.726	21.588
12	24.530	24.528	**21.584**
13	24.380	24.373	21.640
14	24.280	24.272	21.780
15	24.250	24.242	21.980
16	**24.242**	**24.240**	22.120
17	24.320	24.310	22.360
18	24.380	24.360	22.640
19	24.570	24.550	22.780

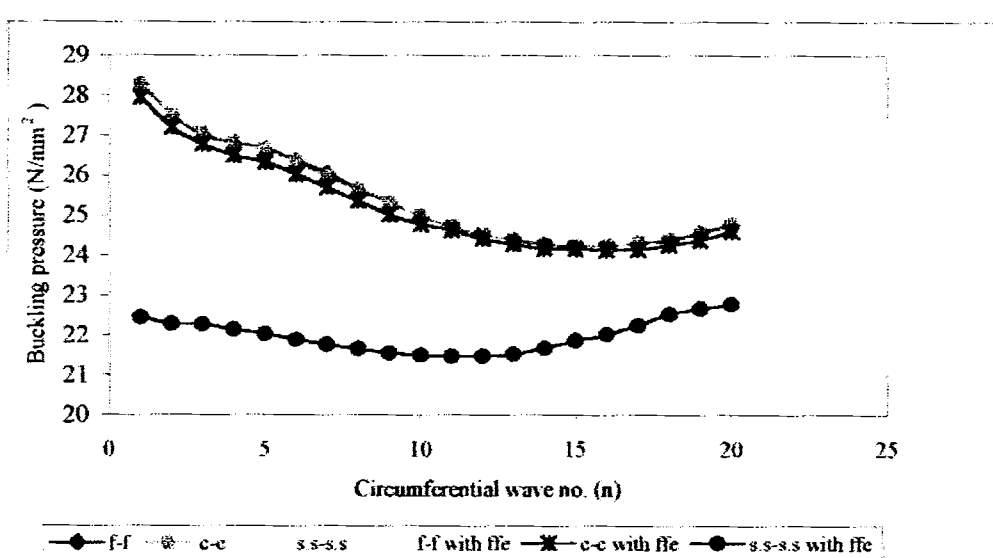

Fig. 4.9 Interdeepframe linear buckling pressures for M1 for various boundary conditions

The collapse pressure values are 24.242 N/mm^2 (n =16) for f-f, 24.240 N/mm^2 (n=16) for c-c and 21.584 N/mm^2 (n=12) for s.s-s.s boundary conditions for M1.

For M2 the buckling pressure values for various n values are shown in table 4.9. Variation of Pcr with n is shown in fig. 4.10.

Table 4.9 Interdeepframe linear buckling pressures for M2 for various boundary conditions.

Circumferential wave no. (n)	Buckling pressure (N/mm^2)		
	f-f	c-c	s,s-s,s
1	18.280	18.260	16.330
2	17.930	17.920	15.980
3	17.368	17.360	15.030
4	16.882	16.860	15.580
5	16.242	16.220	14.020
6	15.542	15.520	13.380
7	14.860	14.840	13.080
8	14.240	14.220	12.680
9	13.640	13.620	12.320
10	13.140	13.120	11.960
11	12.710	12.680	11.680
12	13.364	12.340	11.380
13	12.090	12.060	11.210
14	11.868	11.840	11.090
15	11.780	11.752	11.040
16	11.730	11.710	**10.990**
17	**11.660**	**11.610**	11.020
18	11.690	11.660	11.120
19	11.810	11.780	11.320
20	11.950	11.900	11.520

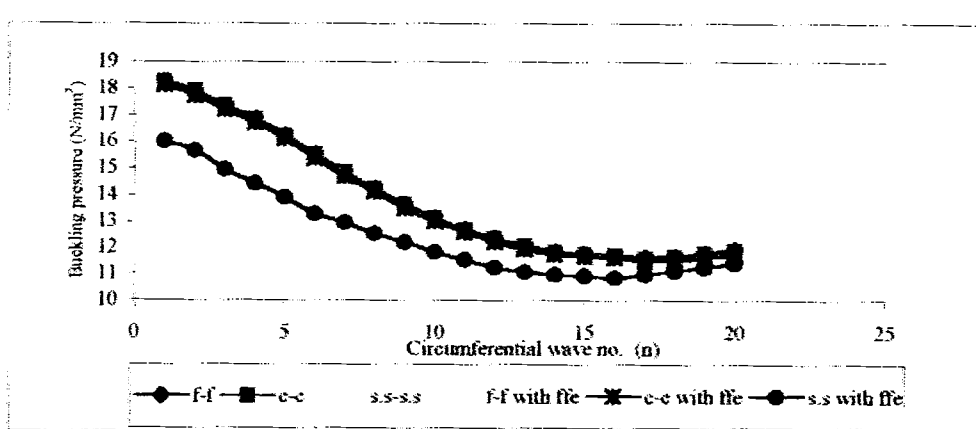

Fig. 4.10 Interdeepframe linear buckling pressures for M2 for various boundary conditions

The collapse pressure values for M2 are 11.660 N/mm^2 (n = 17), 11.610 N/mm^2 (n = 17) and 10.990 N/mm^2 (n= 16) respectively.

Percentage reduction in linear buckling pressure value for change in end condition from rotation restraint (f-f and c-c) to s.s-s.s is 11 for M1 and 6 for M2. The buckling pressure is not much influenced by axial restraint (u) and the change in buckling pressure by the release of axial restraint is negligibly small.

It is observed that the linear buckling pressures for interdeepframe configuration are less susceptible to boundary conditions compared to interstiffener buckling pressures.

The shell between deepframes can be considered as a short shell having L/R ratio 0.43 and 0.57 for M1 and M2 respectively. The various factors influencing the interdeepframe linear buckling pressure are L/R and R/t ratios of the shell as well as the strength and spacing of stiffeners between deepframes. The observation is that there is a reduction in buckling pressure by 50% irrespective of the type of boundary condition.

4. 6.6 Interbulkhead Buckling Analysis of Submarine Models

The buckling pressure values for M1 for various n values are shown in table 4.10. The critical values are shown in bold. Variation of Pcr with n is shown in fig. 4.11.

Table 4.10 Interbulkhead buckling pressures of stiffened cylindrical shell for M1 for various boundary conditions

Circumferential waves no. (n)	Buckling pressure (N/mm^2)		
	f-f	c-c	s.s-s.s
1	19.724	19.720	10.696
2	**15.226**	**10.194**	**10.146**
3	16.090	16.084	16.080
4	17.694	17.688	17.682
5	20.492	20.488	20.482
6	22.992	22.986	22.980
7	23.872	23.868	23.860
8	24.320	24.312	24.306
9	24.636	24.628	24.622
10	24.818	24.838	24.804
11	24.816	24.581	24.802
12	25.436	25.430	25.424
13	25.690	25.684	25.680
14	25.990	25.986	25.982
15	26.310	26.306	26.304
16	26.650	26.646	26.642

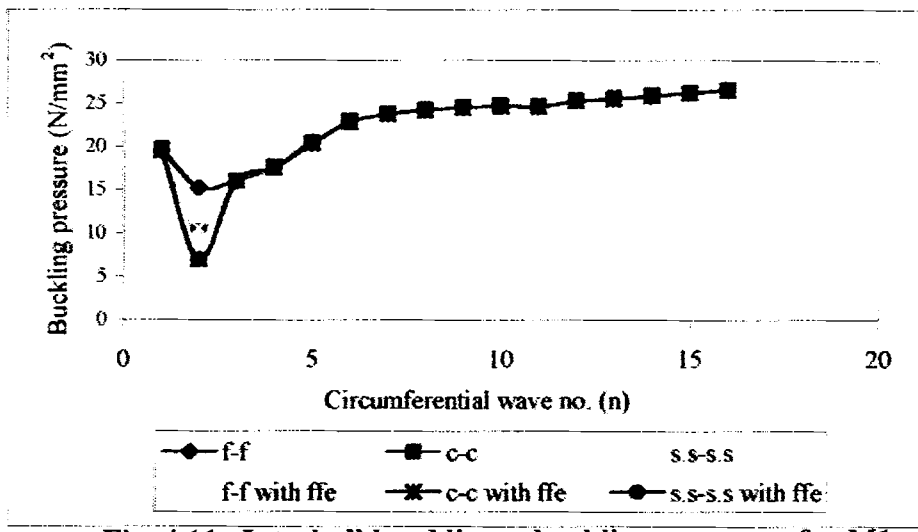

Fig. 4.11 Interbulkhead linear buckling pressures for M1 for various boundary conditions

The buckling pressure values for M2 for various n values are given in table 4.12. The variation of Pcr with n is shown in fig. 4.12.

Table 4.11 Interbulkhead buckling pressures of stiffened cylindrical shell for M2 for various boundary conditions

Circumferential wave no. (n)	Buckling pressure (N/mm^2)		
	f-f	c-c	s.s-s.s
1	10.062	10.058	10.044
2	**7.150**	**6.740**	**6.510**
3	7.740	7.150	7.120
4	10.068	10.064	10.062
5	13.984	13.982	13.980
6	14.906	14.902	14.900
7	14.902	13.998	13.994
8	14.726	14.722	14.720
9	14.548	14.544	14.542
10	14.446	14.444	14.442
11	14.422	14.418	14.416
12	14.486	14.482	14.478
13	14.602	14.598	14.596
14	14.806	14.802	14.798
15	15.006	15.002	15.000
16	15.340	15.336	15.334
17	15.706	15.702	15.698

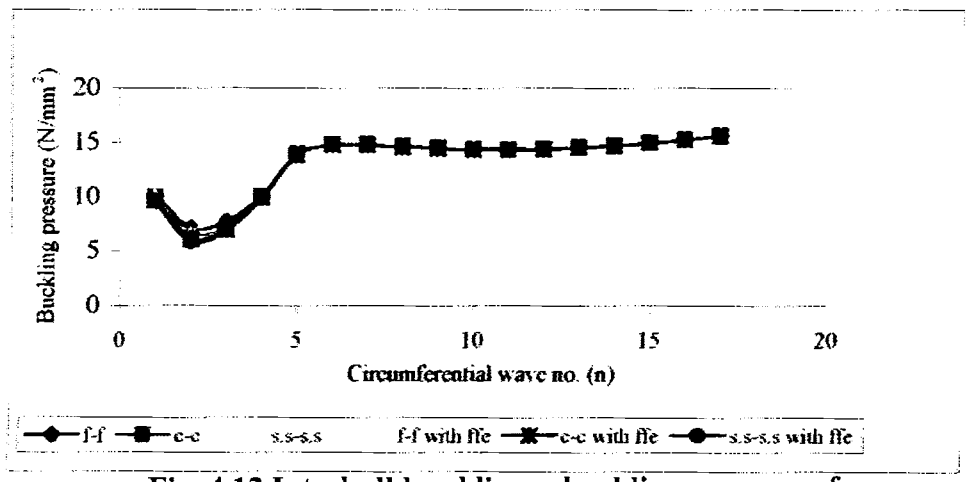

Fig. 4.12 Interbulkhead linear buckling pressures for M2 for various boundary conditions

The buckling pressure values are 15.226 N/mm^2, 10.194 N/mm^2 and 10.146 N/mm^2 (all for n=2) for M1 and 7.150 N/mm^2, 6.740 N/mm^2 and 6.510 N/mm^2 (all for n=2) for M2 for f-f, c-c and s.s-s.s boundary conditions. On considering the shell between bulkheads, which is comparatively a long shell (L/R ratio is 3.42 for M1 and 4.59 for M2) the shell buckles in bending mode with n=2. The cylinders collapse in an overall manner. The general instability failure occurs at a circumferential wave number 2. Thereafter the buckling pressure increases and apparently reaches a maximum value and decline again to give a second local minimum at a harmonic number of 12 or 13 depending upon the boundary conditions.

Percentage reduction in linear buckling pressure value for change in end condition from rotation restraint (c-c) to s.s-s.s is less than 1 and 3 for M1 and M2. But there is a considerable reduction in buckling pressure due to the release of axial restraint (u). The reduction of buckling pressure is 33% for M1 and 6% for M2. The observation, made by Brush and Almroth (1975) that for general instability failure the rotational restraint ($w_x = 0$) is less influential than axial restraint (u=0) is reflected in this work. Collapse pressure values for M1 & M2 are 10.146 N/mm^2 and 6.510 N/mm^2 respectively and occur at n=2.

For linear buckling analysis, the buckling pressure is critical on considering the interbulkhead configuration for simply supported boundary condition.

4.6.7 Follower Force Effect of Hydrostatic Pressure

Interstiffener buckling pressure values for M1, for various n values, with follower force effect incorporated, are shown in table 4.12. The minimum buckling

pressures and corresponding n values are given in bold. Variation of Pcr with n is shown in fig. 4.7. The corresponding values for M2 are given in table 4.13 and is shown in fig. 4.8.

Table 4.12 Interstiffener linear buckling pressures for M1 for various boundary conditions with follower force effect

Circumferential wave no. (n)	Buckling pressure (N/mm^2)		
	f-f	c-c	s.s-s.s
1	65.760	65.426	20.280
2	65.362	65.026	20.120
3	64.681	64.360	19.860
4	63.781	63.520	19.520
5	62.683	62.460	19.120
6	61.422	61.250	18.700
7	60.020	59.902	18.260
8	58.540	58.471	17.842
9	57.021	56.971	17.441
10	55.462	55.422	17.082
11	53.920	53.881	16.780
12	52.422	52.382	16.562
13	50.981	50.940	16.380
14	49.601	49.560	16.280
15	48.300	48.260	16.260
16	47.100	47.060	**16.260**
17	45.982	45.940	16.402
18	44.982	44.941	16.580
19	44.061	44.025	16.802
20	43.260	43.220	17.063
21	42.560	42.520	17.404
22	41.940	41.901	17.780
23	41.421	41.381	18.220
24	41.001	40.961	18.700
25	40.681	40.641	
26	40.442	40.402	
27	40.339	40.298	
28	40.280	40.240	
29	40.252	40.202	
30	**40.248**	**40.202**	
31	40.380	40.311	
32	40.582	40.360	
33	40.840	40.550	
34	41.160	40.900	
35	41.540	41.240	
35	41.982	41.730	
37	42.482	42.140	
38	43.042	42.670	
39	43.642	43.410	
40	44.080	43.810	

Table 4.13 Interstiffener linear buckling pressures for M2 for various boundary conditions with follower force effect

Circumferential wave no. (n)	Buckling pressure (N/mm^2)		
	f-f	c-c	s.s-s.s
1	31.260	31.220	16.640
2	30.560	30.490	16.392
3	29.850	29.770	16.281
4	29.062	29.000	15.869
5	27.879	27.800	15.351
6	26.600	26.523	14.870
7	25.402	25.342	13.305
8	24.132	24.069	13.780
9	22.900	22.831	13.302
10	21.780	21.702	12.872
11	20.798	20.720	12.520
12	19.820	19.762	12.220
13	19.002	18.971	11.982
14	18.304	18.259	11.800
15	17.687	17.619	11.681
16	17.167	17.107	**11.600**
17	16.735	16.685	11.620
18	16.440	16.391	11.640
19	16.027	15.97	11.680
20	15.90	15.859	11.800
21	**15.92**	**15.830**	11.940
22	15.91	15.860	12.102
23	16.068	15.990	12.342
24	16.1612	16.1002	12.640

Buckling pressures for f-f, c-c and s.s-s.s boundary conditions for M1 has been obtained as 40.428 N/mm^2 (n=30), 40.202 N/mm^2 (n=30) and 16.260 N/mm^2 (n=16) respectively.

And the corresponding values for M2 have been obtained as 15.920 N/mm^2 (n= 21), 15.830 N/mm^2 (n =21) and 11.600 N/mm^2 (n = 16) respectively.

The effect of follower force on linear buckling of M1 and M2 are given in table 4.14 and 4.15 respectively.

Table 4.14 Effect of follower force on interstiffener minimum linear buckling pressures of M1

Boundary condition	Buckling pressure (N/mm^2) & (n)		% reduction
	Without follower force effect	With follower force effect	
f–f	40.330(30)	40.248(30)	0.2
c- c	40.283(30)	40.202(30)	0.2
s.s – s.s	16.380(16)	16.260(16)	0.7

Table 4.15 Effect of follower force on minimum linear buckling pressures of M2

Boundary condition	Buckling pressure (N/mm^2)& (n)		% reduction
	Without follower force effect	With follower force effect	
f–f	15.980(21)	15.920(21)	0.4
c- c	15.880(21)	15.830(21)	0.3
s.s – s.s	11.660(16)	11.600(16)	0.5

The reduction in buckling pressures are 0.2%, 0.2% and 0.7% for M1 and 0.4%, 0.3% and 0.5% for M2 for f-f, c-c and s.s-s.s boundary conditions respectively. It is obvious from the results that for interstiffener buckling, where the shell buckles with large number of waves in circumferential direction, the influence of follower force effect is very much limited.

Interdeepframe buckling pressure values for M1 for various n values are given in table 4.16. The minimum buckling pressures and corresponding n values are given in bold. Variation of Pcr with n is shown in fig. 4.9.

Table 4.16 Interdeepframe linear buckling pressures for M1 for various boundary conditions

Circumferential wave no. (n)	Buckling pressure (N/mm^2)		
	f-f	c-c	s.s-s.s
1	27.980	27.952	22.460
2	27.224	27.194	22.298
3	26.804	26.782	22.288
4	26.502	26.498	22.158
5	26.352	26.334	21.924
6	26.042	26.024	22.898
7	25.710	25.696	21.768
8	25.332	25.310	21.664
9	25.220	25.210	21.566
10	24.902	24.894	21.506
11	24.640	24.636	21.484
12	24.420	24.416	**21.482**
13	24.280	24.278	21.542
14	24.182	24.180	21.680
15	24.162	24.160	21.878
16	**24.144**	**24.144**	22.024
17	24.160	24.152	22.258
18	24.270	24.263	22.532
19	24.390	24.381	22.676
20	24.610	24.600	22.788

Buckling pressures for f-f, c-c and s.s-s.s boundary conditions for M1 has been obtained as 24.144 N/mm^2 (n=16), 24.144 N/mm^2 (n=16) and 21.482 N/mm^2 (n=12) respectively.

Interdeepframe buckling pressure values for M2 for various n values are givenn in table 4.17. The minimum buckling pressures and corresponding n values are given in bold. Variation of Pcr with n is shown in fig. 4.10.

Table 4.17 Interdeepframe linear buckling pressures for M2 for various boundary conditions

Circumferential wave no. (n)	Buckling pressure (N/mm^2)		
	f-f	c-c	s.s-s.s
1	18.150	18.132	16.014
2	17.750	17.734	15.850
3	17.230	17.212	14.908
4	16.730	16.708	14.434
5	16.150	16.114	13.902
6	15.410	15.380	13.250
7	14.720	14.692	12.950
8	14.150	14.118	12.530
9	13.520	13.480	12.202
10	13.032	13.000	11.840
11	12.618	12.580	11.530
12	12.250	12.216	11.250
13	11.980	11.940	11.089
14	11.780	11.742	10.974
15	11.700	11.670	10.930
16	11.670	11.624	**10.860**
17	**11.538**	**11.500**	10.980
18	11.550	11.520	11.120
19	11.660	11.620	11.250
20	11.786	11.742	11.408

Buckling pressures for f-f, c-c and s.s-s.s boundary conditions for M2 has been obtained as 11.538 N/mm^2 (n=17), 11.500 N/mm^2 (n=17) and 10.860 N/mm^2 (n= 16) respectively.

The effect of follower force on interdeepframe linear buckling pressures of M1 and M2 is given in table 4.18 and table 4.19 respectively.

Table 4.18 Effect of follower force on interdeepframe minimum linear buckling pressures of M1

Boundary condition	Buckling pressure (N/mm^2) & (n)		% reduction
	Without follower force effect	With follower force effect	
f–f	24.242(16)	24.144(16)	0.4
c- c	24.240(16)	24.144(16)	0.4
s.s – s.s	21.584(12)	21.482(12)	0.5

Table 4.19 Effect of follower force on interdeepframe minimum linear buckling pressures of M2

Boundary condition	Buckling pressure (N/mm^2) & (n)		% reduction
	Without follower force effect	With follower force effect	
f–f	11.660(17)	11.538(17)	1.0
c- c	11.610(17)	11.500(17)	1.0
s.s – s.s	10.990(16)	10.860(16)	1.1

There is a reduction in buckling pressure by 0.4%, 0.4% and 0.5% for M1 and 1.0% 1.0% and 1.1% for M2 for f-f, c-c and s.s-s.s boundary conditions. The follower force effect is negligible since the shell is a short one and buckles with more number of circumferential waves.

Interbulkhead buckling pressure values for M1 for various n values are given in table 4.20. The minimum buckling pressures and corresponding n values are given in bold. Variation of buckling pressure with n is shown in fig. 4.11.

For M2 the buckling pressure values for various n values are given in table 4.21. The critical values are shown in bold. Variation of Pcr with n is shown in fig. 4.12.

Table 4.20 Interbulkhead linear buckling pressures for M1 for various boundary conditions

Circumferential wave no.(n)	Buckling pressure (N/mm^2)		
	f-f	c-c	s.s-s.s
1	19.570	19.566	19.562
2	**10.582**	**6.986**	**6.944**
3	15.996	15.992	15.986
4	17.556	17.552	17.548
5	20.352	20.348	20.342
6	22.858	22.854	22.848
7	23.732	23.728	23.722
8	24.176	24.170	24.164
9	24.516	24.510	24.506
10	24.676	24.672	24.664
11	24.638	24.632	24.626
12	25.312	25.308	25.304
13	25.576	25.568	25.562
14	25.876	25.872	25.864
15	26.218	26.212	26.204
16	26.554	26.550	26.546

Table 4.21 Interbulkhead linear buckling pressures for M2 for various boundary conditions

Circumferential wave no. (n)	Buckling pressure (N/mm^2)		
	f-f	c-c	s.s-s.s
1	9.620	9.618	9.616
2	**6.540**	**6.160**	**5.950**
3	6.950	6.948	6.942
4	9.960	9.956	9.952
5	13.846	13.844	13.840
6	14.766	14.762	14.760
7	14.766	14.764	14.762
8	14.588	14.584	14.582
9	14.428	14.426	14.424
10	14.326	14.324	14.322
11	14.308	14.304	14.302
12	14.368	14.364	14.360
13	14.510	14.508	14.506
14	14.710	14.706	14.704
15	14.968	14.964	14.962
16	15.270	15.266	15.264
17	15.588	15.584	15.578

The collapse pressure values for general instability failure are 10.582 N/mm^2, 6.986 N/mm^2 and 6.944 N/mm^2 (all for n=2) for M1 and 6.540 N/mm^2, 6.160 N/mm^2 and 5.950 N/mm^2 (all for n=2) for M2 for f-f, c-c and s.s-s.s boundary conditions.

The effect of follower force on interbulkhead buckling of M1 and M2 are given in table 4.22 and table 4.23 respectively.

Table 4.22 Effect of follower force on interbulkhead minimum linear buckling pressures of M1

Boundary condition	Buckling pressure (N/mm^2)& (n)		% reduction
	Without follower force effect	With follower force effect	
f–f	15.226(2)	10.582(2)	30.5
c- c	10.194(2)	6.986(2)	31.5
s.s – s.s	10.146(2)	6.944(2)	31.6

Table 4.23 Effect of follower force on interbulkhead minimum linear buckling pressures of M2

Boundary condition	Buckling pressure (N/mm^2)& (n)		% reduction
	Without follower force effect	With follower force effect	
f–f	7.150(2)	6.540(2)	8.5
c- c	6.740(2)	6.160(2)	8.6
s.s – s.s	6.510(2)	5.950(2)	8.6

There are reductions in buckling pressures by 30.5%, 31.5% and 31.5% for M1 and 8.5%, 8.6% and 8.6% for M2 for f-f, c-c and s.s-s.s boundary conditions.

The follower force effect of hydrostatic pressure has very high detrimental effect in the case of general instability failure, which is the case of long shells in which shell buckles with 2 or 3 waves in the circumferential direction. The collapse pressure reduction due to pressure rotation effect is about 31% for M1 and 9% for M2.

For linear buckling analysis with follower force effect, interbulkhead buckling pressure for s.s-s.s boundary condition becomes critical. Design pressure for two submarines has been 3.016 N/mm^2 corresponding to diving depth of 300m. Subsequent safety factor is 3.364 and 2.158 for M1 and M2 respectively.

CHAPTER 5
GEOMETRIC NONLINEAR ANALYSIS

5.1 INTRODUCTION

The geometric nonlinearity arising from nonlinear strain displacement relations is considered in the present study. The follower force effect together with geometric nonlinearity is considered further.

The concept of equilibrium path plays a central role in explaining nonlinear structural analysis. An attempt is made to plot the equilibrium path for stiffened cylindrical shell under external pressure loading. Determination of equilibrium path involves elastic and geometric stiffness matrix in the deformed configuration. Deformations are computed at intermediate load levels by iterative procedure. The pressure at which the stiffness of the structure vanishes is taken as nonlinear buckling pressure

5.2 HYDROSTATIC PRESSURE AS RADIAL PRESSURE LOAD

5.2.1 Methodology

Hydrostatic pressure is considered to be radial to the undeformed cylinder and can be treated as dead load in the analysis. For this conservative loading, the equilibrium equations can be derived from the principle of stationary potential energy.

In the finite element geometric nonlinear analysis the basic problem is to develop equilibrium equations corresponding to applied loads in the deformed geometry, taking into account all nonlinearities and to seek the solution of these algebraic equations through out the complete history of load application (Bathe, 2001). Tangent stiffness matrix and the load vector are used to generate the equilibrium equation at a particular load step.

A load–control incremental-iterative procedure (Cook et al, 1989) is adopted for the geometric nonlinear analysis in the present study. In this method several

monotonically increasing load levels are required to predict the state-control response (fig. 5.1).

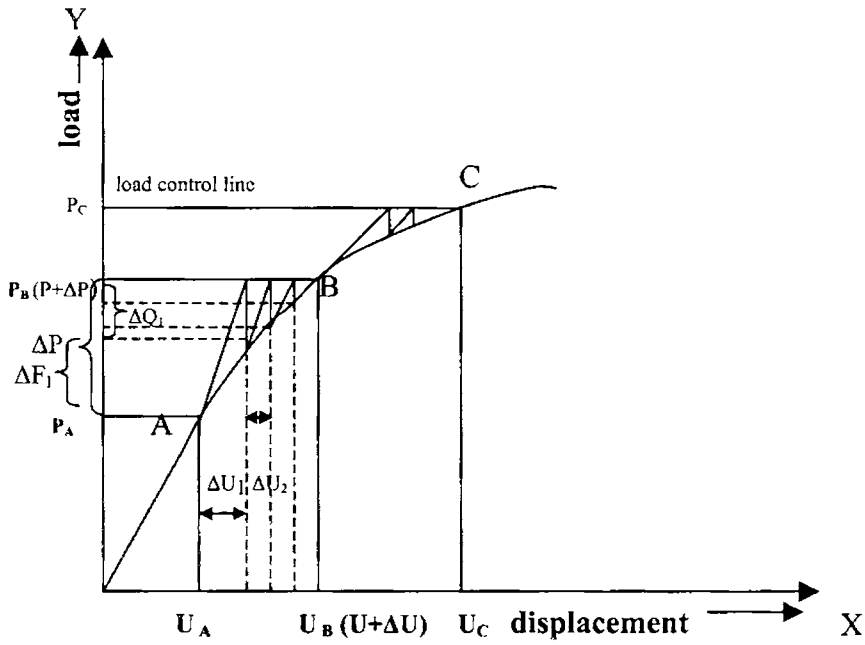

Fig. 5.1 Load control incremental - iterative procedure

The analysis starts from a linear solution and then tries to follow the behaviour of the system as actions applied to it are changed by small steps called increments. To eliminate or reduce the drifting error, the incremental step is followed by one or more iteration steps (Felippa, 1999).

Load control incremental - iterative procedure can be summarized as follows. The solution for the discrete load step P (P_A) is known and that the solution for the next load step P+ΔP (P_B) is required, where ΔP is the suitably chosen load increment. Hence for the load step P_A+ΔP the equilibrium equation relating the external nodal load and the internal forces can be written as

$$^{P+\Delta P}\{R\} - {}^{P+\Delta P}\{F\} = 0 \qquad \text{..... (5.1)}$$

Where $^{P+\Delta P}\{R\}$ is the equivalent nodal loads and $^{P+\Delta P}\{F\}$ is the resistive forces developed due to internal stresses (the left superscript denotes the load step level P+ΔP).

Since the solution is known at the level P only and ${}^{P+\Delta P}\{F\}$ cannot be computed directly, the equation is written as

$$ {}^{P+\Delta P}\{R\} - {}^{P}\{R\} = \{\Delta R\} = \{\Delta F\} \qquad \text{.....} (5.2) $$

Where $\{\Delta R\}$ is the increase in equivalent nodal loads due to increase in load level $\{\Delta P\}$and $\{\Delta F\}$ is the increment in internal nodal forces

$$ \{\Delta R\} = {}^{t}[{}^{P}K_T]\ \{\Delta U\}_1. \qquad \text{.....} (5.3) $$

where ${}^{t}[{}^{P}K_T]$ is the initial tangent stiffness matrix at the load level P and $\{\Delta U\}_1$ the displacements at the first iteration. From the Eqn. 5.3

$$ \{\Delta U\}_1 = {}^{t}[{}^{P}K_T]^{-1}\{\Delta R\} \qquad \text{.....} (5.4) $$

These displacements are transferred to the elements to get the deformed configuration.

Assuming each element to be in the new coordinate axes, which is the rotated one, the tangent stiffness matrix ${}^{t}[{}^{P+\Delta P}K_T]_1$ is calculated. The new incremental equivalent force vector, $\{\Delta F\}_1$ is calculated using the relation

$$ {}^{t}[{}^{P+\Delta P}K_T]_1\{\Delta U\}_1 = \{\Delta F\}_1 \qquad \text{.....} (5.5) $$

The difference load vector $\{\Delta Q\}_1$ is calculated at the first iterative level

$$ \{\Delta Q\}_1 = \{\Delta F\} - \{\Delta F\}_1 = \{\Delta R\} - \{\Delta F\}_1 \qquad \text{.....} (5.6) $$

and $\{\Delta Q\}_1$ is used for the recovery of the displacements $\{\Delta U\}_2$

$$ \{\Delta U\}_2 = {}^{t}[{}^{P+\Delta P}K_T]_1^{-1}\{\Delta Q\}_1 \qquad \text{.....} (5.7) $$

These displacements are further added to nodal coordinates to get the current deformed configuration and hence the new tangent stiffness matrix ${}^{t}[{}^{P+\Delta P}K_T]_2$

At the end of iteration, the solution obtained should be checked for convergence using the condition

$$\frac{\{\Delta U\}_i}{\{\Delta U\}} <= \varepsilon D \qquad \text{..... (5.8)}$$

Where εD is the displacement convergence tolerance limit.

(Since the vector $\{\Delta U\}$ is not known, it can be taken as equal to $\Sigma\{\Delta U\}_i$). This process is continued to the next incremental step (P_B to P_c).

Finite element formulation for geometric nonlinear analysis in the present study is based on corotational kinematics, which accommodates the large displacement matrix (eqn.4.3) by adjusting the element coordinates in the computation of stiffness (Zienkiewicz, 1979). It is effective in problems involving finite rotations and small strains. Besides existing small strain (linear) finite element libraries can effectively be adopted to such formulation (Crisfield, 1981).

5.2.2 Corotational Kinematics and Generation of Total Tangent Stiffness Matrix

Corotational kinematics is used to generate relevant stiffness matrices (Felippa, 1999) and is described subsequently. In corotational description the reference configuration is split up or decomposed into initial or base configuration and corotated configuration. The corotated configuration follows the element like a shadow. The total displacement of the structure is considered to be composed of rigid body and deformational displacement. Purely geometric approach is implemented for the separation of deformational displacement, which is measured with respect to corotated configuration, from the rigid body motion. Strain energy expression is based on the strains and the stresses from purely deformational displacements, expressed in terms of total displacements. Tangent stiffness is derived from this strain energy expression.

Fig. 5.2 gives the corotational motion description of the element. (Deformations are grossly exaggerated for better visibility.)

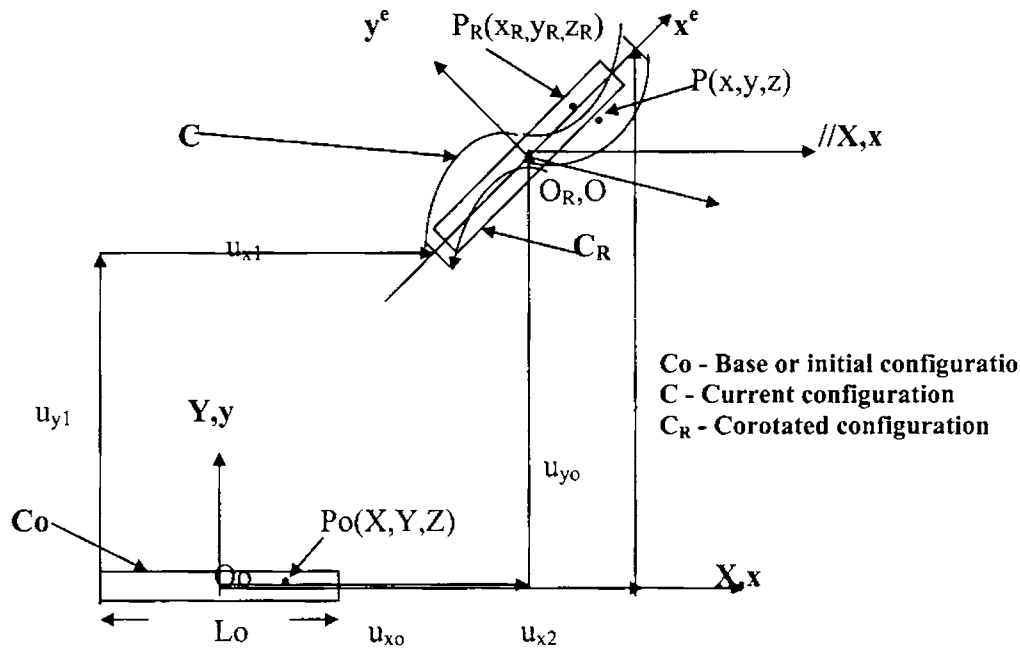

Fig. 5.2 Corotational kinematics (Felippa, 1999)

Assume that the element is in the global X-axis in the reference configuration C_o with the origin located at the mid point. The motion in the (X, Y, Z) space carries it to the current configuration C. The corotated configuration C_R follows C and occupies a symmetric position. An element coordinate system, also called the local system is denoted by (x_o^e, y_o^e,z_o^e) in the initial stage and (x^e,y^e,z^e) in the corotated stage.

This system follows the element motion so that x^e is aligned to the element longitudinal axis. In the reference configuration C_o, the element axes (x_o^e, y_o^e, z_o^e) coincide with (X, Y, Z). In the corotated configuration the element axes (x_R^e, y_R^e, z_R^e) coincide with (x^e, y^e, z^e). The figure depicts the motion of a typical particle, P_o (X, Y, Z) to P_R (x_R, y_R, z_R) in C_R and P (x, y, z) in C.

The total particle displacement in the global coordinate is

$$\{u\} = \{x - X\} = \begin{Bmatrix} x-X \\ y-Y \\ z-Z \end{Bmatrix} \qquad \text{.....(5.9)}$$

The total displacement is spilt into a rigid body displacement u_R and purely deformational displacement u

$$u = u_R + \overline{u} = (x_R - X) + (x - x_R) \qquad \text{..... (5.10)}$$

where

$$\{x_R\} = \begin{Bmatrix} x_R \\ y_R \\ z_R \end{Bmatrix} = \begin{bmatrix} l_1 & m_1 & n_1 \\ l_2 & m_2 & n_2 \\ l_3 & m_3 & n_3 \end{bmatrix}^T \begin{Bmatrix} X \\ Y \\ Z \end{Bmatrix} + \begin{Bmatrix} u_{xo} \\ u_{yo} \\ u_{zo} \end{Bmatrix} = [T_r]^T X + u_o \qquad \text{.....(5.11)}$$

where $[T_r]$ is called the coordinate rotation matrix and l, m and n are the direction cosines

$$\{x\} = \begin{Bmatrix} x \\ y \\ z \end{Bmatrix} = \begin{Bmatrix} X + u_x \\ Y + u_y \\ Z + u_z \end{Bmatrix} = X + u = [I]\, X + u \qquad \text{..... (5.12)}$$

where [I] is the unit matrix

On extracting the deformational displacement

$$\{\overline{u}\} = \begin{Bmatrix} u_x \\ u_y \\ u_z \end{Bmatrix} = \begin{Bmatrix} x - x_R \\ y - y_R \\ z \quad z_R \end{Bmatrix} = \begin{bmatrix} 1-l_1 & -l_2 & -l_3 \\ -m_2 & 1-m_2 & -m_3 \\ -n_1 & -n_2 & 1-n_3 \end{bmatrix} \begin{Bmatrix} X \\ Y \\ Z \end{Bmatrix} + \begin{Bmatrix} u_x - u_{xo} \\ u_y - u_{yo} \\ u_z - u_{zo} \end{Bmatrix} \qquad \text{.... (5.13)}$$

In the matrix form

$$\overline{u} = [I - Tr^T]\, X + u - u_o \qquad \text{..... (5.14)}$$

This can be transformed into element coordinates

$$\overline{u^e} = [T_r]\, \overline{u} = [T_r - 1]\, X + T_r (u - u_o) \qquad \text{..... (5.15)}$$

The extraction of deformational displacements is nonlinear since direction cosines are nonlinear functions of global displacements.

The strain energy can be derived from only purely deformational motion (not including the rigid body motion) using the eqn.5.15. The second variation of the energy expression of the circular cylindrical shell subjected to dead surface pressure can be utilized for the derivation of tangent stiffness matrices as suggested by Brush and Almroth (1975). Matricisation of it gives rise to element total tangent stiffness matrix in the current configuration.

$$^{t}[k_T] = \frac{\partial^2 U}{\partial u_i \partial u_j} \qquad \text{..... (5.16)}$$

The total element tangent stiffness matrix $^{t}[k_T]$ in the current configuration can be decomposed as below.

$$^{t}[k_T] = [T_R]^T [k_T][T_R] \qquad \text{..... (5.17)}$$

where $[k_T]$ is the total element tangent stiffness matrix in the previous configuration, which may be the undeformed configuration in the first iteration and is obtained by adding elastic stiffness and geometric stiffness matrices $[k]$ and $[k_G]$.

$$[k_T] = [k] + [k_G] \qquad \text{..... (5.18)}$$

$[T_R]$ is the transformation matrix and is given below as eqn.5.19.

$$T_R = \begin{pmatrix} Tr & 0 & 0 & 0 \\ 0 & Tr & 0 & 0 \\ 0 & 0 & Tr & 0 \\ 0 & 0 & 0 & Tr \end{pmatrix} \qquad \text{..... (5.19)}$$

where $[T_r]$ is called the coordinate rotation matrix explained in eqn.5.11.

The pre and post multiplication of transformation matrix, which contains trigonometric function, imparts nonlinearity to the total stiffness matrix.

5.2.3 Transformation Matrix

The transformation matrix is derived from coordinate rotation matrix, which is implicitly defined by node displacements through trigonometric relations derived from the orientation of the element with respect to global axis. The coordinate rotation matrix for the finite element considered is given as expression 5.20.

$$Tr = \begin{pmatrix} C_X & C_Y & C_Z \\ \dfrac{C_X C_Y \cos\alpha - C_Z \sin\alpha}{\sqrt{(C_X^2+C_Z^2)}} & \sqrt{(C_X^2+C_Z^2)}\cos\alpha & \dfrac{-C_Y C_Z \cos\alpha + C_X \sin\alpha}{\sqrt{(C_X^2+C_Z^2)}} \\ \dfrac{C_X C_Y \sin\alpha - C_Z \cos\alpha}{\sqrt{(C_X^2+C_Z^2)}} & -\sqrt{(C_X^2+C_Z^2)}\sin\alpha & \dfrac{-C_Y C_Z \sin\alpha + C_X \cos\alpha}{\sqrt{(C_X^2+C_Z^2)}} \end{pmatrix} \quad (5.20)$$

where

$$\left.\begin{array}{l} C_X = X_L/L,\ C_Y = Y_L/L,\ C_Z = Z_L/L \\ \text{Where} \\ L = \sqrt{(X_L^2+Y_L^2+Z_L^2)},\ L_O = \sqrt{(X_O^2+Y_O^2+Z_O^2)} \\ X_L = X_O + u_2 - u_1,\ Y_L = Y_O + v_2 - v_1,\ Z_L = Z_O + w_2 - w_1 \end{array}\right\} \quad \ldots\ldots\ldots\ldots\ldots\ldots\ldots\ldots (5.21)$$

X_O is the undeformed length of the element, L_O and Y_O and Z_O are zeroes in the undeformed configuration and changes on each iteration step accordingly.

$$\text{Sin}\ \alpha = z_{k\gamma}/\sqrt{(y^2_{k\gamma} + z^2_{k\gamma})},\ \text{Cos}\ \alpha = y_{k\gamma}/\sqrt{(y^2_{k\gamma}+z^2_{k\gamma})} \quad \ldots\ldots\ldots\ldots\ldots\ldots (5.22)$$

where $x_{k\gamma}$ $y_{k\gamma}$ and $z_{k\gamma}$ are the coordinates of the additional node chosen lying on the element principal plane with respect to the rotated system of axes (Krishnamoorty,1987).

5.2.4 Tangent Stiffness Matrix

The tangent stiffness matrix is developed using the eqn.5.17 and eqn.5.18. In the eqn.5.18 linear elastic stiffness matrix [k] is from the section 3.3 and section 3.4 and geometric stiffness matrix [k_G] from section 4.2.

5.3 FOLLOWER FORCE EFFECT OF HYDROSTATIC PRESSURE

In the geometric nonlinear analysis treating hydrostatic pressure as a follower force, the pressure stiffness matrix is to be updated in every iteration. This is implemented through modifying the conventional tangent stiffness matrix by the addition of pressure stiffness matrix.

$$[k_T] = [k] + [k_G] + [kp] \qquad \text{..... (5.23)}$$

In the expression 5.23 linear elastic stiffness matrix [k] is described in the section 3.3 and section 3.4 and geometric stiffness matrix $[k_G]$ in section 4.2 and the pressure stiffness matrix in subsection 4.3.1.

The tangent stiffness matrix in the current configuration is obtained by pre and post multiplication of the initial tangent stiffness matrix by the transformation matrix given in eqn.5.19.

$$^{t}[k_T] = [T_R]^T [k_T] [T_R] \qquad \text{..... (5.24)}$$

The methodology adopted is same as that explained in subsection 5.2.1.

5.4 SOFTWARE DEVELOPMENT

Software is developed in C language for geometric nonlinear analysis of stiffened cylindrical shell, treating hydrostatic pressure as radial and as follower force.

5.4.1 Flow Chart

The schematic diagram is given fig. 5.3a and the hierarchal order of operations is given in the flowchart (fig. 5.3b).

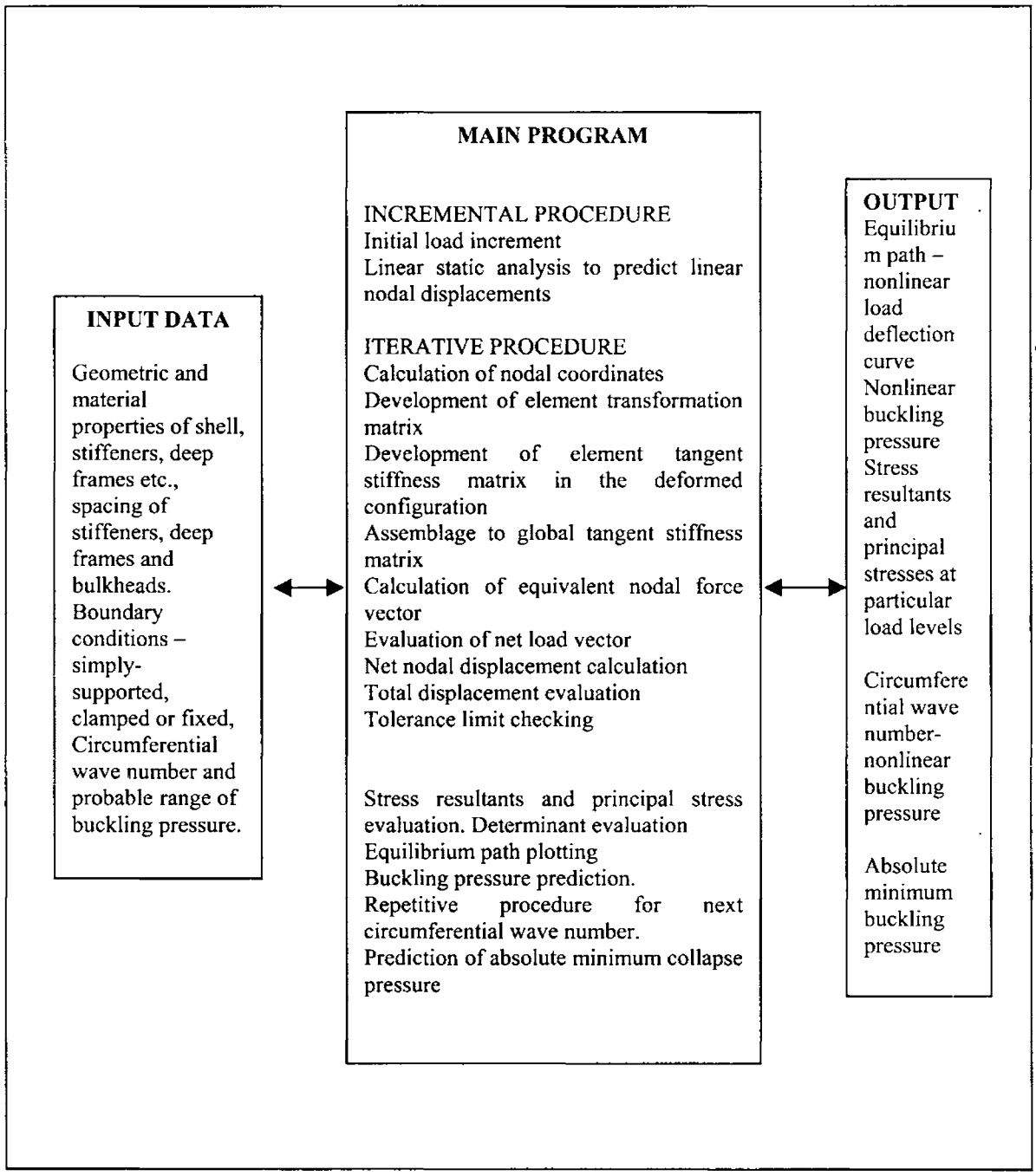

Fig. 5.3a Schematic diagram of geometric nonlinear analysis

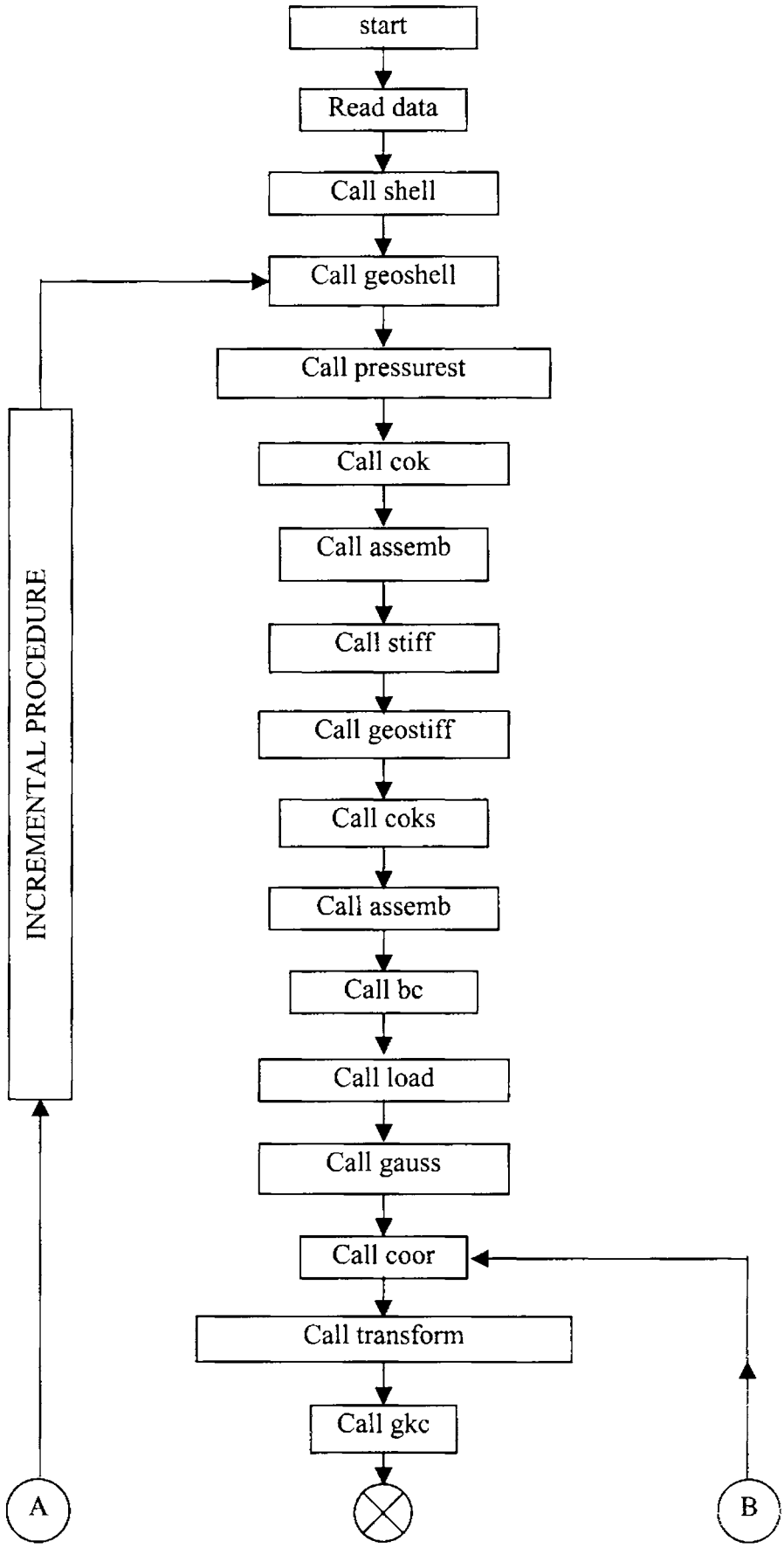
start
Read data
Call shell
Call geoshell
Call pressurest
Call cok
Call assemb
Call stiff
Call geostiff
Call coks
Call assemb
Call bc
Call load
Call gauss
Call coor
Call transform
Call gkc
INCREMENTAL PROCEDURE
A
B

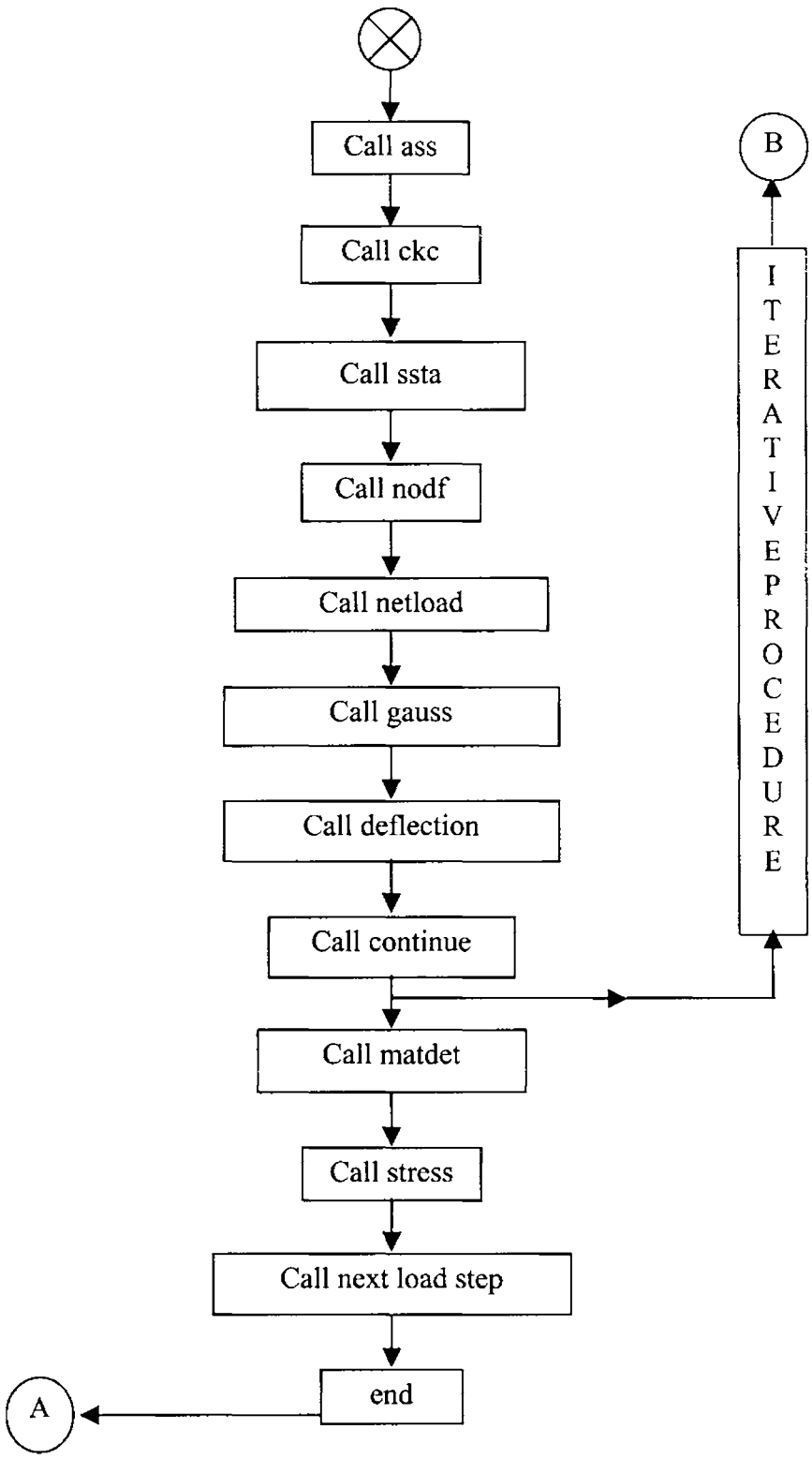

Fig. 5.3b Flowchart for geometric nonlinear analysis

5.4.2 Description of the Program *MAIN*

The function *MAIN* initially calculates elastic geometric and pressure stiffness matrices of the cylindrical shell. It also calculates elastic and geometric matrices of the stiffener. It assembles total stiffness matrix and incorporates the effects of stiffeners. The boundary conditions are accommodated and the equivalent joint loads are calculated. The displacements are calculated as per linear static analysis, and are used to predict the coordinates of the deformed configuration.

As the next step, based on these new coordinates, the transformation matrix and subsequently tangent stiffness matrix of each element are developed. Tangent stiffness matrix is then assembled to get the global tangent stiffness matrix. The net nodal loads based on current displacements are calculated by subtracting the nodal forces from the equivalent joint loads. Using these net nodal loads, the incremental displacement is calculated by performing Gauss elimination. The displacement after first iteration will be the sum of initial displacements and incremental displacements. The iteration is continued till tolerance limit is attained. Determinant of total tangent stiffness matrix is evaluated. Then the procedure is repeated to next load increment. The stresses are calculated at each load levels. This software is developed exclusively to calculate the buckling pressure of stiffened cylindrical shells. However, using the functions, deflection and stress, the deflections, stress resultants and principal stresses can also be determined.

5.4.3 Description of Functions

The functions *shell, stiff, bc, load* and *gauss* from the linear static analysis (section 3.5.3) and functions *geoshell, geostiff, pressurest* and *matdet* from linear buckling analysis (section 4.4.3) are used with some modifications. Functions developed for geometric nonlinear analysis besides those mentioned above are explained subsequently.

Function *cok*

This function is used to incorporate the effects of elastic stiffness matrix $[k_o]$, geometric stiffness matrix $[k_G]$ and pressure stiffness matrix $[k_P]$ of the shell element to get $[k_T]$.

G9047

Function *coks*

It is used to incorporate the combined effects of elastic stiffness matrix $[k_s]$ and geometric stiffness matrix $[k_{gs}]$ of the stiffener.

Function *assemb*

Function *assemb* is used to get the assembled global stiffness matrix [K] of the unstiffened cylindrical shell.

Function *stassemb*

This function includes the stiffness matrices of the stiffeners to get the global stiffness matrix $[K_S]$ of the stiffened cylindrical shell.

Function *coor*

This function calculates the new displaced co-ordinates of nodal points of each element after the displacement evaluation by Gauss elimination procedure (step for generating tangent stiffness matrix).

Function *transform*

Function *transform* develops the transformation matrix for each element based on the new displaced position.

Function *ckc*

ckc calculates the tangent stiffness matrix of each element based on the corresponding transformation matrix.

Function *ass*

This function assembles the tangent stiffness matrices to get global tangent stiffness matrix.

Function *ssta*

Function *ssta* incorporates the effect of stiffeners.

UNIVERSITY LIBRARY ★ COCHIN UNIVERSITY OF SCIENCE AND TECHNOLOGY ★
Cochin - 682 022

Function *nodf*

It calculates the nodal loads based on first iteration.

Function *netload*

Function *netload* calculates the net effective load by subtracting nodal forces from equivalent joint load.

Function *tolerance*

Function *tolerance* determines whether the iteration is to be stopped or continued.

5.5 NUMERICAL INVESTIGATIONS

Validation of the program is done using the benchmark problem (BMP4) suggested by Moradi and Parsons (1993). The geometric features of ring stiffened cylindrical shell are shown in fig. 5.4.

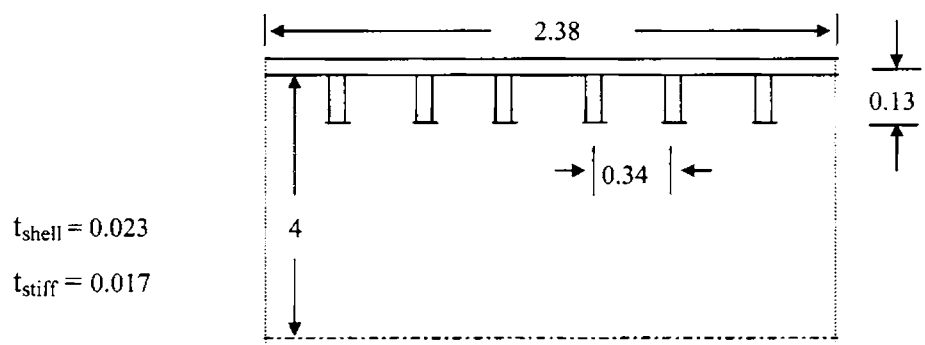

Fig. 5.4 Geometric features of ring stiffened cylindrical shell (BMP4) (All dimensions are in inches)

Modulus of elasticity of the material of the cylinder is 1.04 x10^7 psi and Poisson's ratio is 0.3. s.s-s.s boundary condition has been adopted.

Linear buckling pressure and results from geometric nonlinear analysis have been compared for BMP2 (Kendrick, 1970), the geometry of which is given in fig. 4.2a. The variations of buckling pressures with circumferential wave numbers are predicted and the critical values are compared. The influence of various boundary conditions viz., fixed-fixed, clamped-clamped and simply supported-simply supported on nonlinear buckling pressure is investigated. A comparative study is made between linear and nonlinear buckling (limit point) pressures for above-

mentioned boundary conditions. Equilibrium path is drawn for simply supported–simply supported boundary condition and the limit point pressure is observed.

Geometric nonlinear analysis has been conducted on stiffened cylindrical shell of Kendrick's example (BMP3), which has been shown in fig. 4.3a. The shell skin is modeled using all-cubic axisymmetric shell element and stiffeners using discrete ring stiffener element. The variations of buckling pressures with circumferential wave numbers are predicted. Influence of f-f, c-c and s.s-s.s boundary conditions on nonlinear buckling pressure is investigated. A comparative study is made between linear and nonlinear buckling pressures for the above-mentioned boundary conditions. Equilibrium path is drawn for f–f boundary conditions.

Geometric nonlinear analysis has been carried out for stiffened cylindrical hull of attack submarine models M1 and M2 have been given in section 3.6.2. Geometric features of stiffened cylindrical shells of submarine M1 and M2 are given earlier in table 3.2 and in figs. 3.6a, 3.6b, 3.7a and 3.7b. Geometric nonlinear analysis has been carried out for the three configurations dealt in the linear buckling analysis viz., cylindrical shell between stiffeners (interstiffener), stiffened cylindrical shell between deepframes (interdeepframe) and stiffened cylindrical shell between bulkheads (interbulkhead). The variations of buckling pressures with circumferential wave numbers are predicted. The scope of the numerical investigations has been extended to realize the influence of possible boundary conditions.

A comparative study is made between linear and nonlinear buckling pressure for M1 and M2 for the above-mentioned configurations, for f-f, c–c and s.s-s.s boundary conditions. The equilibrium paths or nonlinear load deflection curves are plotted with maximum radial deflection Vs hydrostatic pressure for M1 and M2 for the three configurations for f-f boundary conditions for wave numbers corresponding to minimum buckling pressures. The limit point buckling pressures can be observed from that. For a comparative study the linear load deflection curves are also plotted along with the equilibrium path diagrams.

The follower force effect of hydrostatic pressure is also investigated for M1 and M2 for the three configurations. The influence of various boundary conditions viz., fixed-fixed, clamped-clamped and simply supported-simply supported on nonlinear buckling pressure with follower force effect is investigated. The equilibrium paths are drawn including pressure rotation effects. The linear load deflection curves are also plotted along with the equilibrium path diagrams. A comparative study is made between linear and nonlinear buckling pressure for M1 and M2 for the above-mentioned configurations.

5.6 RESULTS AND DISCUSSION

5.6.1 Validation

The buckling pressure evaluated from geometric nonlinear analysis of BMP4 for s.s-s.s boundary conditions are given in table 5.1. The minimum buckling pressure and corresponding n value is given in bold. The nonlinear buckling pressures Pcr against circumferential wave numbers (n) for s.s-s.s boundary conditions are shown in fig. 5.5.

Table 5.1 Nonlinear buckling pressures corresponding to wave numbers for BMP4

Circumferential wave no. (n)	Minimum buckling pressure (psi)
1	636
2	608
3	420
4	299
5	262
6	**243**
7	258
8	324

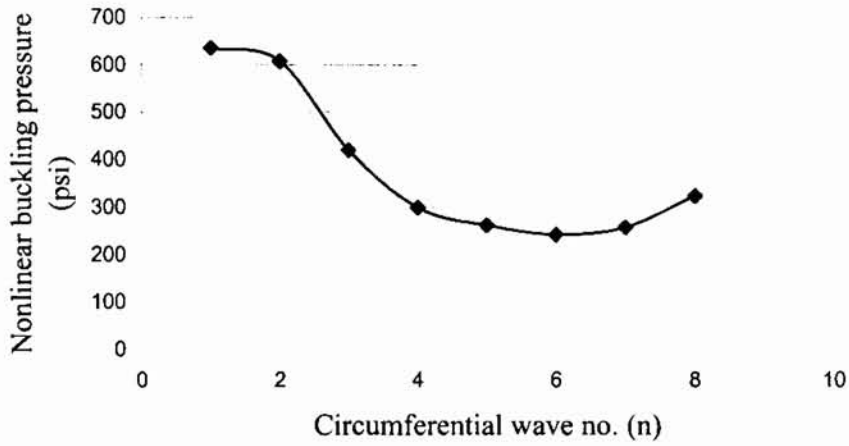

Fig. 5.5 Nonlinear buckling pressures corresponding to wave numbers for BMP4

For s.s-s.s boundary condition the minimum buckling pressure obtained 243 psi (n=6). The nonlinear buckling pressure predicted using four nodded shell element in ABAQUS is 241 psi (Moradi and Parsons, 1993). The obtained result is 0.8% upper bound.

Equilibrium path with maximum radial deflection Vs hydrostatic pressure for s.s-s.s boundary condition is given fig. 5.6. Linear load–deflection curve is also plotted along with the equilibrium path. In the equilibrium path an almost linear regime is followed by a softening regime and there is no substantial redistribution of stresses due to changes in geometry and the structure eventually collapses at the limit point. From the nonlinear path it is observed that the collapse occurs at a pressure of 243 psi.

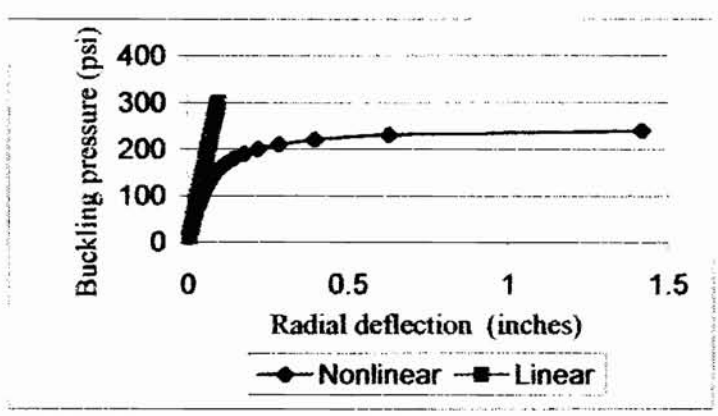

Fig. 5.6 Linear and nonlinear load deflection curve of BMP4 for s.s-s.s boundary condition (n = 6)

5.6.2 Interstiffener Analysis of BMP2

The buckling pressure evaluated from geometric nonlinear analysis of Kendrick's model (BMP2) for f-f, c-c and s.s-s.s boundary conditions are given in table 5.2. The minimum buckling pressures and corresponding n values are given in bold.

Table 5.2 Nonlinear interstiffener buckling pressures corresponding to wave numbers for BMP2 for various boundary conditions

Circumferential waves no. (n)	Nonlinear buckling pressure (psi)		
	f-f	c-c	s.s-s.s
1	2800	2680	1225
2	2757	2440	1200
3	2670	1860	890
4	2526	1295	745
5	2315	1057	685
6	2095	882	630
7	1390	814	610
8	1080	782	594
9	930	**760**	**580**
10	860	775	600
11	**840**	780	630
12	855	805	665
13	882	820	710
14	920	850	776
15	970	920	820
16	1027	980	890
17	1094	1020	978

The variation of nonlinear buckling pressure Pcr against circumferential wave number n for the three boundary conditions are shown in fig. 5.7.

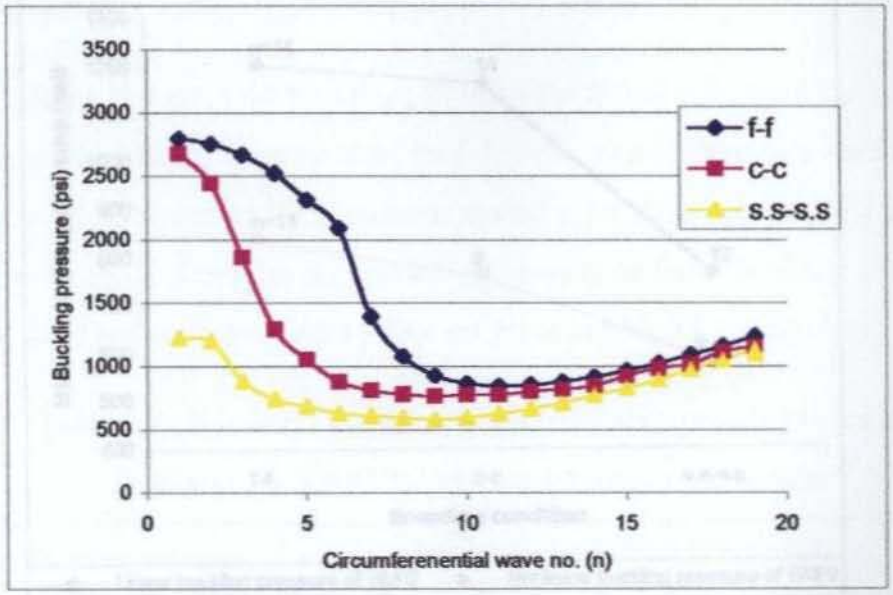

Fig. 5.7 Nonlinear interstiffener buckling pressures corresponding to wave numbers for BMP2 for various boundary conditions

For f-f, c-c and s.s-s.s boundary conditions, minimum buckling pressures are 840 psi (n = 11), 760 psi (n = 9) and 580 psi (n = 9) respectively. Comparative study between linear and nonlinear buckling pressures for f–f, c–c and s.s–s.s boundary conditions are given in table 5.3 and fig. 5.8.

Table 5.3 Comparison of linear and nonlinear buckling pressures of BMP2 for various boundary conditions

Boundary condition	Buckling pressure (psi) & (n)		% reduction
	Linear	Nonlinear	
f-f	1202(14)	840(11)	30.1
c-c	1163(14)	760(9)	34.6
s-s	765(12)	580(9)	24.8

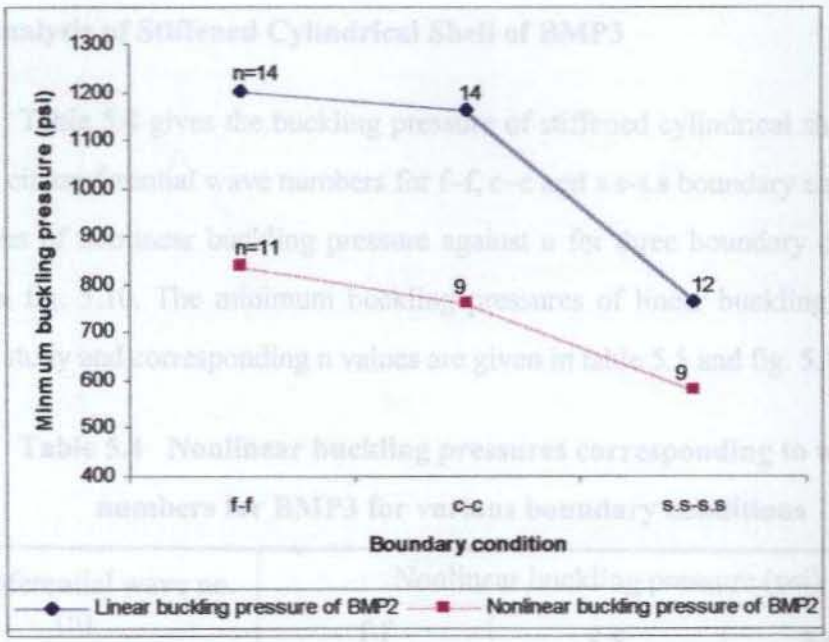

Fig. 5.8 Minimum linear and nonlinear buckling pressures for various boundary conditions for BMP2

Nonlinearity induces a reduction in buckling pressure by 30.1% for f–f, 34.6% for c-c and 24.8% for s.s-s.s boundary conditions. In the geometric nonlinear analysis change in geometry as the structure deforms is taken into account and hence depicts the actual situation of shell buckling at a lower pressure.

Equilibrium path or nonlinear load deflection curve with maximum radial deflection Vs hydrostatic pressure for s.s-s.s boundary condition is fig. 5.9. Linear load deflection curve is also plotted along with the equilibrium path. From the nonlinear path it is observed that the collapse occurs at a pressure of 580 psi.

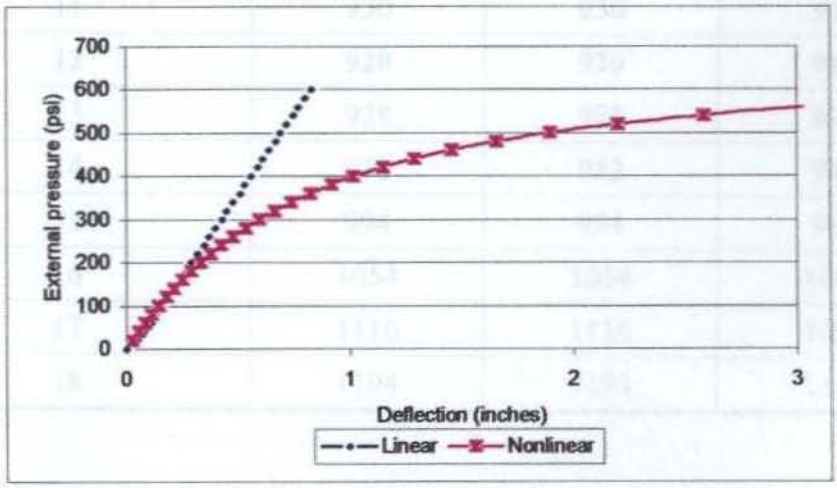

Fig. 5.9 Equilibrium path and linear load deflection curve of BMP2 for f–f boundary condition (n = 11)

5.6.3 Analysis of Stiffened Cylindrical Shell of BMP3

Table 5.4 gives the buckling pressure of stiffened cylindrical shell BMP3 for various circumferential wave numbers for f–f, c–c and s.s-s.s boundary conditions. The variations of nonlinear buckling pressure against n for three boundary conditions are given in fig. 5.10. The minimum buckling pressures of linear buckling analysis and present study and corresponding n values are given in table 5.5 and fig. 5.11.

Table 5.4 Nonlinear buckling pressures corresponding to wave numbers for BMP3 for various boundary conditions

Circumferential wave no. (n)	Nonlinear buckling pressure (psi)		
	f-f	c-c	s.s-s.s
1	2722	2488	2254
2	2470	2370	2234
3	2178	2078	2042
4	2128	2018	1956
5	1436	1420	1402
6	1364	1360	1349
7	1178	1194	1178
8	1128	1122	1121
9	1040	1040	1038
10	968	968	964
11	930	930	924
12	**920**	**920**	**910**
13	928	928	920
14	952	952	946
15	994	994	988
16	1054	1054	1007
17	1116	1116	1091
18	1194	1194	1154

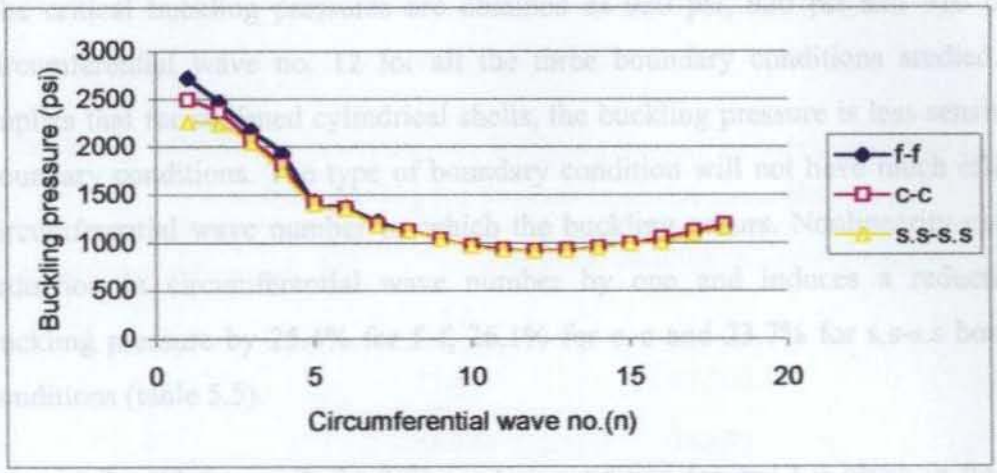

Fig. 5.10 Nonlinear buckling pressures corresponding to wave numbers of stiffened cylindrical shell of BMP3 for various boundary conditions

Table 5.5 Comparison of linear and nonlinear buckling pressures of BMP3 for f-f, c-c and s.s-s.s boundary conditions

Boundary condition	Buckling pressure (psi) & (n)		% reduction
	Linear	Nonlinear	
f-f	1233(13)	920(12)	25.4
c-c	1231(13)	920(12)	26.1
s.s-s.s	1193(13)	910(12)	23.7

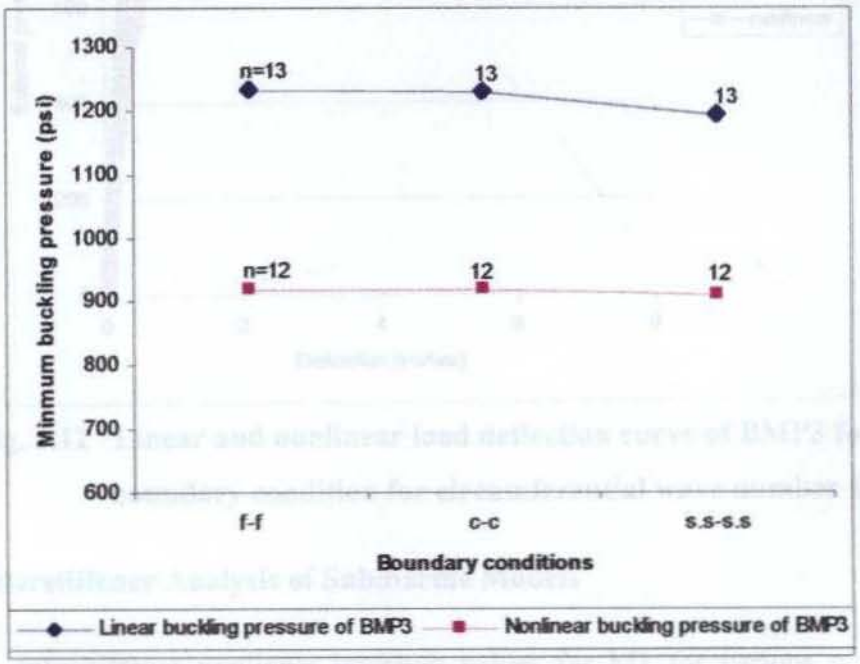

Fig. 5.11 Minimum linear and nonlinear buckling pressures for various boundary conditions for BMP3

The critical buckling pressures are obtained as 920 psi, 920 psi and 910 psi for circumferential wave no. 12 for all the three boundary conditions studied. This implies that for stiffened cylindrical shells, the buckling pressure is less sensitive to boundary conditions. The type of boundary condition will not have much effect on circumferential wave number on which the buckling occurs. Nonlinearity causes a reduction in circumferential wave number by one and induces a reduction in buckling pressure by 25.4% for f–f, 26.1% for c–c and 23.7% for s.s-s.s boundary conditions (table 5.5).

Equilibrium path for f–f boundary condition for n=12 is given in fig. 5.12. Linear load–deflection curve is also plotted along with the equilibrium path. The figure displays the limit point pressure value as 920 psi.

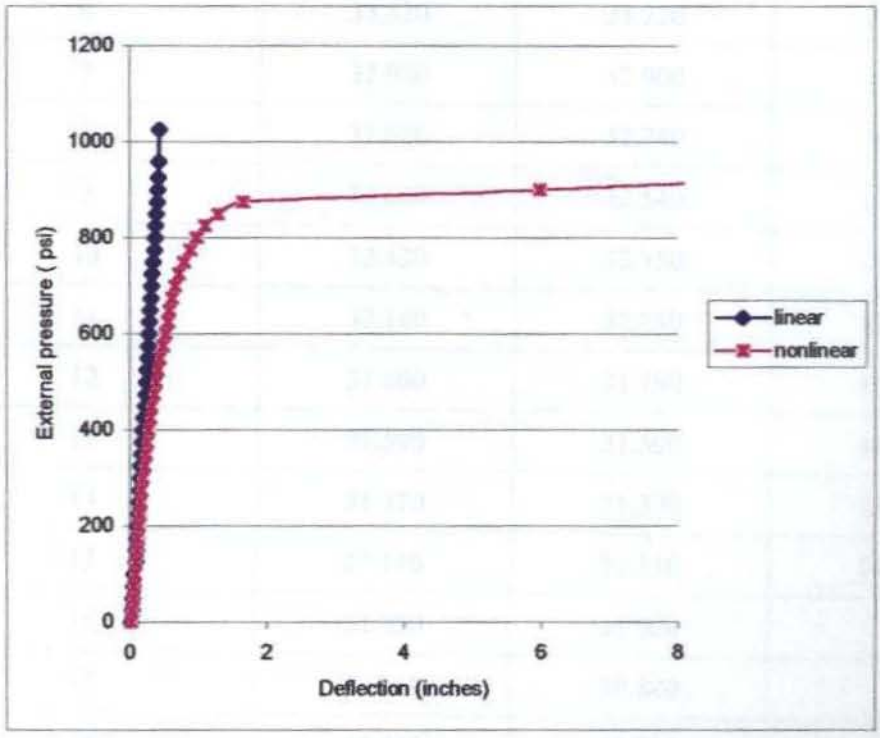

Fig. 5.12 Linear and nonlinear load deflection curve of BMP3 for f–f boundary condition for circumferential wave number 12

5.6.4 Interstiffener Analysis of Submarine Models

Interstiffener nonlinear buckling values for M1 for various n values are shown in table 5.6. Variations of Pcr with n are shown in fig. 5.13. The minimum

buckling pressures and the corresponding n values for linear buckling analysis and geometrically nonlinear analysis are given in table 5.7 and fig. 5.14.

Table 5.6 Nonlinear interstiffener buckling pressures corresponding to wave numbers for M1 for various boundary conditions

Circumferential wave no. (n)	Nonlinear buckling pressure (N/mm^2)		
	f-f	c-c	s.s-s.s
1	33.840	33.760	15.480
2	33.780	33.680	15.320
3	33.720	33.620	15.270
4	33.680	33.560	15.220
5	33.570	33.440	15.140
6	33.330	33.220	15.070
7	32.980	32.900	14.940
8	32.820	32.740	14.120
9	32.620	32.540	13.780
10	32.420	32.350	**13.180**
11	32.140	32.080	13.340
12	31.860	31.790	13.540
13	31.590	31.500	13.670
14	31.370	31.300	13.940
15	31.170	31.110	14.030
16	31.050	31.000	
17	30.910	30.840	
18	**30.840**	**30.780**	
19	30.840	30.790	
20	30.990	30.900	
21	31.150	31.050	

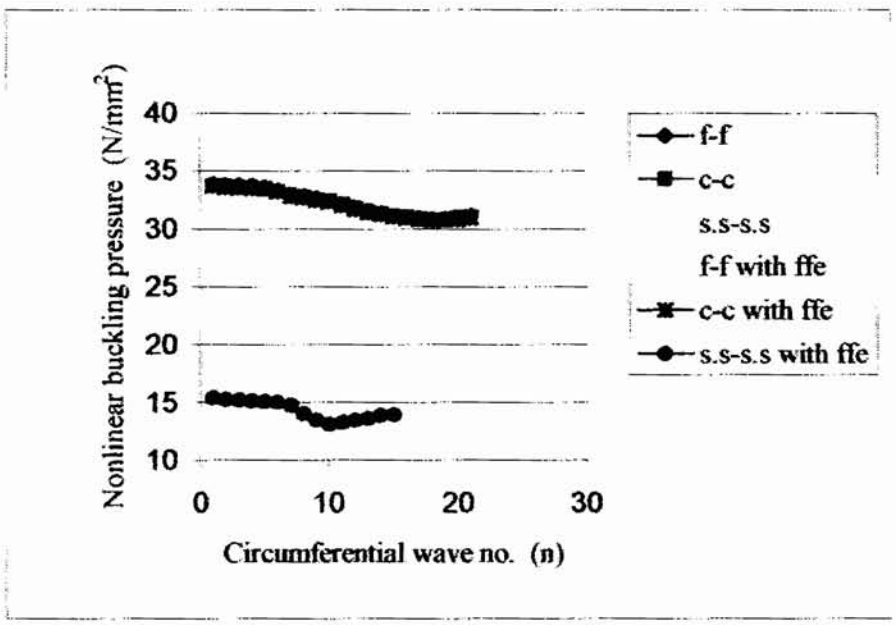

Fig. 5.13 Nonlinear interstiffener buckling pressures for M1 with and without follower force effect for various boundary conditions

For M1 the minimum buckling pressures are 30.840 N/mm^2 (n=18), 30.780 N/mm^2 (n= 18) and 13.180 N/mm^2 (n=10) respectively for f-f, c-c and s.s-s.s boundary conditions. Comparative study is made between linear and nonlinear buckling pressures for f–f, c–c and s.s-s.s boundary conditions and is given in table 5.7. Nonlinearity induces a reduction in buckling pressure by 23.5% for f–f, 23.6% for c–c and 19.5% for s.s-s.s boundary conditions.

Table 5.7 Comparison of linear and nonlinear interstiffener buckling pressures of M1 for f-f, c-c and s.s-s.s boundary conditions

Boundary condition	Buckling pressure (N/mm^2) & (n)		% reduction
	Linear	Nonlinear	
f-f	40.330(30)	30.840(18)	23.5
c-c	40.283(30)	30.780(18)	23.6
s.s-s.s	16.380(16)	13.180(10)	19.5

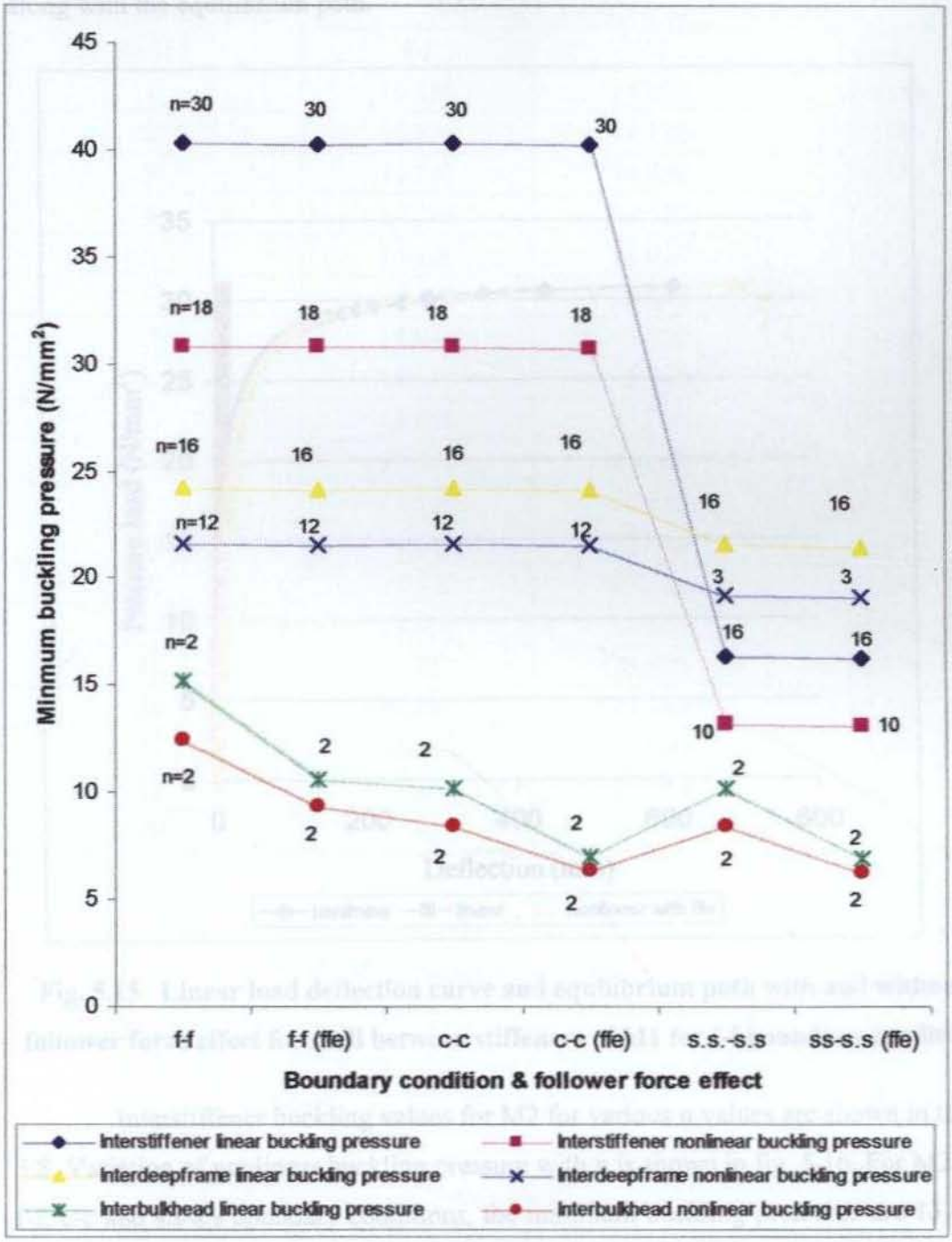

Fig. 5.14 Minimum linear and nonlinear buckling pressures for various configurations and boundary conditions with and without follower force effect for M1

Equilibrium path for M1 for f–f boundary condition for circumferential wave number 18 is given in fig. 5.15. Linear load – deflection curve is also plotted along with the equilibrium path.

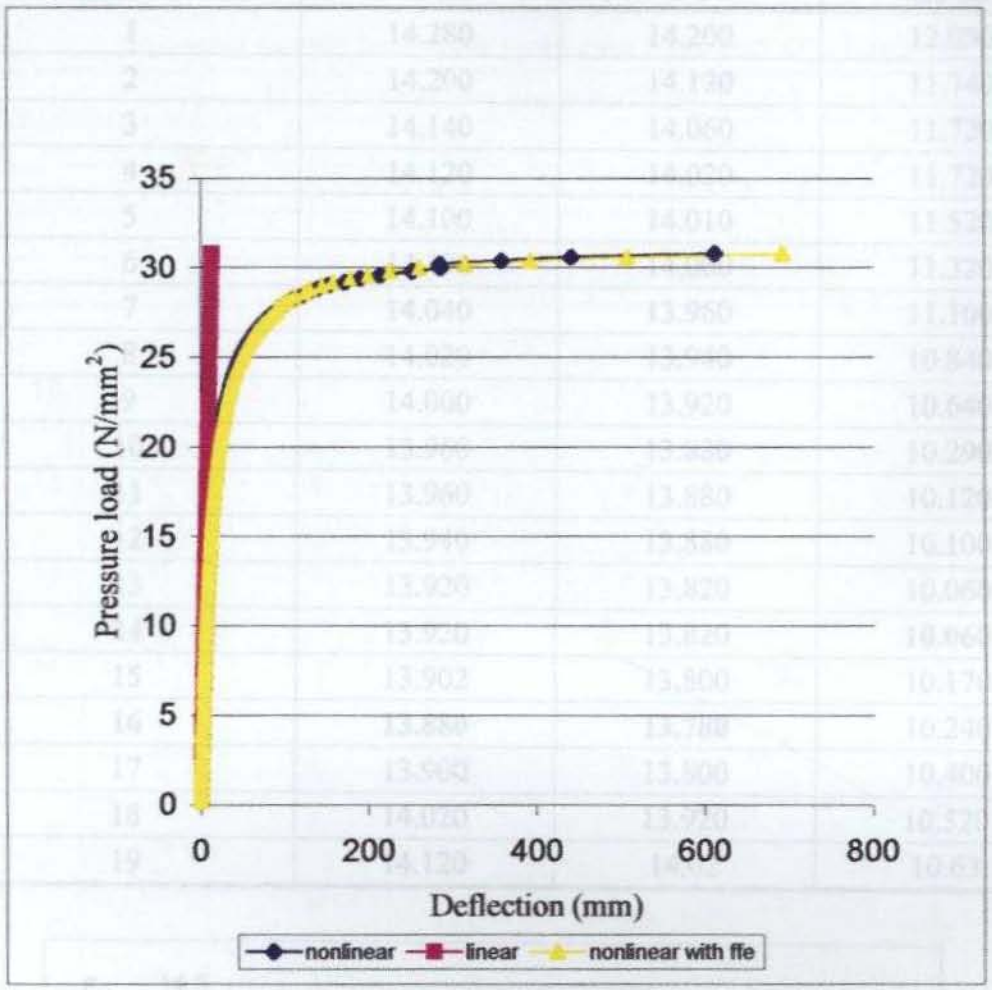

Fig. 5.15 Linear load deflection curve and equilibrium path with and without follower force effect for shell between stiffeners of M1 for f-f boundary condition

Interstiffener buckling values for M2 for various n values are shown in table 5.8. Variation of nonlinear buckling pressure with n is shown in fig. 5.16. For M2 for f-f, c-c and s.s-s.s boundary conditions, the minimum buckling pressures are 13.880 N/mm^2 (n =16), 13.770 N/mm^2 (n =16) and 10.060 N/mm^2 (n=14) respectively.

Table 5.8 Nonlinear interstiffener buckling pressures corresponding to wave numbers for M2 for various boundary conditions

Circumferential wave no. (n)	Nonlinear buckling pressure (N/mm^2)		
	f-f	c-c	s.s-s.s
1	14.280	14.200	12.030
2	14.200	14.120	11.740
3	14.140	14.060	11.720
4	14.120	14.020	11.720
5	14.100	14.010	11.520
6	14.100	14.000	11.320
7	14.040	13.960	11.100
8	14.020	13.940	10.840
9	14.000	13.920	10.640
10	13.960	13.880	10.290
11	13.960	13.880	10.120
12	13.940	13.880	10.100
13	13.920	13.820	10.060
14	13.920	13.820	**10.060**
15	13.902	13.800	10.170
16	**13.880**	**13.780**	10.240
17	13.900	13.800	10.400
18	14.020	13.920	10.520
19	14.120	14.02	10.63

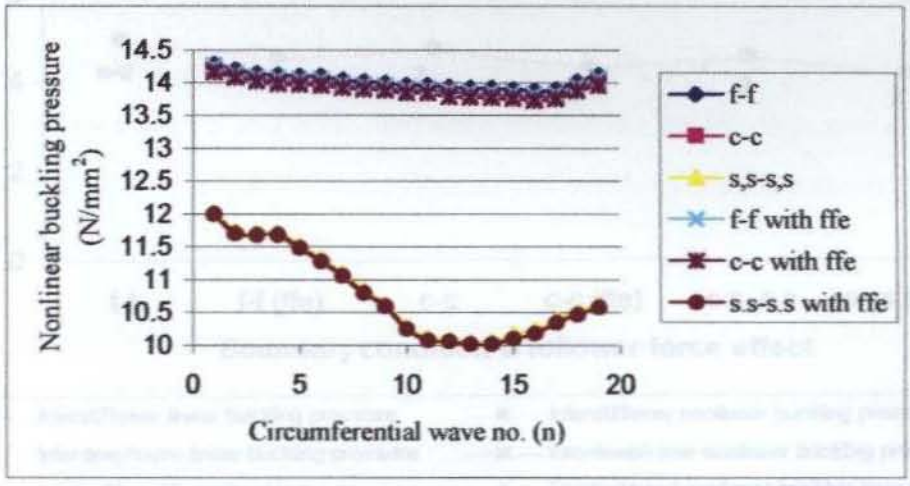

Fig. 5.16 Nonlinear interstiffener buckling pressures of M2 with and without follower force effect for various boundary conditions

Linear and nonlinear minimum buckling pressures for f–f, c–c and s.s-s.s boundary conditions are given in table 5.9 and fig. 5.17. Nonlinearity induces a reduction in buckling pressure by 13.1% for f–f, 13.3% for c-c and 13.7% for s.s-s.s boundary conditions.

Table 5.9 Comparison of linear and nonlinear interstiffener buckling pressures for M2 for f-f, c-c and s.s-s.s boundary conditions

Boundary condition	Buckling pressure (N/mm^2) & (n)		% reduction
	Linear	Nonlinear	
f-f	15.980(21)	13.880(16)	13.1
c-c	15.880(21)	13.770(16)	13.3
s.s-s.s	11.660(16)	10.060(14)	13.7

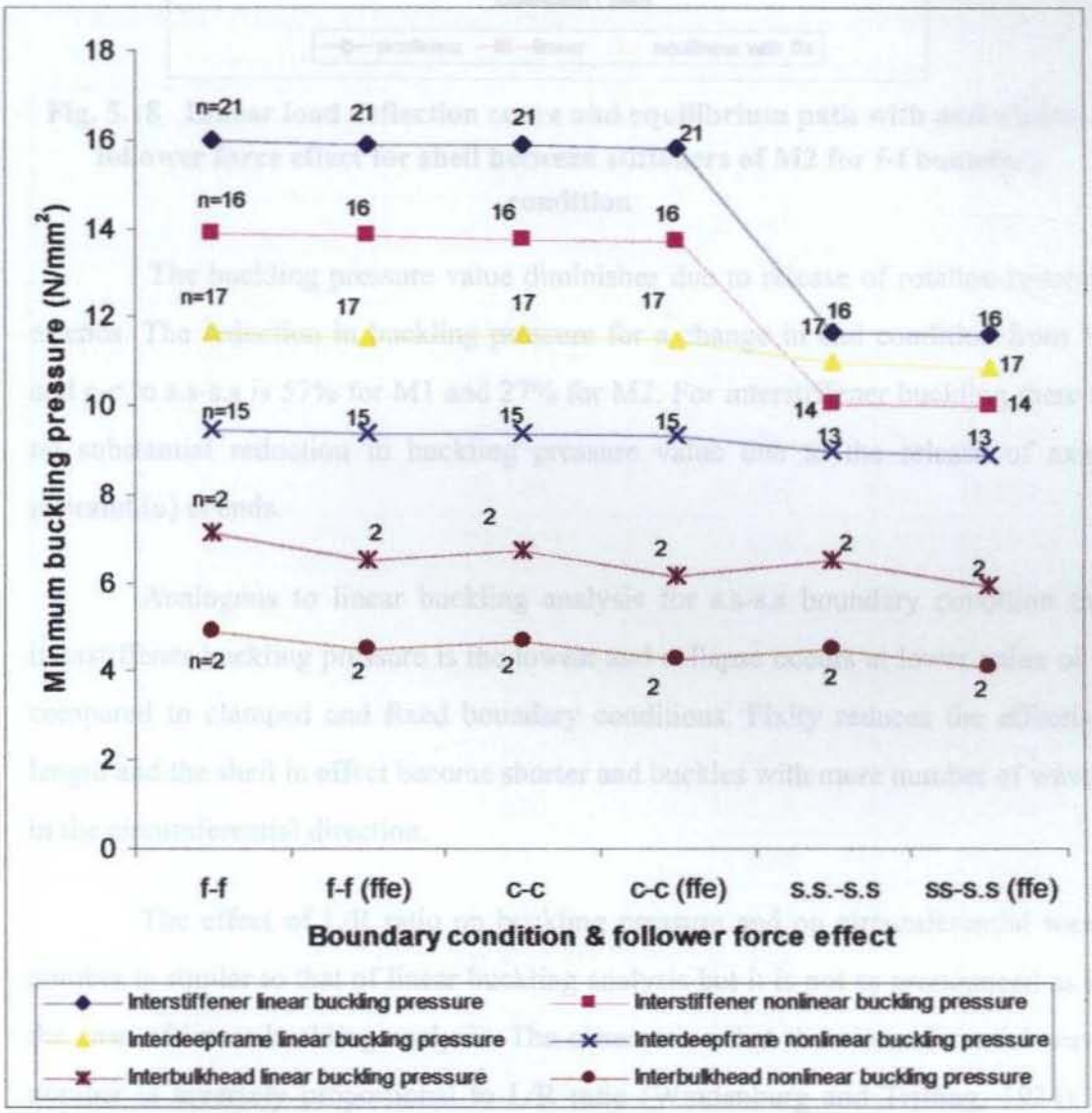

Fig. 5.17 Minimum linear and nonlinear buckling pressures for various configurations and boundary conditions with and without follower force effect for M2

Nonlinearity induces flexibility to the structure such that the shell buckles with less number of waves in the circumferential direction. Equilibrium path for f–f boundary condition for M2 is given in fig. 5.18.

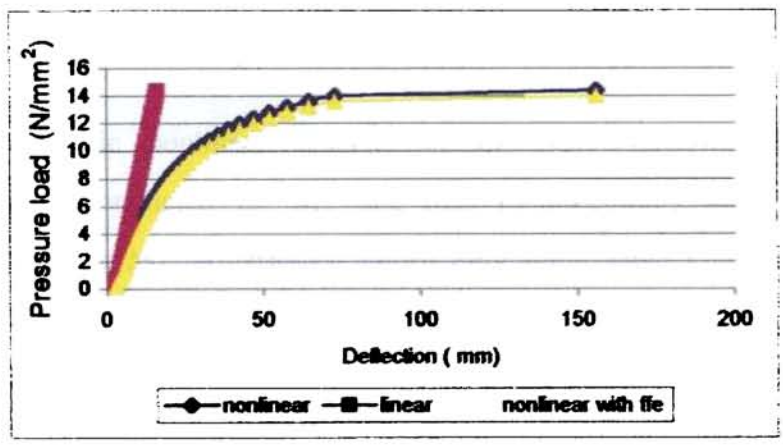

Fig. 5.18 Linear load deflection curve and equilibrium path with and without follower force effect for shell between stiffeners of M2 for f-f boundary condition

The buckling pressure value diminishes due to release of rotation restraint at ends. The reduction in buckling pressure for a change in end condition from f-f and c-c to s.s-s.s is 57% for M1 and 27% for M2. For interstiffener buckling there is no substantial reduction in buckling pressure value due to the release of axial restraint (u) at ends.

Analogous to linear buckling analysis for s.s-s.s boundary condition the interstiffener buckling pressure is the lowest and collapse occurs at lower value of n compared to clamped and fixed boundary conditions. Fixity reduces the effective length and the shell in effect become shorter and buckles with more number of waves in the circumferential direction.

The effect of L/R ratio on buckling pressure and on circumferential wave number is similar to that of linear buckling analysis but it is not as pronounced as in the case of linear buckling analysis. The observation that the circumferential wave number is inversely proportional to L/R ratio (Windenburg and Trilling, 1934) is reflected in the results of geometric nonlinear analysis also.

The reduction in buckling pressure due to geometric nonlinearity is not much influenced by the change in boundary condition. The reduction in buckling pressure is 23% for M1 and 13% for M2, irrespective of the boundary condition.

5.6.5 Interdeepframe Analysis of Submarine Models

Geometric nonlinear analysis of stiffened cylindrical shell between deepframes is conducted for M1 and M2. Interdeepframe nonlinear buckling pressure values for M1 for various n values are given in table 5.10 and are shown in fig 5.19.

Table 5.10 Nonlinear interdeepframe buckling pressures corresponding to wave numbers for M1 for various boundary conditions

Circumferential wave no. (n)	Nonlinear buckling pressure (N/mm^2)		
	f-f	c-c	s.s-s.s
1	22.080	22.040	20.690
2	21.880	21.840	20.390
3	21.900	21.860	**19.230**
4	22.000	21.960	20.890
5	22.120	22.080	21.570
6	22.100	22.060	21.550
7	22.050	21.998	21.410
8	21.940	21.900	21.370
9	21.800	21.770	21.350
10	21.720	21.690	21.330
11	21.660	21.640	21.310
12	**21.620**	**21.610**	21.384
13	21.630	21.620	21.430
14	21.700	21.678	21.550
15	21.820	21.794	21.690
16	22.020	21.988	21.890
17	22.520	22.450	22.110
18	23.090	22.980	22.390

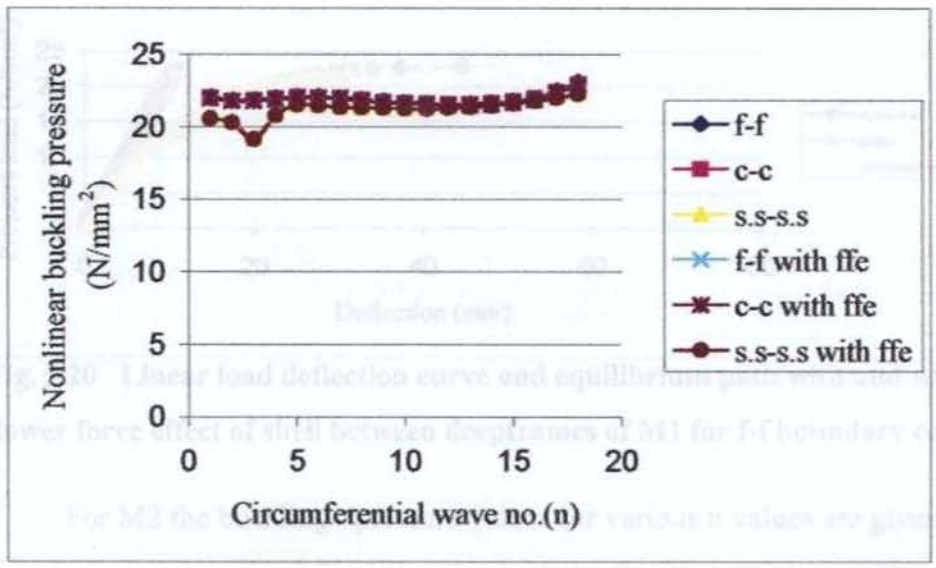

Fig. 5.19 Nonlinear interdeepframe buckling pressures corresponding to wave numbers with and without follower force effect of M1 for various boundary conditions

For M1 for f-f, c-c and s.s-s.s boundary conditions, the minimum buckling pressures are 21.620 N/mm^2 (n= 12), 21.610 N/mm^2 (n= 12) and 19.230 N/mm^2 (n =3) respectively. Comparative study is made between linear and nonlinear buckling pressures for the above mentioned boundary conditions and are given in table 5.11 and fig. 5.14. Nonlinearity induces a reduction in buckling pressure by 10.8% for f-f and c–c and 10.9% for s.s–s.s boundary conditions.

Table 5.11 Comparison of linear and nonlinear interdeepframe buckling pressures for M1 for f-f, c-c and s.s-s.s boundary conditions

Boundary condition	Buckling pressure (N/mm^2) & (n)		% reduction
	Linear	Nonlinear	
f-f	24.242(16)	21.620(12)	10.8
c-c	24.240(16)	21.610(12)	10.8
s.s-s.s	21.584(12)	19.230(3)	10.9

Equilibrium path for f–f boundary condition for M1 (n=12) is given in fig. 5.20. Linear load–deflection curve is also plotted along with the equilibrium path.

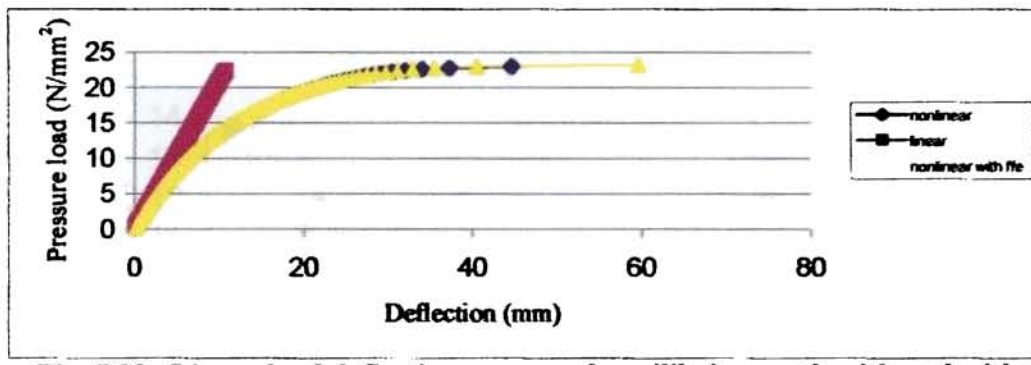

Fig. 5.20 Linear load deflection curve and equilibrium path with and without follower force effect of shell between deepframes of M1 for f-f boundary condition

For M2 the buckling pressure values for various n values are given in table 5.12 and are shown in fig. 5.21.

Table 5.12 Nonlinear interdeepframe buckling pressures corresponding to wave numbers for M2 for various boundary conditions

Circumferential wave no. (n)	Nonlinear buckling pressure (N/mm^2)		
	f-f	c-c	s.s-s.s
1	13.800	13.760	13.330
2	13.600	13.580	13.130
3	13.400	13.30	12.940
4	12.890	12.850	11.400
5	11.780	11.750	10.820
6	10.800	10.760	10.220
7	10.250	10.210	9.820
8	9.890	9.830	9.510
9	9.880	9.820	9.410
10	9.720	9.670	9.210
11	9.600	9.560	9.080
12	9.560	9.540	9.000
13	9.510	9.520	**9.000**
14	9.460	9.420	9.020
15	**9.460**	**9.400**	9.050
16	9.520	9.420	9.060
17	9.650	9.580	9.120
18	9.871	9.720	9.190
19	10.050	9.910	9.280

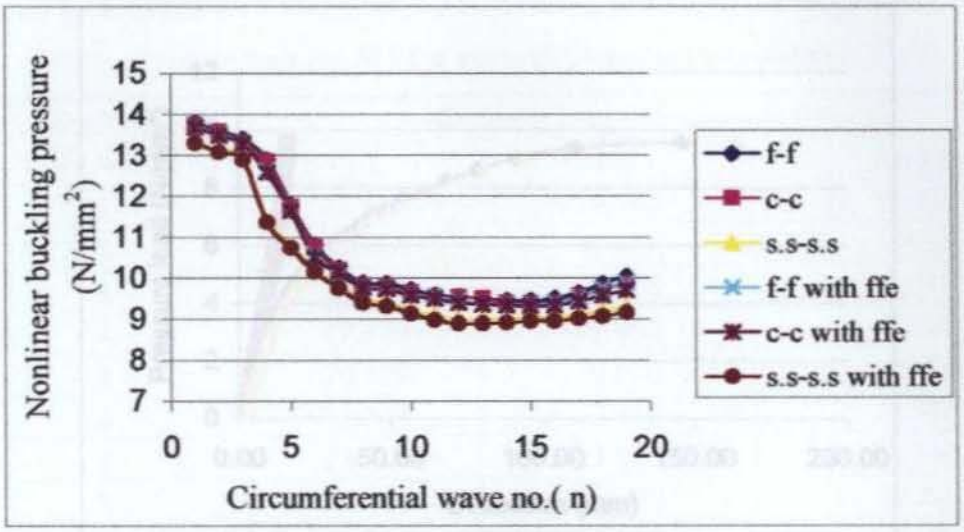

Fig. 5.21 Nonlinear interdeepframe buckling pressures for M2 with and without follower force effect for various boundary conditions

The collapse pressure values are 9.460 N/mm^2 (n=15), 9.400 N/mm^2 (n =15) and 9.000 N/mm^2 (n=3) for f–f, c–c and s.s-s.s boundary conditions. Comparative study is made between linear and nonlinear buckling pressures for f–f, c–c and s.s-s.s boundary conditions and is given in table 5.13 and fig. 5.17. Nonlinearity induces a reduction in buckling pressure by 18.9% for f–f, 19.0% for c–c and 18.1% for s.s-s.s boundary conditions.

Equilibrium path for f–f boundary condition for M2 is given in fig. 5.22. Linear load deflection curve is also plotted along with the equilibrium path.

Table 5.13 Comparison of linear and nonlinear interdeepframe buckling pressures of M2 for f-f, c-c and s.s-s.s boundary conditions

Boundary condition	Buckling pressure (N/mm^2) & (n)		% reduction
	Linear	Nonlinear	
f-f	11.660(17)	9.460(16)	18.9
c-c	11.610(17)	9.400(16)	19.0
s.s-s.s	10.990(8)	9.000(13)	18.1

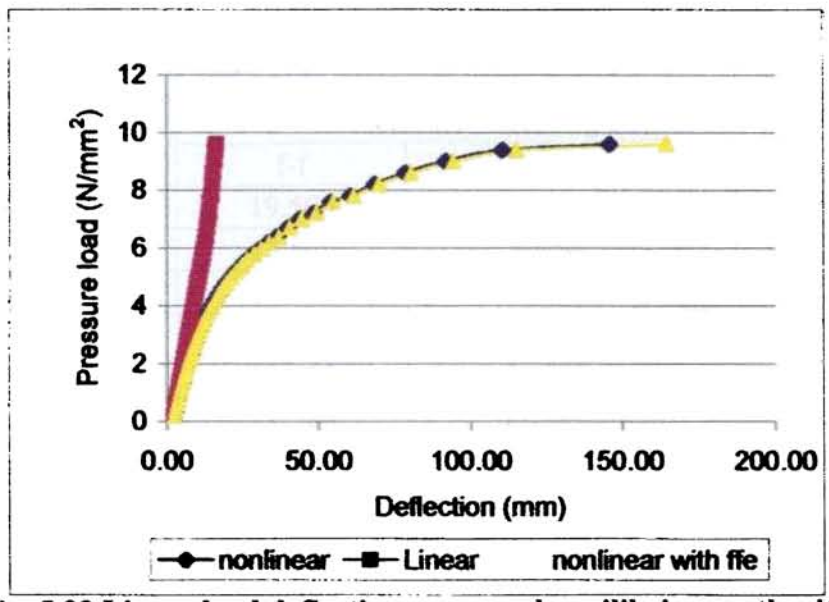

Fig. 5.22 Linear load deflection curve and equilibrium path with and without follower force effect for shell between deepframes of M2 for f-f boundary condition (n=15)

Reduction in nonlinear buckling pressure for release of end condition from rotation restraint (from f-f and c-c to s.s-s.s) is 11% for M1 and 4.6% for M2. Almost same values are reported in linear buckling analysis. The effect of axial restraint (u) reflected by the buckling pressure of f-f and c-c is negligible (less than 1%). The interdeepframe nonlinear buckling pressures are less susceptible to boundary conditions, compared to interstiffener buckling pressures.

The reduction in buckling pressure due to geometric nonlinearity is not much influential to boundary condition. There is a reduction in buckling pressure by 11% for M1 and 19% for M2, irrespective of the boundary condition.

5.6.6 Interbulkhead Analysis of Submarine Models

Between bulkheads, the nonlinear buckling pressure values for M1 for various n values are given in table 5.14 and summarized in table 5.15. The variation of Pcr with n is shown in fig. 5.23.

Table 5.14 Nonlinear interbulkhead buckling pressures corresponding to wave numbers for M1 for various boundary conditions

Circumferential wave no. (n)	Nonlinear buckling pressure (N/mm^2)		
	f-f	c-c	s.s-s.s
1	19.500	19.460	19.400
2	**12.400**	**8.450**	**8.450**
3	15.380	15.320	15.080
4	17.110	17.060	16.940
5	20.100	20.020	19.990
6	22.500	22.440	22.390
7	23.700	23.620	23.580
8	23.900	23.840	23.80
9	24.300	24.200	24.100
10	24.900	24.820	24.720
11	25.100	25.020	24.920
12	25.300	25.200	25.100
13	25.400	25.360	25.300
14	25.600	25.520	25.420
15	25.720	25.620	25.500
16	26.100	26.020	25.900
17	26.300	26.200	26.100

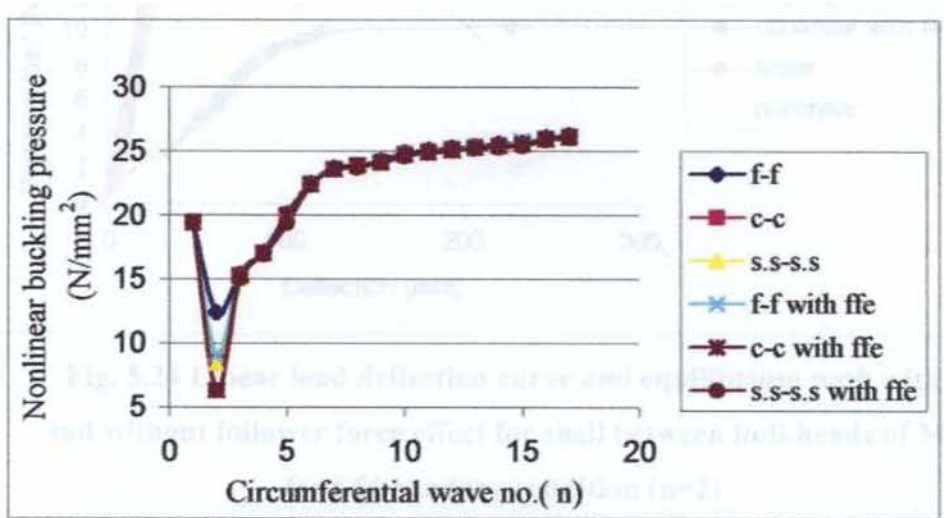

Fig. 5.23 Nonlinear interbulkhead buckling pressures corresponding to wave numbers of M1 with and without follower force effect for various boundary conditions

The collapse pressure values are 12.400 N/mm^2 (n=2), 8.450 N/mm^2 (n =2) and 8.450 N/mm^2 (n=2) for f–f, c–c and s.s-s.s boundary conditions. Linear and

nonlinear minimum buckling pressures for f–f, c–c and s.s-s.s boundary conditions are given in table 5.15 and fig. 5.14.

Table 5.15 Comparison of linear and nonlinear interbulkhead buckling pressures for M1 for f-f, c-c and s.s-s.s boundary conditions

Boundary condition	Buckling pressure (N/mm^2) & (n)		% reduction
	Linear	Nonlinear	
f-f	15.226(2)	12.400(2)	18.6
c-c	10.194(2)	8.450(2)	17.1
s.s-s.s	10.146(2)	8.450(2)	16.7

Nonlinearity induces a reduction in buckling pressure by 18.6% in f–f, 17.1% for c–c 16.7% for s.s-s.s boundary conditions. Equilibrium path for f–f boundary condition for M1 is given in and fig. 5.24.

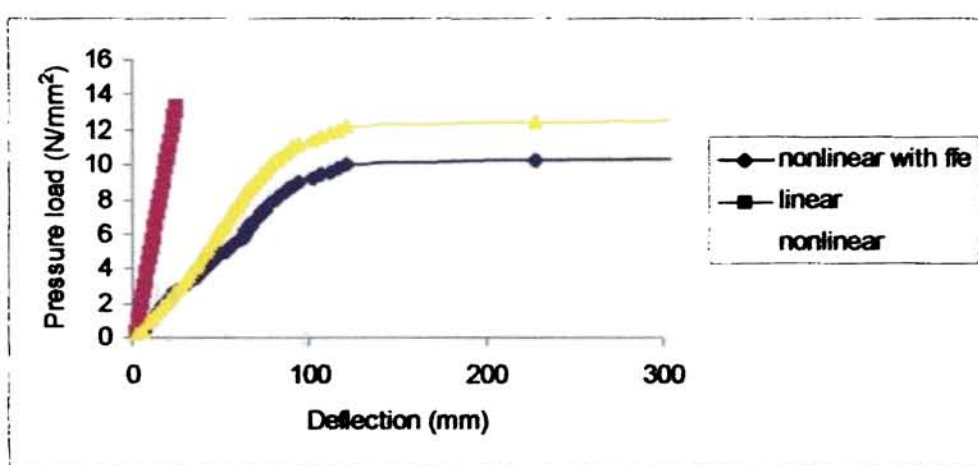

Fig. 5.24 Linear load deflection curve and equilibrium path with and without follower force effect for shell between bulkheads of M1 for f-f boundary condition (n=2)

For M2 the buckling pressure values for various n values are shown in table 5.16 and summarised in table 5.17. The variation of Pcr with n is shown in fig. 5.25.

Table 5.16 Nonlinear interbulkhead buckling pressures corresponding to wave numbers for M2 for various boundary conditions

Circumferential wave no. (n)	Nonlinear buckling pressure (N/mm^2)		
	f-f	c-c	s.s-s.s
1	6.620	6.480	6.340
2	**4.900**	**4.700**	**4.500**
3	6.560	6.460	6.360
4	9.840	9.600	9.200
5	13.630	13.430	13.310
6	13.690	13.510	13.310
7	13.710	13.610	13.410
8	13.550	13.450	13.400
9	13.370	13.320	13.300
10	13.270	13.220	13.210
11	13.250	13.200	13.180
12	13.310	13.260	13.210
13	13.440	13.340	13.290
14	13.650	13.560	13.500
15	13.890	13.790	13.710
16	14.190	14.100	14.080

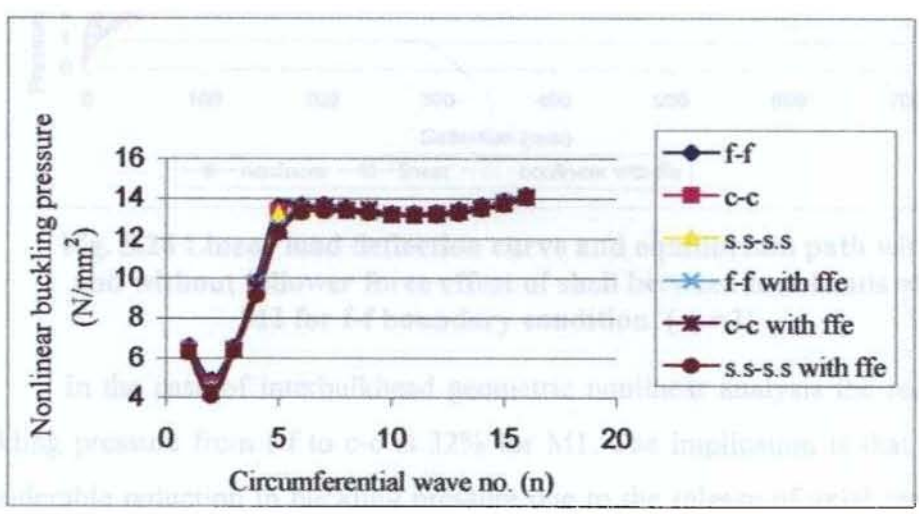

Fig. 5.25 Nonlinear interbulkhead buckling pressures corresponding to wave numbers of M2 with and without follower force effect for various boundary conditions

The collapse pressure values are 4.900 N/mm^2 (n=2), 4.700 N/mm^2 (n =2) and 4.500 N/mm^2 (n=2) for f–f, c–c and s.s-s.s boundary conditions. Comparative

study between linear and nonlinear buckling pressures for f–f, c–c and s.s-s.s boundary conditions are given in table 5.17 and fig. 5.17.

Table 5.17 Comparison of linear and nonlinear interbulkhead buckling pressures of M2 for f-f, c-c and s.s-s.s boundary conditions

Boundary condition	Buckling pressure (N/mm^2) & (n)		% reduction
	Linear	Nonlinear	
f-f	7.150(2)	4.900(2)	31.2
c-c	6.740(2)	4.700(2)	30.3
s.s-s.s	6.510(2)	4.500(2)	30.9

Equilibrium path for f–f boundary condition for M2 is given in fig. 5.26. Linear load–deflection curve is also plotted. Nonlinearity induces a reduction in buckling pressure by 31.2% for f–f, 30.3% for c–c and 30.9% for s.s-s.s boundary conditions.

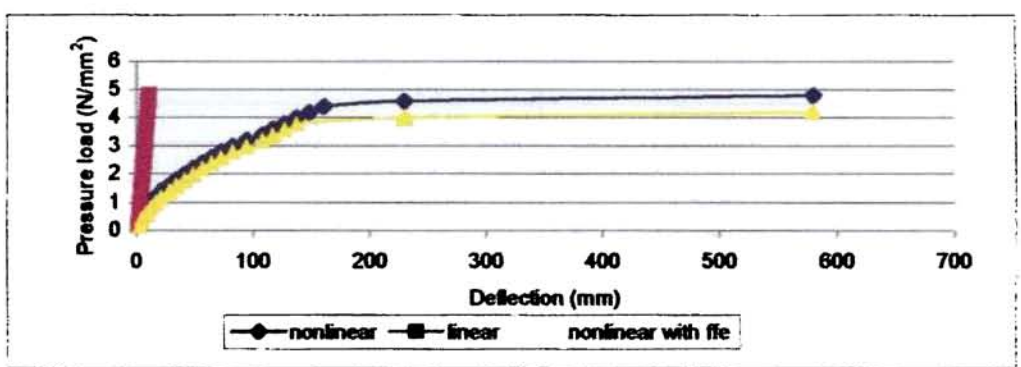

Fig. 5.26 Linear load deflection curve and equilibrium path with and without follower force effect of shell between bulkheads of M2 for f-f boundary condition (n =2)

In the case of interbulkhead geometric nonlinear analysis the reduction in buckling pressure from f-f to c-c is 32% for M1. The implication is that there is a considerable reduction in buckling pressure due to the release of axial restraint (u). But there is no such reduction in buckling pressure due to the release of rotation restraint. The observation that in general instability failure, the influence of rotation restraint is nominal (Brush and Almroth) substantiates authoress' results.

For interbulkhead analysis the reduction in buckling pressure due to geometric nonlinearity is not much sensitive to boundary condition. There is a

reduction in buckling pressure by 18% for M1 and 30% for M2 irrespective of boundary conditions.

For geometric nonlinear analysis, the buckling pressure predicted is critical while considering the interbulkhead configuration with s.s-s.s boundary conditions.

5.6.7 Follower Force Effect of Hydrostatic Pressure

Effect of follower force on nonlinear buckling pressure is analysed for various configurations and boundary conditions. Results are tabulated. Buckling pressure in general is reduced when follower force effect is taken into account. Interstiffener buckling values for M1 for various n values are given in table 5.18. The variation of Pcr with n is shown in fig. 5.13.

Table 5.18 Nonlinear interstiffener buckling pressures for M1 with follower force effect for various boundary conditions

Circumferential wave no. (n)	Nonlinear buckling pressure (N/mm^2)		
	f-f	c-c	s.s-s.s
1	33.740	33.680	15.400
2	33.680	33.602	15.240
3	33.620	33.544	15.202
4	33.580	33.496	15.164
5	33.512	33.446	15.084
6	33.260	33.196	15.012
7	32.916	32.824	14.882
8	32.758	32.688	14.042
9	32.554	32.484	13.704
10	32.364	32.302	**13.100**
11	32.084	32.024	13.282
12	31.790	31.702	13.478
13	31.520	31.440	13.602
14	31.312	31.260	13.882
15	31.110	31.030	13.942
16	30.990	30.902	
17	30.850	30.792	
18	**30.780**	**30.720**	
19	30.800	30.742	
20	30.866	30.800	
21	30.998	30.922	
22	31.140	31.080	
23	31.240	31.188	

For M1 for f-f, c-c and s.s-s.s boundary conditions, the minimum buckling pressures are 30.780 N/mm^2 (n=18), 30.720 N/mm^2 (n=18) and 13.100 N/mm^2 (n=10). The effect of follower force on nonlinear buckling pressure is given in table 5.19 and fig. 5.14.

Table 5.19 Effect of follower force on nonlinear interstiffener buckling pressures for M1 for f-f, c-c and s-s boundary conditions

Boundary condition	Nonlinear buckling pressure (N/mm^2) & (n)		% reduction
	Without follower force effect	With follower force effect	
f-f	30.840(18)	30.780(18)	0.2
c-c	30.780(18)	30.720(8)	0.2
s.s-s.s	13.180(10)	13.100(10)	0.6

The reductions in buckling pressures are 0.2%, 0.2% and 0.6% for f–f, c-c and s.s-s.s boundary conditions respectively. Equilibrium path with and without including follower force effects for f–f boundary condition for M1 is given in fig. 5.15

Interstiffener buckling values for M2 for various n values are shown in table 5.20. The variation of Pcr with n is shown in fig. 5.16.

Table 5.20 Nonlinear interstiffener buckling pressures with follower force effect for M2 for various boundary conditions

Circumferential wave no. (n)	Nonlinear buckling pressure (N/mm^2)		
	f-f	c-c	s.s-s.s
1	14.270	14.160	12.000
2	14.160	14.080	11.700
3	14.100	14.020	11.680
4	14.080	13.980	11.680
5	14.060	13.970	11.480
6	14.060	13.960	11.280
7	14.000	13.920	11.060
8	13.980	13.900	10.800
9	13.960	13.880	10.600
10	13.920	13.840	10.250
11	13.920	13.840	10.080
12	13.900	13.790	10.060
13	13.880	13.780	10.020
14	13.880	13.770	**10.020**
15	13.860	13.760	10.100
16	**13.830**	**13.730**	10.180
17	13.850	13.750	10.340
18	13.960	13.870	10.470
19	14.080	13.960	10.580
20	14.180	13.970	

For M1 for f-f, c-c and s.s-s.s boundary conditions, the minimum buckling pressures are 13.830 N/mm^2 (n = 16), 13.730 N/mm^2 (n =16) and 10.020 N/mm^2 (n=14) respectively.

Table 5.21 Effect of follower force on nonlinear interstiffener buckling pressures corresponding to wave numbers for M2 for f-f, c-c and s.s-s.s boundary conditions

Boundary condition	Nonlinear buckling pressure (N/mm^2) & (n)		% reduction
	Without follower force effect	With follower force effect	
f-f	13.880(16)	13.830(16)	0.4
c-c	13.770(16)	13.730(16)	0.3
s.s-s.s	10.060(14)	10.020(14)	0.4

The effect of follower force on nonlinear buckling pressure is shown in table 5.21 and fig. 5.17. The reduction in buckling pressures are 0.4%, 0.3% and 0.4% for f–f, c-c and s.s–s.s boundary conditions respectively. In general for interstiffener buckling the reduction in buckling pressure due to follower force effect is less than 1% for all types of boundary conditions. For interstiffener buckling, where the shell buckles with large number of waves in circumferential direction, the pressure rotation effect is very much limited. Short shells are not much susceptible to pressure rotation effects (Rajagopalan, 1993) and this feature is reflected in the results.

Equilibrium path with and without follower force effects for f–f boundary condition for M2 is given in fig. 5.18.

Interdeepframe buckling pressure values for M1 for various n values are shown in table 5.22 and summarized in table 5.23 and fig. 5.14. Variation of Pcr with n is shown in fig. 5.19.

Table 5.22 Nonlinear interdeepframe buckling pressures with follower force effect corresponding to wave numbers for M1 for various boundary conditions

Circumferential wave no. (n)	Nonlinear buckling pressure (N/mm^2)		
	f-f	c-c	s.s-s.s
1	22.028	21.998	20.604
2	21.808	21.802	20.302
3	21.824	21.820	**19.150**
4	21.946	21.930	20.808
5	22.034	22.012	21.524
6	22.012	21.988	21.508
7	21.934	21.988	21.360
8	21.820	21.802	21.344
9	21.720	21.684	21.302
10	21.644	21.610	21.280
11	21.582	21.560	21.246
12	**21.540**	**21.530**	21.308
13	21.552	21.540	21.366
14	21.624	21.588	21.486
15	21.738	21.694	21.604
16	21.918	21.884	21.804
17	22.408	22.360	22.020
18	22.978	22.898	22.280

Table 5.23 Effect of follower force on nonlinear interdeepframe buckling pressures for M1 for f-f, c-c and s.s-s.s boundary conditions

Boundary condition	Nonlinear buckling pressure (N/mm^2) & (n)		% reduction
	Without follower force effect	With follower force effect	
f-f	21.620(12)	21.540(12)	0.4
c-c	21.610(12)	21.539(12)	0.3
s.s-s.s	19.230(3)	19.150(3)	0.4

The collapse pressure values for interdeepframe are 21.540 N/mm^2 (n=12), 21.530 N/mm^2 (n=12) and 19.150 N/mm^2 (n=3) for f–f, c–c and s.s-s.s boundary conditions. The effect follower force on nonlinear buckling pressure is given in table 5.23. The reductions in buckling pressures are by 0.4%, 0.3% and 0.4% for M1 for the corresponding boundary conditions. Linear load deflection curve and equilibrium path with and without follower force effects for f–f boundary condition for M1 are given in fig. 5.20.

For M2 the buckling pressure values for various n values are shown in table 5.24 and summarized in table 5.25 and fig.5.17. Variation of Pcr with n is shown in fig. 5.21.

Table 5.24 Nonlinear interdeepframe buckling pressures corresponding to wave numbers with follower force effect for M2 for various boundary conditions

Circumferential wave no. (n)	Nonlinear buckling pressure (N/mm^2)		
	f-f	c-c	s.s-s.s
1	13.730	13.690	13.300
2	13.520	13.480	13.080
3	13.320	13.280	12.890
4	12.640	12.580	11.360
5	11.680	11.644	10.740
6	10.580	10.508	10.160
7	10.108	10.160	9.760
8	9.804	9.770	9.410
9	9.780	9.740	9.326
10	9.620	9.584	9.146
11	9.564	9.502	8.984
12	9.460	9.400	8.902
13	9.400	9.370	**8.900**
14	9.380	9.340	8.924
15	**9.370**	**9.320**	8.955
16	9.420	9.340	8.966
17	9.550	9.440	9.024
18	9.760	9.584	9.078
19	9.894	9.712	9.168

Table 5.25 Effect of follower force on interdeepframe nonlinear buckling pressures for M2 for f-f, c-c and s.s-s.s boundary conditions

Boundary condition	Nonlinear buckling pressure (N/mm^2) & (n)		% reduction
	Without follower force effect	With follower force effect	
f-f	9.460(15)	9.370(15)	1.0
c-c	9.400(15)	9.320(15)	0.9
s.s-s.s	9.000(13)	8.900(13)	1.1

The effect of follower force on nonlinear buckling pressure is obtained by comparing the values given in table 5.25. The collapse pressure values are 9.370 N/mm^2 (n=15), 9.320 N/mm^2 (n=15) and 8.900 N/mm^2 (n=13) for f–f, c–c and s.s-s.s boundary conditions. There is a reduction in buckling pressure by 1.0%, 0.9% and 1.1% for M2 for the above-mentioned boundary conditions. The follower force effect is negligible, since the shell is a short one and buckles with more number of waves in the circumferential direction. Linear load deflection curve and equilibrium path with and without including follower force effects for f–f boundary condition M2 is given in fig. 5.22.

Interbulhead buckling pressure values for M1 for various n values are shown in table 5.26 and summarized in table 5.27 and fig. 5.14. Variation of Pcr with n is shown in fig. 5.23.

Table 5.26 Nonlinear interbulkhead buckling pressures with follower force effect for M1 for various boundary conditions

Circumferential wave no. (n)	Nonlinear buckling pressure (N/mm^2)		
	f-f	c-c	s.s-s.s
1	19.440	19.400	19.360
2	**9.100**	**6.310**	**6.300**
3	15.320	15.280	15.020
4	17.060	17.020	16.890
5	20.020	19.980	19.370
6	22.480	22.400	22.320
7	23.640	23.580	23.520
8	23.900	23.900	23.700
9	24.200	24.120	24.060
10	24.820	24.700	24.600
11	25.020	24.920	24.880
12	25.200	25.100	25.020
13	25.360	25.300	25.200
14	25.500	25.400	25.300
15	25.820	25.560	25.420
16	26.020	25.940	25.880

Table 5.27 Effect of follower force on nonlinear interbulkhead buckling pressures for M1 for f-f, c-c and s.s-s.s boundary conditions

Boundary condition	Nonlinear buckling pressure (N/mm^2) & (n)		% reduction
	Without follower force effect	With follower force effect	
f-f	12.400(2)	9.320(2)	24.8
c-c	8.450(2)	6.310(2)	25.3
s.s-s.s	8.450(2)	6.300(2)	25.4

The effect of follower force on nonlinear buckling pressure is obtained by comparing the values given in table 5.27 and fig. 5.14. The collapse pressure values for general instability failure are 9.320 N/mm^2 (n=2), 6.310 N/mm^2 (n =2) and 6.300 N/mm^2 (n=2) for M1. There is a reduction in buckling pressure by 24.8%, 25.3% and 25.4% for M1 for f–f, c–c and s.s-s.s boundary conditions. Equilibrium path including pressure rotation effects along with linear load – deflection curve for f–f boundary condition for M1 is given in fig. 5.24

For M2 the buckling pressure values for various n values are shown in table 5.28 and summarized in table 5.29 and fig. 5.17. Variation of Pcr with n is shown in fig. 5.25.

Table 5.28 Nonlinear interbulkhead buckling pressures corresponding to wave numbers with follower force effect for M2 for various boundary conditions

Circumferential wave no. (n)	Nonlinear buckling pressure (N/mm^2)		
	f-f	c-c	s.s-s.s
1	6.480	6.320	6.280
2	**4.500**	**4.300**	**4.120**
3	6.500	6.410	6.310
4	9.790	9.530	9.130
5	12.580	12.370	12.280
6	13.620	13.460	13.280
7	13.670	13.570	13.380
8	13.510	13.410	13.360
9	13.320	13.480	13.260
10	13.240	13.190	13.160
11	13.210	13.160	13.140
12	13.250	13.210	13.170
13	13.400	13.310	13.252
14	13.612	13.526	13.464
15	13.854	13.742	13.686
16	14.156	14.064	14.022

Table 5.29 Effect of follower force on nonlinear buckling pressures for shell between bulkheads of M2 for f-f, c-c and s.s-s.s boundary conditions

Boundary condition	Nonlinear buckling pressure (N/mm^2) & (n)		% reduction
	Without follower force effect	With follower force effect	
f-f	4.900(2)	4.500(2)	8.2
c-c	4.700(2)	4.300(2)	8.5
s.s-s.s	4.500(2)	4.120(2)	8.4

The collapse pressure values for general instability failure are 4.500 N/mm^2 (n=2), 4.300 N/mm^2 (n=2) and 4.120 N/mm^2 for M2 for f–f, c–c and s.s-s.s boundary conditions.

The effect of follower force on nonlinear buckling pressure effect is obtained by comparing the values given in table 5.29. There is a reduction in buckling pressure by 8.2%, 8.5% and 8.4% for M2 for f–f, c–c and s.s-s.s boundary conditions. The follower force effect of hydrostatic pressure has very high detrimental effect in the case of general instability failure, exhibited by long shells in which shell buckles with 2 or 3 waves in the circumferential direction. The collapse pressure reduction due to pressure rotation effect is about 25% for M1.

Equilibrium path or nonlinear load deflection curve with and without including pressure rotation effects for f–f boundary condition for M2 is given in fig. 5.26. Linear load – deflection curve is also plotted along with the equilibrium path.

The buckling pressure predicted is minimum for interbulkhead configuration and has to be dealt with prime importance. The critical value of buckling pressure is obtained by considering both geometric nonlinearity and follower force effect together for s.s-s.s boundary condition for M1 and M2.

5.6.8 Combined Effect of Geometric Nonlinearity and Follower Force on Buckling Pressure

The reduction in buckling pressures on considering the geometric nonlinearity and follower force effect in various configurations and boundary conditions are summarized in table 5.30.

Table 5.30 The overall % reduction in buckling pressures on considering the geometric nonlinearity and follower force effect for M1 &M2

Submarine models	Cylindrical shell configuration	Boundary condition	Overall % reduction in buckling pressure
M1	Interstiffener	f-f	23.7
		c-c	23.7
		s.s-s.s	20.0
	Interdeepframe	f-f	11.1
		c-c	11.2
		s.s-s.s	11.3
	Interbulkhead	f-f	38.8
		c-c	38.1
		s.s-s.s	37.9
M2	Interstiffener	f-f	13.5
		c-c	13.5
		s.s-s.s	14.1
	Interdeepframe	f-f	19.6
		c-c	19.7
		s.s-s.s	19.0
	Interbulkhead	f-f	37.1
		c-c	36.2
		s.s-s.s	36.7

For interstiffener analysis, the reduction in buckling pressures are 23.7%, 23.7% and 20.0% for M1 and 13.5%, 13.5% and 14.1% for M2 for f–f, c-c and s.s-s.s boundary conditions respectively.

For between deepframes analysis, the reduction in buckling pressures are 11.2%, 11.2% and 11.3% for M1 and 19.6%, 19.7% and 19.0% for M2 for f–f, c–c and s.s-s.s boundary conditions respectively.

For between bulkheads analysis, the reduction in buckling pressures are 38.8%, 38.1% and 37.9% for M1 and 37.1%, 36.2% and 36.7% for M2 for f–f, c–c and s.s-s.s boundary conditions respectively.

5.6.9 Safety Factor

Safety factors (i.e., ratio of collapse pressures to the design pressures) for stiffened cylindrical hull of attack submarines M1 and M2 from numerical investigations based on finite element method are calculated for various configurations and boundary conditions. The values are given in table 5.31.

Table 5.31 Safety factor against buckling for various configurations and boundary conditions for M1 &M2

Submarine models	Cylindrical shell configuration	Boundary condition	Safety factor
M1	Interstiffener	f-f	10.20
		c-c	10.18
		s.s-s.s	4.34
	Interdeepframe	f-f	8.58
		c-c	7.13
		s.s-s.s	6.34
	Interbulkhead	f-f	3.09
		c-c	2.09
		s.s-s.s	2.08
M2	Interstiffener	f-f	4.58
		c-c	4.55
		s.s-s.s	3.32
	Interdeepframe	f-f	3.10
		c-c	3.09
		s.s-s.s	2.95
	Interbulkhead	f-f	1.49
		c-c	1.42
		s.s-s.s	1.36

Classical solutions for radial deflection, shell buckling, shell yielding and general instability are available in literature and are reviewed in chapter 2. A software is developed based on these equations and numerical investigations are carried out for M1 and M2. The details of the equations, software and numerical

investigations are given in Appendix B. Table 5.32 gives the collapse pressure and safety factor predicted for M1 and M2.

Table 5.32 Collapse pressure predicted and safety factors from classical solutions for M1 and M2

Model	Classical solution	Collapse pressure (N/mm^2)	Safety factor
M1	Windenburg's formula (shell buckling)	39.978	13.25
	Bryant's formula (general instability)	25.37 (n=2)	8.41
	Yielding at midbay (Von Sanden and Gunther)	16.60	5.50
	Yielding at frame (Von Sanden and Gunther)	13.33	4.42
M2	Windenburg's formula (shell buckling)	19.51	6.47
	Bryant's formula (general instability)	38.23(n=2)	12.68
	Yielding at midbay (Von Sanden and Gunther)	6.72	2.22
	Yielding at frame (Von Sanden and Gunther)	9.45	3.13

On considering the shell buckling, the minimum value of safety factor will be for simply supported boundary condition i.e., 4.34 and 3.32 for M1 and M2 respectively (table 5.31). On considering the Windenburg's formula the corresponding values are 13.25 and 6.47 (table 5.32), which are closer to the values while considering f-f boundary conditions i.e., 10.20 and 4.58 for M1 and M2 respectively. Collapse pressure predicted by Windenburg's equation is much higher than the corresponding value predicted by finite element method.

On considering the case of general instability, between bulkhead's analyses gives the minimum buckling pressure. The safety factor on considering the simply supported boundary condition is 2.088 and 1.366 for M1 and M2 respectively. According to Bryant's formula the safety factor values are 8.41 and 12.67 for M1 and M2 respectively. The analysis of results pinpoints to the necessity of proper finite element analysis.

The empirical relation i.e., von Sanden and Gunther's relation to find the yield stress gives a safety factor against yielding at midbay as 5.50 and 2.22 for M1

and M2. The inference is that the classical solution of von Sanden and Gunther is less conservative compared to finite element solution.

The various rulebooks for the design of submarines, IS, LRS and DnV give provisions for the prediction of design pressure of stiffened cylindrical shells for the given scantlings. A software based on these provisions is available elsewhere (Sreekala, 1997). The design pressure for M1and M2 based on IS, LRS and DnV code provisions are estimated using the above- mentioned software and is shown in table 5.33.

Table 5.33 Design pressure predicted by Rulebooks for M1 and M2

No.	Rulebook	Design pressure predicted (N/mm^2)	
		M1	M2
1	IS 2825	3.389	1.864
2	LRS	7.693	6.812
3	DnV	4.103	3.633

The design pressure predicted by IS 2825 are 3.389 N/mm^2 and 1.864 N/mm^2 for M1 and M2 respectively. The corresponding values predicted by LRS are 7.693 N/mm^2 and 6.812 N/mm^2 and by DnV are 4.103 N/mm^2 and 3.633 N/mm^2 for M1 and M2 respectively. On analysing the results, a comparative study of various code provisions is made. The critical study of code provisions highlights the under estimation or over estimation of strength, which may cause conservative or inadequate design. On analyzing the results it may be concluded that IS code is more conservative than LRS and DnV and may be advised for a revision.

CHAPTER 6
CONCLUSIONS

6.1 GENERAL

Software has been developed based on the finite element formulations for the elastic and buckling analysis of stiffened cylindrical shells. Numerical investigations are conducted using the software and the results have been discussed. Conclusions and major observations from this study are presented under the subsequent headings, linear static analysis, linear buckling analysis and geometric nonlinear analysis.

6.2 LINEAR STATIC ANALYSIS

Software has been developed for linear static analysis of stiffened cylindrical submarine shells based on discrete stiffener cylindrical shell finite element model in which shell is modeled using all-cubic axisymmetric cylindrical shell finite element and stiffeners using discrete ring stiffener element. The software has been validated using Flugge's problem.

A linear static analysis has been carried out for stiffened cylindrical shells of attack submarine models M1 and M2, having a design operational depth of 300m. The submarine cylindrical hull has been analysed for three configurations, viz., cylindrical shell between stiffeners (interstiffener), stiffened cylindrical shell between deepframes (interdeepframe) and stiffened cylindrical shell between bulkheads (interbulkhead). The analysis has been carried out for fixed-fixed boundary condition and stress resultants, principal stresses and displacements are plotted.

The maximum values of principal stresses occur at the outer layer of midbay of stiffeners while considering the shell between bulkheads, which can be considered critical.

6.3 LINEAR BUCKLING ANALYSIS

Software has been developed for linear buckling analysis of stiffened cylindrical shells using all-cubic axisymmetric cylindrical shell element and discrete ring stiffener element using relevant geometric stiffness matrices of the above-mentioned elements and has been validated using Kendrick's problems. The element has shown satisfactory convergence.

The influence of derivatives of displacements used as degrees of freedom on buckling pressure has been studied. It has been concluded that arresting these degrees of freedom has nominally (4.7%) increased the buckling pressure. The influence of support restraint on linear buckling pressure has been studied by considering the end conditions as simply supported-simply supported, clamped – clamped and fixed – fixed. Kendrick's problem has been analysed for interstiffener buckling and descending order of buckling pressure is observed from fixed-fixed to simply supported-simply supported boundary condition.

Stiffened cylindrical shell of Kendrick' example has been investigated incorporating various boundary conditions. The influence of end restraint is nominal and is in the descending order from fixed-fixed to clamped-clamped to simply supported-simply supported as expected.

Linear buckling analysis has been carried out for stiffened cylindrical shells of attack submarines. Linear buckling analysis has been carried out for interstiffener, interdeepframe and interbulkhead configurations and may be considered as a parametric study for various L/R ratios.

The scope of the numerical investigation includes the study to realize the influence of various boundary conditions, which reflects the effect of end restraint.

From the interstiffener buckling analysis results, it can be observed that for simply supported boundary condition the interstiffener buckling pressure is the lowest and collapse occurs at less value of n compared to clamped and fixed boundary conditions. The collapse pressure predicted for fixed boundary condition is

the highest and is at a higher value of n, which shows the significance of the selection of appropriate boundary condition in the investigation.

For simply supported boundary condition the ends will have more flexibility and hence will have more effective length and buckling occurs with less number of circumferential waves. Fixity reduces the effective length and the shell in effect becomes shorter and buckles with more number of waves in the circumferential direction.

On considering the influence of end restraints on interstiffener buckling pressure the following conclusions have been arrived at. For short shells buckling pressure is susceptible to rotation restraints at the ends indicated by higher buckling pressure for fixed-fixed and clamped-clamped boundary conditions. The effect of rotation restraint is smoothened on increasing L/R ratio. The influence of axial restraint 'u' is not significant indicated by the same value of buckling pressure for fixed-fixed and clamped-clamped boundary conditions and becomes prominent on increasing the L/R ratio.

In general, with same end restraint shorter shell buckles with higher waveform. The effect of L/R ratio on buckling pressure and on circumferential wave number is more pronounced in the case of fixed and clamped (rotation restraint) boundary condition. But for simply supported boundary condition this effect is not there because of greater flexibility at the boundary.

The shell between deepframes can be considered as a short shell in both cases (M1 is shorter and thicker than M2). The failure occurs by interframe buckling rather than by general instability. Interframe buckling is less susceptible to boundary conditions compared to interstiffener buckling cases. In the case of interframe buckling the shell buckles with more lobes in longitudinal direction (rapidly varying function) and hence less vulnerable to end restraints. There is not much difference in circumferential wave numbers corresponding to the lowest buckling pressure for various boundary conditions.

The effect of end restraint becomes smoothened on transition from interstiffener to interdeepframe configuration and change in buckling pressure due to the release of axial restraint is negligibly small.

In M2 the stiffeners are well arranged between deepframes such that there is not much difference between interstiffener and interdeepframe buckling pressures. Comparison of values with interstiffener collapse pressure gives an impression that the spacing and size of stiffeners are adequate. Two types of failures occur simultaneously, which can be considered as the optimum design criteria. But in the case of M1, the spacing between stiffeners and bulkheads can be slightly increased. From a few trials optimum dimensions and spacing of stiffeners can be found out, which satisfies the functional requirements.

On considering the shell between bulkheads, which is comparatively a long shell (L/R ratio 3.42 for M1 and 4.59 for M2) the shell buckles with less number of waves in the circumferential direction. The cylinders will collapse in an overall manner. The general instability failure occurs at a circumferential wave number 2 or 3. Thereafter the buckling pressure increases and apparently reaches a maximum value and decline again to give a second local minimum at a harmonic number of 11 or 12, depending on the boundary conditions. The lower value of n refers to general instability i.e., one lobe in the longitudinal direction. The higher value of n refers to interframe buckling mode with as many longitudinal lobes as the frame spaces.

For interbulkhead buckling, the effect of rotation restraint becomes negligibly small indicated by the same buckling pressure for clamped-clamped and simply supported-simply supported boundary conditions. The change in buckling pressure due to the release of axial restraint becomes more significant as indicated by a considerable reduction in buckling pressure from fixed-fixed to clamped–clamped boundary condition.

The follower force effect of hydrostatic pressure on linear buckling pressure has been investigated for M1 and M2 for the three configurations – viz., interstiffener, interdeepframe and interbulkhead for the above-mentioned boundary conditions, the following conclusions are derived from the results.

For interstiffener and interdeepframe buckling where shell buckles with large number of waves in circumferential direction, follower force effect is less significant (reduction in buckling pressure is less than 1%). The above-mentioned observation may be due to the reason that in those cases the buckling displacement functions are rapidly varying functions of circumferential coordinates.

Between bulkhead analysis follower force effect is much more significant. There is a reduction in buckling pressure by 31%for M1 and 9% for M2 for various boundary conditions. The follower force effect of hydrostatic pressure has very high detrimental effect in the case of general instability failure, which is the case of long shells in which shell buckles with 2 or 3 waves in the circumferential direction.

For M1, failure may be due to one lobe in longitudinal direction and two waves in circumferential direction and follower force effect becomes prominent since there is no abrupt change in direction. But in the case of M2, which is longer with two intermediate deepframes, the shell buckles with three lobes in longitudinal direction and hence the reduction in buckling pressure due to follower force effect is less.

6.4 GEOMETRIC NONLINEAR ANALYSIS

Software has been developed for geometric nonlinear analysis of stiffened cylindrical submarine shells based on discrete stiffener cylindrical shell finite element model in which shell is modeled using all-cubic axisymmetric cylindrical shell finite element and stiffeners using discrete ring stiffener element. Methodology adopted is load control incremental iterative procedure. Corotational kinematics is used for the generation of tangent stiffness matrix. The software has been validated using Moradi and Parsons' problem.

Equilibrium path is drawn and the limitpoint buckling pressure is determined and almost in all cases the tangent stiffness matrix becomes singular in the vicinity of the limit point.

From the results of geometric nonlinear analysis for Kendrick's example BMP2 for fixed-fixed, clamped-clamped and simply supported-simply supported boundary conditions, it is observed that there is a considerable reduction in buckling

pressure due to geometric nonlinearity, which demands to the necessity of geometric nonlinear analysis in the prediction of collapse pressure.

Geometric nonlinear analysis has been extended to stiffened cylindrical shell of Kendrick's model BMP3 and it is seen that there is about 25% reduction in buckling pressure irrespective of boundary conditions. Analogous to the observations in linear buckling analysis, the nonlinear buckling pressure is less susceptible to boundary conditions. The type of boundary condition does not have much effect on the circumferential wave number at which the buckling occurs.

Geometrically nonlinear analysis has been carried out for stiffened cylindrical shells of M1 and M2. Analysis has been conducted for the three configurations viz., interstiffener, interdeepframe and interbulkhead. The variations of buckling pressures with circumferential wave numbers are predicted and compared. The scope of the numerical investigations has been extended to realize the influence of possible boundary conditions. The ends have been treated as fixed–fixed, clamped–clamped and simply supported - simply supported. A comparative study has been made between linear and nonlinear buckling pressures for M1 and M2 for the above-mentioned configurations and boundary conditions.

For interstiffener configuration the buckling pressures are reduced by 23% for M1 and 13% for M2 for f–f and c–c boundary conditions and also a reduction in circumferential wave number as well.

The prebuckling deformations of the unstiffened shell cause softening of the shell, resulting in lower buckling pressure as well as lower circumferential wave number. The nonlinear buckling pressure value is less vulnerable to higher circumferential wave number indicated by the flattening of Pcr Vs n curve compared to that of linear buckling analysis.

The effect of L/R ratio on buckling pressure and on circumferential wave number has been found similar to that of linear buckling analysis but is not as pronounced as in the case of linear buckling analysis. The reduction in buckling

pressure due to the incorporation of geometric nonlinearity is not much influenced by the effect of boundary condition.

For the interdeepframe configuration geometric nonlinearity reduces buckling pressure and the corresponding circumferential wave number.

Reduction in nonlinear buckling pressure for the release of rotation restraint is analogous to that of linear buckling pressure. The effect of axial restraint (u) is negligible. The interdeepframe nonlinear buckling pressures are less susceptible to boundary conditions compared to interstiffener buckling pressures.

For interbulkhead configuration there is considerable reduction of buckling pressure reported (32.0% for M1) by virtue of release of axial restraint. But there is no such reduction in buckling pressure due to the release of rotation restraint.

In all the three configurations, the change in percentage reduction in nonlinear buckling pressure by the change boundary has been meager.

The follower force effect of hydrostatic pressure has been studied for M1 and M2 for various configurations and boundary conditions and following conclusions are arrived at. The follower force effect is less pronounced in geometrically nonlinear analysis compared to linear buckling analysis and its effect is almost negligible in the case of interstiffener and interdeepframe analyses. Whereas, the follower force effect of hydrostatic pressure has very high detrimental effect for interbulkhead configuration in which the shell buckles with 2 or 3 waves in the circumferential direction. The collapse pressure has been reduced by the pressure rotation effect by about 25% for M1 and 8% for M2.

6.5 OVERALL REDUCTION IN BUCKLING PRESSURE

From the observation of critical buckling pressure values for various configurations and boundary conditions it has been concluded that the reduction in buckling pressure is maximum for general instability failure between bulkheads and is about 38% for M1 and 37% for M2. Based on the present study, the geometric

nonlinear interbulkhead analysis is found critical and hence recommended for submarine pressure hull design.

6.6 SAFETY FACTOR FROM CLASSICAL SOLUTIONS AND DESIGN PRESSURE FROM RULEBOOK PROVISIONS

The software for the estimation of safety factor for submarine cylindrical shell, based on Windenburg's formula, Bryant's formula and von Sanden and Gunther's formulae is operational in pc environment.

The safety factors for M1 and M2 evaluated using this software shows wide deviations (4.42 to 13.25 and 2.22 to 12.68 respectively)

The software for the calculation of the design pressure of stiffened cylindrical shell based on provisions in IS 2825, LRS and DnV is operational and has been used to estimate the design pressure of M1 and M2.

These values vary from 3.4 to 7.7 N/mm^2 and 1.9 and 6.8 N/mm^2 respectively against 3.016 N/mm^2 (pressure considered for the design based on operational depth).

The classical solutions and Rulebook provisions overestimate the safety factor. These may be used for the preliminary design of scantlings where as geometric nonlinear finite element analysis has to be adopted for the prediction of collapse pressure.

6.7 SCOPE FOR FUTURE WORK

Instead of a shell-discrete ring stiffener model, a ring stiffened cylindrical shell element itself may be developed.

The analysis can be extended by incorporating nonlinearity due to large strains and material nonlinearity together with geometric nonlinearity.

The inertia matrix can also be included along with elastic, geometric and pressure stiffness matrices to predict the nonlinear buckling pressure to check whether it is a dynamic criterion.

By incorporating classical solutions and finite element analysis a package for optimum design of stiffened cylindrical hull based on reliability criteria can be developed.

REFERRENCES

1. Arentzen, E.S., Mandel, P., Naval Architectural Aspects of Submarine Design, Transaction of SNAME, Vol. 68, pp. 622-692, 1960.
2. Barlag, S., Robert, H., An Idealization Concept for the Stability Analysis of Ring Reinforced Cylindrical Shells Under External Pressure, International Journal of Nonlinear Mechanics, Vol.37, Issue 4-5, pp. 745-756, 2002.
3. Baruch, M., Singer, J., Effect of Eccentricity of Stiffeners on the General Instability of Stiffened Cylindrical Shell Under Hydrostatic Pressure, Journal Mechanical Engineering Sciences, Vol. 5, No. 1, pp. 23-27, 1963.
4. Batdorf, S.B., A simplified Method of Elastic Stability for Thin Cylindrical Shells, NACA Report No.874, 1947.
5. Bathe, K. J., Finite Element Procedures in Engineering Analysis, Prentice Hall, pp. 485-641, New Jersey, 2001.
6. Bijlaard, P.P., Buckling Under External Pressure of Cylindrical Shells Evenly Stiffened by Rings Only, Journal of Aerospace Sciences, June1957.
7. Bodner, S.R., On the Conservativeness of Various Distributed Force Systems. Journal of the Aeronautical Sciences, Vol. 25, pp. 132-133, 1958.
8. Bodner, S.R., Analysis of General Instability of Ring Reinforced Circular Cylindrical Shells of Orthotropic Shell Theory, Journal of Applied Mechanics, Vol. 24, No. 2, 1957.
9. Brush, D.O. and Almroth, Buckling of Bars, Plates and Shells, McGraw-Hill, Kogakusha. Ltd., pp. 40-189, 1975.
10. BS 5500, British Standard Institution specification for Unfired Fusion Welded Pressure Vessels, HMSO, 1976.
11. Burcher, R., Rydill, L., Concepts in Submarine Design, Cambridge Ocean Technology Series-2, Cambridge University Press, pp. 71-99, 1994.
12. Bushnell, D. and Bushnell, W.D., An Approximate Method for the Optimum Design of Ring and Stringer Stiffened Cylindrical Panel and Shells with Local Inter-ring and General Buckling Modal Imperfections. Computers and structures, Vol. 59, No.3, pp. 489-527, 1996.

13. Carnoy, E.G., Guennoun, N., Sander, G., Static Buckling Analysis of Shells Submitted to Follower Pressure by the Finite Element Method, Computers & Structures, Volume 19, Issues 1-2, pp. 41-49, 1984.

14. Chen, Wen, Ren,Wen-Min,Zhang Wei, Buckling Analysis of Ring Stiffened Cylinderical Shells with Cutouts BY Mixed Method of Finite Strip and Finite Element, Computer and Structures, Vol. 53, Issue 4, pp. 811-816, 1994.

15. Combescure, A., Gusic, G., Nonlinear Buckling of Cylinders Under External Pressure with Nonaxisymmetric Thickness Imperfections Using the COMI Axisymmetric Shell Element, International Journal of Solids and Structures, Vol.38, Issues 34-35, pp. 6207-6226, August 2001.

16. Cook, R.D., Malkus, D.S., Plesha, M.E., Concepts and Applications of Finite Element Analysis, John Wiley & Sons, pp. 529-533, 1989.

17. Cook, W.A., A Finite Element Model for Nonlinear Shells of Revolution, International Journal for Numerical Methods in Engineering, Vol.15, pp. 135-142, 1982.

18. Cormstock, P. M., Principles of Naval Architecture, 3rd Ed., Society of Naval Architects and Marine Engineers, New York, pp. 206-219, 1988.

19. Correia, I.F.P., Barbosa, J.I., Critovao, M., Soares, M.,Carlos, A, Soares, M.A., Finite Element Semi analytical Model for Laminated Axisymmetric Shells, Static, Dynamic and Buckling, Computers and Structures, Vol. 76, pp. 299-317, 2000.

20. Crisfield, M.A., Incremental/Iterative Solution Procedures for Nonlinear Structural Analysis in Numerical Methods for Nonlinear Problems, Pineridge Press, Swansea, U.K., pp. 1-22, 1980.

21. Crisfield, M.A., Incremental/Iterative Algorithm that Handles Snapthrough, Computers and Structures, Vol. 13, pp. 55-62, 1981.

22. Daniel, R.J., Considerations Influencing Submarine Design. Proceedings of the Symposium of Naval Submarines, London, United Kingdom, May 1983.

23. Das, P.K., Zanic, Vendran, Faulkner, Douglas, Reliability based Design Procedure for Stiffened Cylinder Using Multimedia Optimization Technique.

Proceedings of 25th Annual Offshore Technology Conference, Part 3, USA, 1997.

24. Det Norske Veritas, Design of Submarine Hulls, 1996.

25. Donnell, L.H, Beams, Plates and Shells, McGraw Hill, New York, 1976.

26. Faulkner, D., The Collapse Strength and Design of Submarines, Proceedings of the Symposium on Naval Submarines, May 17, London, RINA, 1983.

27. Felipp.a, C.A., Lecture Notes in Nonlinear Finite Element Method, Center for Aerospace Structures, Boulder, Colorado, 1999.

28. Flugge, W., Stresses in Shells, Springer-Verlag, Berlin, 1962.

29. Galletly, G.D., Slankard, R.C., Wenk, E., General Instability of Ring Stiffened Cylindrical Shells Under External Pressure- A Comparison of Theory and Experiment, ASME, 1957.

30. Giacofci, T.A., Modeling Techniques for ADINA Analysis of Stiffened Shell Structures, Computers and Structures, Vol. 13, pp. 601-605,1981.

31. Gorman, J.J., Louie L. L., Submersible Pressure Hull Design Parametrics, SNAME Transactions, Vol. 9, pp. 119-146, 1991.

32. Goswami, S., Mukopadhyay, M., Geometrically Nonlinear Analysis of Laminated Stiffened Shells, Journal of Reinforced Plastics and Composites, Vol.14, No. 12, Dec 1995.

33. Gould, P.L, Finite Element Analysis of Shells of Revolution, Pitman, Marshfield, 1985.

34. Gould, P. L., Hara T., Recent Advances in Local–Global FE Analysis of Shells of Revolution, Thin-Walled Structures, Vol. 40, Issues 7-8, pp. 641-649, 2002.

35. Grafton, P.E. and Strome, D.R. Analysis of Axisymmetric Shells by Direct Stiffness Method, AIAA Journal 1, pp. 2342-2347,1963.

36. Greene, B.E., Strome, D.R., Weikel, R.C., Application of Stiffness Method to the Analysis of Shell Structures, Proc. of Conference of ASME, Los Angeles, 1961.

37. Gusic, G., Comberscure, A., Jullien, J.F., The Influence of Circumferential Thickness Variations on the Buckling of Cylindrical Shells Under External Pressure, Computers and Structures, Vol. 74, pp. 461-477, 2000.

38. Hasegawa, A., Matsuno, T., Nistino, F., Elastic Instability and Nonlinear Analysis of Thin Walled Members Under Nonconservative Forces, Structural Engineering/Earth Quake Engineering, Vol. 5, No.1, pp. 1055-1185, 1988.

39. Herrmann, G., Bungay, R.W., On Stability of Elastic Systems Subjected to Nonconservative Forces, Transactions of ASME, pp. 435-440,1964.

40. Hibbit, H.D., Some Follower Forces and Load Stiffness, IJNME. Vol.14, pp. 937-41, 1979.

41. Huang, J., Wierzbicki, T., Plastic Tripping of Ring Stiffeners, Journal of Structural Engineers, Vol. 119, No. 5, pp. 1623-1642, 1993.

42. Hughes, T.J.R., Hinton, E., Finite Element Method for Plate and Shell Structures, Vol. 1: Element Technology; Vol. 2 Formulation and Algorithms, Pineridge, Swansea, 1986.

43. Indian Standard Code for Unfired Pressure Vessels, IS 2825,1977.

44. Jackson, H.A., Submarine Parametrics, Proceedings of the Symposium of Naval Submarines, London, United Kingdom, RINA, 1983.

45. Jackson, H.A., Fundamentals of Submarine Concept Design, SNAME Transactions. Vol.100, pp. 419-448, 1992.

46. Jacob, A.S., Design of 3000 Tonnes Attack Submarine Speed 22 Knots, Undergraduate Project Report, Department of Ship Technology, CUSAT, 1989.

47. Kaminsky, E.L., General Instability of Ring Stiffened Cylinders with Clamped Edges under External Pressure by Kendrick's Method, D.T Report No.855, 1954.

48. Karabalis, D.L., Simplified Analysis of Stiffened Cylindrical Shells With Cutouts, Computers and Structures, vol. 7, pp. 47-58, 1992.

49. Kasagi,A., Sridharan,S., Imperfection Sensitivity of Layered Composite Cylinders, Journal of Engineering Mechanics, pp. 810-818, July,1995.

50. Kempner, Joseph, Misovec, A. D., and Herzner F. C., Ring Stiffened Orthotropic Circular Cylindrical Shell Under Hydrostatic Pressure, Ocean Engineering, Vol.1, Issue 5, pp. 575-595, February 1970.

51. Kendrick, S. B., Buckling Under External Pressure of Ring Stiffened Circular Cylinders with Evenly Spaced Frames, NCRE Report R-244, 1953.

52. Kendrick, S.B., Buckling Under External Pressure of Ring Stiffened Circular Cylinders, Trans. of RINA, Vol.107, No.1, pp. 139 –155, 1965.

53. Kendrick, S.B., Externally Pressurized Vessels. Stress Analysis of Pressure Vessels and Pressure Vessel Components, Pergamon Press, London, 1970.

54. Kohnke, C.P, Schnobrich,W.C, Analysis of Eccentrically Stiffened Cylindrical Shells, Journal of Structural Division, Proceedings of ASCE, Vol. 7, No.98, pp. 1493-1510,1972.

55. Koiter, W.T., Elishakoff, I., Li, Y.W., Buckling of an Axially Compressed Cylindrical Shell of Variable Thickness, International Journal of Solids and Structures, Vol. 31, No.6, pp. 797-805, 1994.

56. Kraus, H., Thin Elastic Shells, Wiley, New York, 1967.

57. Krishnamoorthy, C.S., The Finite Element Analysis-Theory and Programming, Tata McGraw Hill Book Company, 1987.

58. Li, Y.B., Peter, B.J., Tim, W.B., Adaptive Finite Element Analysis of Stiffened Shells, Advances in Software, Vol. 28, No. 8, pp. 501-507, 1997.

59. Loganathan, R., Chang, S.C., Gallenger, R.H., Abel, J.F., Short Communications- Finite Element Representation and Pressure Stiffness in Shell Stability Analysis. International Journal for Numerical Methods in Engineering, Vol.14, pp. 1413-1429, 1979.

60. Mang, H.A., Symmetricability of Pressure Stiffness Matrix for Shells with Loaded Free Edges, International Journal for Numerical Methods in Engineering, Vol.15, pp. 981-990, 1980.

61. McDonald, J.R. and White, K.R., Effect of out-of Roundness on Elastic Instability of Thin Circular Cylindrical Shells, Proceedings Symposium on Hydromechanically Loaded Shells, University Press, Hawaii, Honolulu, pp. 442-456, 1973.

62. Moradi, B. and Parsons, I.D., A Comparison of Techniques for Computing the Buckling Loads of Stiffened Shells, Computers and Structures, Vol. 46, No. 3, pp. 505-514, 1993.

63. Mutoh, Itaru, Kato,Shiro, Chiba Y., Alternate Lower Bound Analysis of Thin Shells of Revolution. Engineering Computations, Vol.13, No.24, pp. 41-75, 1996.

64. Nash, W.A., General Instability of Ring Stiffened Cylindrical Shell Subject to Hydrostatic Pressure, Proc. 2nd National Congress of Applied Mechanics, 1954.

65. Navaratna, D.R., Pian, T.H.H., Witmer, E.A., Stability of Shells of Revolution by Finite Element Method, AIAA Journal, Vol. 6, No.2, pp. 355-361, 1968.

66. Neto, Miguel Mattar, Miranda Carlos A.J., Evaluation of Collapse Pressure of a Ring Stiffened Cylindrical Shell Under External Hydrostatic Pressure using Code Formulations and FER, Pressure Vessels and Piping Division, ASME, Vol. 338, No. 1, 1996.

67. Novozhilov, V.V., Theory of Thin Elastic Shells, Groningen, 1959.

68. Oden, J.J, Note on Approximate Method for Computing Nonconservative Generalized Forces on Finitely Deformed Finite Elements, AIAA Journal, Vol. 8, No. 11, pp. 2088-2090, 1970.

69. Omurtag, M.H., Akoz A.Y., A Compatible Cylindrical Shell Element for Stiffened Cylindrical Shell in a Mixed Finite Element Formulation, Computers and Structures, Vol. 42, No. 5, pp. 751-768,1992.

70. Pegg, N.G., Numerical Study on Dynamic Pulse Buckling of Ring Stiffened Cylinders, Computers and Structures, Vol. 44, No.6, pp. 1205-1214, 1992.

71. Percy, J.H., Pian,T.H.H., Klein,S., and Navaratna, D.R., Application of Matrix Displacement Method for Linear Elastic Analysis of Shells of Revolution, AIAA Journal, pp. 2138-2145,1965.

72. Popov, E.P, Penzien, J. and Lu, Z.A., Finite Element Solution of Axisymmetric Shells, Journal of Engineering Mechanics Division, ASCE, pp. 119-145, 1964.

73. Pradeepkumar,C.T., Design of Attack Submarine, Undergraduate Project Report, Department of Ship Technology, CUSAT, 1988.

74. Rajagopalan, K. and Ganapathy Chettiar, C., Application of Finite Element Method to the Interstiffener Buckling in Submersible Cylindrical Hulls, Journal of Ship Research, Vol. 27, pp. 281-285, 1983.

75. Rajagopalan, K., Finite Element Buckling Analysis of Stiffened Cylindrical Shells, Oxford and IBH Publishing Company, New Delhi, India, 1993.

76. Ramm, E., Stegmuller, H., The Displacement Finite Element Method in Nonlinear Buckling Analysis of Shells, Proceedings of State of The Art Colloquium, 1982.

77. Reis, A.J., and Walker, A.C., Local Buckling Strength of Cylindrical Shells Under External Pressure, Thin Walled Structures, Vol.2, Issue 4, pp. 325-353,1984.

78. Ross, C.T.F., The Instability of Ring-stiffened Circular Cylindrical Shells, Under Uniform External Pressure, Trans. of RINA. Vol.107, No.1, pp. 139 – 155, 1965.

79. Ross, C.T.F., Lobar Buckling of Thin–Walled Cylindrical Shells and Truncated Conical Shells Under External Pressure, Journal of Ship Research, Vol.18, No.4, pp. 272-277, 1974.

80. Ross C.T.F., Vibration and Instability of Ring Reinforced Circular Cylindrical and Conical Shells, Journal of Ship Research, Vol. 20, pp. 22-31, 1976.

81. Ross, C.T.F. and Mackeny, M.D.A., Deformation and Stability Studies of Thin Walled Domes, Under Uniform External Pressure, Journal of Strain Analysis, Vol. 18, No.3, 1983.

82. Ross, C.T.F., Portsmouth, R., Vibrations of Axisymmetric Shells Under External Water Pressure, Proceedings of Institution of Mechanical Engineers, Journal of Mechanical Engineering Science, Vol. 208, No 3, pp. 177-185, 1994.

83. Ross, C.T.F., Plastic Buckling of Ring Stiffened Conical Shells Under Uniform External Pressure, Journal of Ship Research, Vol.39, No.4, pp. 166-175, 1995.

84. Ross, C.T.F., Gill-Carson A., Little A.P.F., The Inelastic Buckling of Varying Thickness Circular Cylinders Under External Hydrostatic Pressure, Structural Engineering and Mechanics, Vol. 9, No.1, pp. 51-68, 2000.

85. Rules and Regulations for the Construction and Classification of Submersibles and Diving Systems, Lloyd's Register of Shipping, Part II, Chapter 1,1988.

86. Sanders, J.L., Nonlinear Theories for Thin Shells, Quart. App.. Math., Vol. 21, No.1, pp. 21-36,1963.

87. Schokker, A.,Sridharan, S., Kasagi, A., Dynamic Buckling of Composite Shells, Computers and Structures, Vol.59, No.1,pp. 443-453,1996

88. Singer, J., Vibration and Buckling of Imperfect Stiffened Shells – Recent Developments. IVTM Symposium on Collapse, Uni. College, London 1982.

89. Sreekala, K., Finite Element Buckling Analysis of Stiffened Cylindrical Shells, Dept. of Ship Technology, CUSAT, Kochi, India, 1997.

90. Sridharan, S., Analysis of Cylindrical Shells Under Interactive Buckling, Proceedings of Engineering Mechanics, ASCE, Vol. 1, pp. 509-512,1995.

91. Sridharan, S., and Kasagi, A., On Buckling and Collapse of Moderately Thick Composite Cylinders under Hydrostatic Pressure, Vol.28, Issue 5-6, pp. 583-596,1997.

92. Srinath, L.S., Advanced Mechanics of Solids, Tata McGraw-Hill Publishing Company Ltd., New Delhi, 1995.

93. Stanley, A.J., Ganesan, N., Free Vibration Characteristics of Stiffened Cylindrical Shells, Computers and Structures, Vol. 65, No. 1, pp. 33-45,1997.

94. Subbiah, J., Natarajan, R., Stability Analysis of Ring Stiffened Shells of Revolution, Computers and Structures, Vol. 13, pp. 497-503,1981.

95. Subbiah, J., Nonlinear Analysis of Geometrically Imperfect Stiffened Shells of Revolution, Journal of Ship Research, Vol. 32, No.1, 1988.

96. Surana, K.S., Geometrically nonlinear Formulation for the Axisymmetric Shell Elements, International Journal for Numerical Methods in Engineering, Vol.18, pp. 477-502,1982.

97. Sze K. Y., Liu X. H. Lo S. H. Popular Benchmark Problems for Geometric Nonlinear Analysis of Shells, Finite Elements in Analysis and Design, Vol. 40, Issue 11, pp. 1551-1569, July 2004,

98. Tian,J.,Wang,C.M., Swaddiwudhipong,S., Elastic Buckling Analysis of Ring Stiffened Cylindrical Shells under General Pressure Loading Via Ritz Method, Thin Walled Structures, Vol. 35, Issue 1, pp. 1-24,1999.

99. Timoshenko, S.P., Krieger,S.W., Theory of Plates and Shells, McGraw-Hill, 1959.

100. Timoshenko, S.P., Gere, Theory of Elastic Stability, McGraw-Hill, 1961.

101. Tomski,L., and Przybyski, J., Post buckling Behaviour of a Clamped Elastically Supported Planar Structures Under Follower Force, AIAA Journal, Vol. 25,No. 4, 1987.

102. Tsang, S.K., Harding, J.E., Ring Stiffened Cylinder Under Interactive Loading, Journal of Structural Division ASCE, Vol. 113, No.9, pp. 1977-1993, 1987.

103. Venkateswara Rao,G., Raju,I.S., Radhamohan, S.K., Buckling of Shells by Finite Element Method, Journal of Engineering Mechanics Division, ASCE, Vol.100, pp. 1092-1096, 1974.

104. Voce,S.J., Buckling Under External Hydrostatic Pressure of Orthotropic Cylidrical Shell with Evenly Spaced Equal Strength Circular Ring Frames, Ocean Engineering,Vol.1, Issue 5, pp. 521-534, July 1969.

105. Wilson, L.B., The Elastic Deformation of a Circular Cylindrical Shell Supported by Equally Spaced Ring Frames Under Uniform External Pressure, Trans. RINA, Vol.108, 1966.

106. Windenburg, D.F., Trilling, C., Collapse by Instability of Thin Cylindrical Shells Under External Pressure, Trans.of ASME, Vol.56, No.11, pp. 819-824, 1934.

107. Wu,D.L.,Zhang,Z, Nonlinear Buckling Analysis of Discretely Stiffened Composite Cylindrical Shells, Composite Structures, Vol.18, Issue1, pp. 31-45,1991.

108. Zhen-yi Ji, Kei-yuan Yeh, General Solution for Nonlinear Buckling of Nonhomogeneous Axial Symmetric Ring and Stringer Stiffened Cylindrical Shells, Computers and Structures, Vol. 4, No. 4, pp. 585-591, 1990.

109. Zienkiewicz, O.C., The Finite Element Method, Mc Graw-Hill Book Company, New York, 1979.

APPENDIX A

ELEMENTS OF STIFFNESS MATRICES OF ALL-CUBIC AXISYMMETRIC ELEMENTS AND DISCRETE STIFFENER ELEMENTS

A.1 Upper Triangular Elements of Elastic Stiffness Matrix [k] of the Shell Element (Rajagopalan, 1993)

$k_{11} = (\pi RLEt / 1-\nu^2)\ [6/5L^2+13(1-\nu)n^2/70R^2]$

$k_{12} = (\pi RLEt / 1-\nu^2)\ [1/10L+11(1-\nu)n^2 L/420R^2]$

$k_{13} = (\pi RLEt / 1-\nu^2)\ [(1-3\nu)n/4RL]$

$k_{14} = -(\pi RLEt / 1-\nu^2)\ [(1+\nu)n L/20R]$

$k_{15} = (\pi RLEt / 1-\nu^2)\ [\nu/2R L]$

$k_{16} = (\pi RLEt / 1-\nu^2)\ [\nu/10R]$

$k_{17} = (\pi RLEt / 1-\nu^2)\ [6/5L^2+9(1-\nu)n^2/140R^2]$

$k_{18} = (\pi RLEt / 1-\nu^2)\ [1/10L+13(1-\nu)n^2 L/840R^2]$

$k_{19} = (\pi RLEt / 1-\nu^2)\ [(1+\nu)n/4R L]$

$k_{110} = -(\pi RLEt / 1-\nu^2)\ [(1+\nu)n L/20R]$

$k_{111} = (\pi RLEt / 1-\nu^2)\ [\nu/2R L]$

$k_{112} = -(\pi RLEt / 1-\nu^2)\ [\nu/10R]$

$k_{22} = (\pi RLEt / 1-\nu^2)\ [2/15+11(1-\nu)n^2 L^2/210R^2]$

$k_{23} = (\pi RLEt / 1-\nu^2)\ [(1+\nu)n L/20R]$

$k_{25} = -(\pi RLEt / 1-\nu^2)\ [\nu/10R]$

$k_{27} = (\pi RLEt / 1-\nu^2)\ [1/10L+13(1-\nu)n^2 L/840R^2]$

$k_{28} = (\pi RLEt / 1-\nu^2)\ [1/30-(1-\nu)n^2 L^2/280R^2]$

$k_{29} = -(\pi RLEt / 1-\nu^2)\ [(1+\nu)n/20R]$

$k_{210} = -(\pi RLEt / 1-\nu^2)\ [(1+\nu)n L/120R]$

$k_{211} = (\pi RLEt / 1-\nu^2)\ [\nu/10R]$

$k_{212} = -(\pi RLEt / 1-\nu^2)\ [\nu L/60R]$

$k_{33} = (\pi RLEt / 1-\nu^2)\ \{[13 n^2/35 R^2+3(1-\nu)/5L^2] + t^2/12[13 n^4/35 R^4+12(1-\nu)/5R^2L^2]\}$

$k_{34} = (\pi RLEt / 1-\nu^2)\ \{[11 n^2 L/210 R^2] + (1-\nu)/20L] + t^2/12[11 n^2 L/210 R^4 + 1-\nu)/5R^2L^2]\}$

$k_{35} = -(\pi RLEt / 1-\nu^2)\ \{[13n/35R^2] + t^2/12[11 n^2 L/210 R^4+6 n(\nu-2)/5R^2L^2]\}$

$k_{36} = (\pi RLEt / 1-\nu^2)\ \{[11 n L/210 R^2] + t^2/12(11 n^3 L/210 R^4 + n(9\nu+2)/10R^2L]\}$

$k_{37} = (\pi RLEt / 1-\nu^2))\ [(1+\nu)n/4R L]$

$k_{38} = (\pi RLEt / 1-\nu^2)$ $[(1+\nu)\, nL /20R]$

$k_{39} = -(\pi RLEt / 1-\nu^2)$ $\{[9\, n^2/70\, R^2 - 3(1-\nu)/5L^2] + t^2/12[9\, n^2/70\, R^4 - 12(1-\nu)/5R^2\, L^2]$

$k_{310} = (\pi RLEt / 1-\nu^2)$ $\{[13\, n^2/420\, R^2 + (1-\nu)/20L] + t^2/12[13\, n^2/420\, R^4 - 12(1-\nu)/5R^2\, L]$

$k_{311} = -(\pi RLEt / 1-\nu^2)$ $\{[9\, n^2/70\, R^2] + t^2/12[9\, n^3/70\, R^4 - 6\, n\, (2-\nu)/5R^2\, L^2]$

$k_{312} = (\pi RLEt / 1-\nu^2))$ $\{[13\, n\, L/420\, R^2 + t^2/12[13\, n^3\, L/420\, R^4 + 6\, n\, (\nu-2/5R^2\, L^2]$

$k_{44} = (\pi RLEt / 1-\nu^2)$ $\{[13\, n^2\, L^2/105\, R^2 + (1-\nu)/15]\, t^2/12(11\, n^2\, L^2/10\, 5R^4 + 4\, (1-\nu)/15R^2]\}$

$k_{45} = -(\pi RLEt / 1-\nu^2)$ $\{[13nL/210R^2] + t^2/12(-11\, n^3\, L/210\, R^4 + n\, (\nu-2)/10R^2L]\}$

$k_{46} = -(\pi RLEt / 1-\nu^2)$ $\{[nL^2/105R^2] + t^2/12(n^3\, L^2/105R^4 + 2n\, (\nu-2)/15R^2]\}$

$k_{47} = -(\pi RLEt / 1-\nu^2)$ $[(1+\nu)n/20R]$

$k_{48} = -(\pi RLEt / 1-\nu^2)$ $[(1+\nu)n\, L/120R]$

$k_{49} = -(\pi RLEt / 1-\nu^2)$ $\{[13n^2L/420R^2 - (1-\nu)/20\, L] + t^2/12(13\, n^2\, L/420\, R^4 - (1-\nu)/5R^2L]\}$

$k_{410} = -(\pi RLEt / 1-\nu^2)$ $\{[n^2L^2/420R^2 - (1-\nu)/60] + t^2/12(n^2\, L^2/140\, R^4 - (1-\nu)/15R^2]\}$

$k_{411} = -(\pi RLEt / 1-\nu^2)$ $\{[13nL/420R^2] + t^2/12(-13\, n^3\, L/420\, R^4 - n\, (2-\nu)/10R^2L]\}$

$k_{412} = -(\pi RLEt / 1-\nu^2)$ $\{[nL^2/140R^2] + t^2/12(n^3/420\, R^4 + (2-\nu)/30R^2]\}L^2$

$k_{55} = (\pi RLEt / 1-\nu^2)$ $[13/35\, R^2] + t^2/12(12/L^4 + 13n^4/35\, R^4 + 12n^2/5R^2\, L^2]\}$

$k_{56} = (\pi RLEt / 1-\nu^2)$ $[11\, L/210\, R^2] + t^2/12(6/L^3 + 11n^4\, L/210\, R^4 + n^2(5\nu + 1/5R^2\, L]\}$

$k_{57} = -(\pi RLEt / 1-\nu^2)$ $[\nu/2R\, L]$

$k_{58} = (\pi RLEt / 1-\nu^2)$ $\nu/10R$

$k_{59} = -(\pi RLEt / 1-\nu^2)$ $[9\, n/70\, R^2] + t^2/12(9n^3/70\, R^4 + 6n(2-\nu)/5R^2L^2]$

$k_{510} = (\pi RLEt / 1-\nu^2)$ $\{[13nL/420R^2] + t^2/12(13\, n^3\, L/420\, R^4 - n\, (2-\nu)/10R^2L]\}$

$k_{511} = (\pi RLEt / 1-\nu^2)$ $[9/70R^2] + t^2/12(9n^4/70\, R^4 + 12/L^4 + 12n^2/5R^2L^2]$

$k_{512} = (\pi RLEt / 1-\nu^2)$ $[13nL/420R^2] + t^2/12(13n^4\, L/420\, R^4 + 6/L^3 + n^2/5R^2L]$

$k_{66} = -(\pi RLEt / 1-\nu^2)$ $[L^2/105R^2]] + t^2/12(4/L^2 + 11n^4\, L^2/10\, 5R^4 + 4n^2/15R^2]\}$

$k_{67} = -(\pi RLEt / 1-\nu^2)$ $\nu/10R$

$k_{68} = -(\pi RLEt / 1-\nu^2)$ $\nu L/60R$

$k_{69} = -(\pi RLEt / 1-\nu^2)$ $[13nL/420R^2] + t^2/12(13n^3\, L/420\, R^4 + n\, (2-\nu)/10R^2L]$

$k_{610} = -(\pi RLEt / 1-\nu^2)) \{ [nL^2/140R^2] + t^2/12(n^3 L^2 /140 R^4 +n(2-\nu)/30R^2]\}$

$k_{611} = -(\pi RLEt / 1-\nu^2)) [13nL/420R^2] + t^2/12(13n^4 L /420 R^4 +6/L^3+n^2/5R^2L]$

$k_{612} = -(\pi RLEt / 1-\nu^2)) [L^2/140R^2] + t^2/12(n^4 L^2 /140 R^4 +2/L^2+n^2/15R^2]$

$k_{77} = (\pi RLEt / 1-\nu^2) [6/5L^2+13(1-\nu)n^2/70R^2]$

$k_{78} = (\pi RLEt / 1-\nu^2) [1/10L+11(1-\nu)n^2 L/420R^2]$

$k_{79} = (\pi RLEt / 1-\nu^2) [(1-3\nu) n /4RL]$

$k_{710} = -(\pi RLEt / 1-\nu^2) [(1+\nu)n L/20R]$

$k_{711} = (\pi RLEt / 1-\nu^2) [\nu/ 2R L]$

$k_{712} = (\pi RLEt / 1-\nu^2) [\nu/ 10R]$

$k_{88} = (\pi RLEt / 1-\nu^2) [2/15+11(1-\nu)n^2 L^2/210R^2]$

$k_{89} = (\pi RLEt / 1-\nu^2) [(1+\nu)n L/20R]$

$k_{811} = -(\pi RLEt / 1-\nu^2) [\nu/ 10R]$

$k_{99} = (\pi RLEt / 1-\nu^2) \{[13 n^2/35 R^2+3(1-\nu)/5L^2] +t^2/12[13 n^4/35 R^4+12(1-\nu)/5R^2L^2]\}$

$k_{910} = (\pi RLEt / 1-\nu^2) \{ [11 n^2 L /210 R^2] +(1-\nu)/20L] + t^2/12[11 n^2 L /210 R^4+ 1-\nu)/5R^2L^2]\}$

$k_{911} = -(\pi RLEt / 1-\nu^2) \{[13n/35R^2] + t^2/12[11 n^2 L /210 R^4+6 n (\nu-2)/5R^2L^2]\}$

$k_{912} = (\pi RLEt / 1-\nu^2) \{[11 n L /210 R^2] + t^2/12(11 n^3 L /210 R^4+ n (9\nu+2)/10R^2L]\}$

$k_{1010} = (\pi RLEt / 1-\nu^2) \{[13 n^2 L^2/105 R^2+(1-\nu)/15] t^2/12(11 n^2 L^2/10 5R^4+ 4 (1-\nu)/15R^2]\}$

$k_{1011} = -(\pi RLEt / 1-\nu^2) \{ [13nL/210R^2] + t^2/12(-11 n^3 L /210 R^4+ n (\nu-2)/10R^2L]\}$

$k_{1012} = -(\pi RLEt / 1-\nu^2) \{[nL^2/105R^2] + t^2/12(n^3 L^2/105R^4+2n (\nu-2)/15R^2]\}$

$k_{1111} = (\pi RLEt / 1-\nu^2) [13 /35 R^2] + t^2/12(12/L^4+13n^4 / 35 R^4+12n^2/5R^2 L^2]\}$

$k_{1112} = -(\pi RLEt / 1-\nu^2) [11 L /210 R^2] + t^2/12(6/L^3+11n^4 L / 210 R^4+n^2(5\nu+1/5R^2 L]\}$

$k_{1212} = (\pi RLEt / 1-\nu^2) [L^2/105R^2]] + t^2/12(4/L^2+n^4 L^2 /10 5R^4+4n^2/15R^2]\}$

A.2 Elements of Stress Resultant Matrix [S]

```
L  = Ls/N;
b = 1/(L*L);

N2 = (1-3*S*S+2*S*S*S)/R;
N3 = (S-2*S*S+S*S*S)/R;

N5 = (3*S*S-2*S*S*S)/R;
N6 = (-S*S+S*S*S)/R;
N7 = (6 - 12*S)/(L*L);
N8 = (6*S-6*S*S)/(R*L);
N9 = S/L;
N10 =(1-4*S-3*S*S)/R;
N11 = (-2*S+3*S*S)/R;
H = (1-nw)/2;
J = t*t/12;
W =E*t/(1-nw*nw);
M[0][0] =-R*N8;
M[0][1] = R*N10;
M[0][2] = nw*n*N2;
M[0][3] = nw*n*L*N3;
M[0][4] = -nw*N2;
M[0][5] =-nw*L*N3;
M[0][6] = R*N8;
M[0][7] = R*N11;
M[0][8] = nw*n*N5;
M[0][9] = nw*n*L*N6;
M[0][10] =-nw*N5;
M[0][11] =-nw*L*N6;

M[1][0] =-nw*R*N8;
M[1][1] = nw*R*N10;
M[1][2] =n*N2;
M[1][3] =n*L*N3;
M[1][4] =-N2;
M[1][5] =-L*N3;
M[1][6] =nw*R*N8;
M[1][7] =nw*R*N11;
M[1][8] =n*N5;
M[1][9] =n*L*N6;
```

```
M[1][10] =-N5;
M[1][11] =-L*N6;

M[2][0] = -H*n*N2;
M[2][1] =-H*n*L*N3;
M[2][2] =-H*R*N8;
M[2][3] =H*R*N10;
M[2][4] =0.0;
M[2][5] =0.0;
M[2][6] =-H*n*N5;
M[2][7] =-H*n*L*N6;
M[2][8] =R*N8;
M[2][9] =R*N11;
M[2][10] =0.0;
M[2][11] =0.0;

M[3][0] =0.0;
M[3][1] =0.0;
M[3][2] =J*nw*n*N2/R;
M[3][3] =-J*nw*n*L*N3/R;
M[3][4] = J*(-N7+-nw*n*n*N2/R);
M[3][5] =J*(-4*b*L+6*N9-nw*(n*n*L*N3/R));
M[3][6] = 0.0;
M[3][7] =0.0;
M[3][8] =J*nw*n*N5/R;
M[3][9] =nw*n*L*N6/R;
M[3][10] =J*(-N7-nw*n*n*N5/R);
M[3][11] =J*(-2*b *L+6*N9-nw*n*n*L*N6/R);

M[4][0] =0.0;
M[4][1] =0.0;
M[4][2] =J*n*N2/R;
M[4][3] =-J*n*L*N3/R;
M[4][4] =J*-(nw*N7+n*n*L*N2/R);
M[4][5] =J*(nw*(-4*b *L+6*N9)-n*n*L*N3/R);
M[4][6] =0.0;
M[4][7] =0.0;
M[4][8] =J*n*N5/R;
M[4][9] =J*n*N6*L/R;
M[4][10] =J*(nw*N7-n*n*N5/R);
```

```
M[4][11] =J*(nw*(-2*b*L+6*N9)-n*n*L*N6/R);

M[5][0] =0.0;
M[5][1] =0.0;
M[5][2] =-H*2*N8;
M[5][3] =H*2*N10;
M[5][4] =H*2*n*N8;
M[5][5] =-H*2*n*N10;
M[5][6] =0.0;
M[5][7] =0.0;
M[5][8] =H*2*N8;
M[5][9] =H*2*N11;
M[5][10] =-H*2*n*N8;
M[5][11] =-H*2*n*N11;
```

A.3 Upper Triangular Elements of Elastic Stiffness Matrix [k_s] of the Stiffener Element (Rajagopalan,1993)

$k_{S11} = \pi G C_R n^2/R_R^3$

$k_{S16} = \pi G C_R e n^2/R_R^3 - \pi G C_R n^2/R_R^2$

$k_{S33} = \pi\, n^2 E A_R R_R/R^2 + \pi\, n^2 E I_R/R_R R^2$

$k_{S35} = \pi\, n E A_R/R[(n^2 e/R)-1] + \pi\, n^3 E I_R/R_R^2 R[(e/R)-1]$

$k_{S55} = \pi\, n E A_R/R_R\, [(n^2 e/R)-1]^2 + \pi\, n^4 E I_R/R_R^3 [(e/R)-1]^2$

$k_{S16} = \pi G C_R n^2/R_R[(e/R_R)+1]^2$

A.4 Upper Triangular Elements of Geometric Stiffness Matrix [kg] of the Shell Element (Rajagopalan, 1993)

$k_{g33} = =(p\pi R^2 L / 2) 13\alpha_2/3R^2$

$k_{g34} = (p\pi R^2 L / 2) 11\alpha_2 L/210R^2$

$k_{g35} = (p\pi R^2 L / 2) 13\alpha_2 n/35R^2$

$k_{g36} = -(p\pi R^2 L / 2) 11\alpha_2\, n\, L/210R^2$

$k_{g39} = (p\pi R^2 L / 2) 9\alpha_2/70R^2$

$k_{g310} = -(p\pi R^2 L / 2) 13\alpha_2/420R^2$

$k_{g311} = -(p\pi R^2 L / 2) 9\alpha_2\, n /70R^2$

$k_{g312} = (p\pi R^2 L / 2) 13\alpha_2\, n\, L /420R^2$

$k_{g44} = (p\pi R^2 L / 2) \alpha_2 L^2/105R^2$

$k_{g45} = -(p\pi R^2 L / 2) 11\alpha_2\, n\, L/210R^2$

$k_{g46} = -(p\pi R^2 L / 2) \alpha_2\, n\, L^2/105R^2$

$k_{g49} = -(p\pi R^2 L / 2) 13\alpha_2/420R^2$

$k_{g410} = -(p\pi R^2 L / 2) \alpha_2 L^2/140R^2$

$k_{g411} = -(p\pi R^2 L / 2) 13\alpha_2\, n /420R^2$

k_{g412}= ($p\pi R^2L$ / 2)α_2 n $L^2/140R^2$
k_{g55}= ($p\pi R^2L$ / 2)($6\alpha_1$ /$5L^2$+$13\alpha_2$n/$35R^2$)
k_{g56}=($p\pi R^2L$ / 2)(α_1 /10L+$11\alpha_2 n^2$ L /$210R^2$)
k_{g59}= -($p\pi R^2L$ / 2)$9\alpha_2$n/$70R^2$
k_{g510}= ($p\pi R^2L$ / 2)$13\alpha_2$ n L /$420R^2$
k_{g511}= -($p\pi R^2L$ / 2)($6\alpha_1$ /$5L^2$ +$9\alpha_2$n/$70R^2$)
k_{g512}=($p\pi R^2L$ / 2)(α_1 /10L+$13\alpha_2 n^2L$ /$420R^2$)
k_{g66}=($p\pi R^2L$ / 2) ($2\alpha_1$ /15+$\alpha_2 n^2L^2$ /$105R^2$)
k_{g69}=-($p\pi R^2L$ / 2) $13\alpha_2$ nL /$420R^2$
k_{g610}= -($p\pi R^2L$ / 2) α_2 nL^2 /$140R^2$
k_{g512}=($p\pi R^2L$ / 2) (α_1 /10L-$13\alpha_2 n^2L$ /$420R^2$)
k_{g99}= -($p\pi R^2L$ / 2)$13\alpha_2$/$35R^2$
k_{g910}= -($p\pi R^2L$ / 2)$11\alpha_2$ n L/$210R^2$
k_{g911}= -($p\pi R^2L$ / 2)$13\alpha_2$ n /$35R^2$
k_{g912}=($p\pi R^2L$ / 2)$11\alpha_2$ n L/$210R^2$
k_{g1010}= ($p\pi R^2L$ / 2)α_2L^2/$105R^2$
k_{g1011}= ($p\pi R^2L$ / 2)$11\alpha_2$ n L/$210R^2$
k_{g1012}= -($p\pi R^2L$ / 2)α_2 n L^2/$105R^2$
k_{g1111}=($p\pi R^2L$ / 2)($6\alpha_1$ /$5L^2$ +$13\alpha_2 n^2$/$35R^2$)
k_{g1112}=($p\pi R^2L$ / 2)(α_1 /10L-$11\alpha_2 n^2L$ /$210R^2$)
k_{g1212}=($p\pi R^2L$ / 2)($2\alpha_1$ /15+$\alpha_2 n^2L^2$ /$105R^2$)

A.5 Upper Triangular Elements of Geometric Stiffness Matrix [k_{gS}] of the Stiffener Element (Rajagopalan, 1993)

k_{gS33} = $\pi p A_R R_R L_s/[R(A_R+tL_s)]$

k_{gS35} =$[n\pi p A_R L_s/(A_R+tL_s)]$ [(e/R)-1]

k_{gS55} =$[n^2\pi p R A_R L_s/R_R (A_R+tL_s)]$ $[(e/R)-1]^2$

A.6 Upper Triangular Elements of Pressure Stiffness Matrix [k_P] of the Shell Element (Rajagopalan, 1993)

k_{P16} = -1/10 ($p\pi RL$)
k_{P111} = -1/2L ($p\pi RL$)
k_{P112} = 1/10 ($p\pi RL$)
k_{P25} =-1/10 ($p\pi RL$)
k_{P211} = -1/10 ($p\pi RL$)
k_{P212} = L/60 ($p\pi RL$)
k_{P33} = 13/35R ($p\pi RL$)
k_{P34} = 11L/210R ($p\pi RL$)
k_{P35} = 13n/35R ($p\pi RL$)
k_{P36} = -11nL/210R ($p\pi RL$)

$k_{P39} = 9/70R\ (p\pi RL)$
$k_{P310} = -13L/420R\ (p\pi RL)$
$k_{P311} = 9n/70R\ (p\pi RL)$
$k_{P312} = -13nL/420R\ (p\pi RL)$
$k_{P44} = -L^2 1/105R\ (p\pi RL)$
$k_{P45} = 11L/210R\ (p\pi RL)$
$k_{P46} = nL^2/105R\ (p\pi RL)$
$k_{P49} = 13L/420R\ (p\pi RL)$
$k_{P410} = -L^2/140R\ (p\pi RL)$
$k_{P411} = 13nL/420R\ (p\pi RL)$
$k_{P412} = -nL^2/40R\ (p\pi RL)$
$k_{P55} = 13/35R\ (p\pi RL)$
$k_{P56} = 11L/210R\ (p\pi RL)$
$k_{P57} = 1/2L\ (p\pi RL)$
$k_{P58} = -1/10\ (p\pi RL)$
$k_{P59} = 9n/70R\ (p\pi RL)$
$k_{P510} = -13nL/420R\ (p\pi RL)$
$k_{P511} = 9/70R\ (p\pi RL)$
$k_{P512} = -13nL/420R\ (p\pi RL)$
$k_{P66} = L^2/105R\ (p\pi RL)$
$k_{P67} = -1/10\ (p\pi RL)$
$k_{P68} = -L/60\ (p\pi RL)$
$k_{P69} = 13nL/420R\ (p\pi RL)$
$k_{P610} = nL^2/140R\ (p\pi RL)$
$k_{P611} = 13L/420R\ (p\pi RL)$
$k_{P612} = -L^2/140R\ (p\pi RL)$
$k_{P712} = -1/10\ (p\pi RL)$
$k_{P811} = -1/10\ (p\pi RL)$
$k_{P99} = 13/35R\ (p\pi RL)$
$k_{P910} = 11L/210R\ (p\pi RL)$
$k_{P911} = 13n/35R\ (p\pi RL)$
$k_{P912} = -11L/210R\ (p\pi RL)$
$k_{P1010} = L^2/105R\ (p\pi RL)$
$k_{P1011} = -11nL/210R\ (p\pi RL)$
$k_{P1012} = nL^2/105R\ (p\pi RL)$
$k_{P1111} = 13/35R\ (p\pi RL)$
$k_{P1112} = -11L/210R\ (p\pi RL)$
$k_{P1212} = L^2/105R\ (p\pi RL)$

APPENDIX B

CLASSICAL SOLUTIONS AND RULEBOOK PROVISIONS

B.1 General

Various classification societies and relevant rulebooks for the design of submersibles give provisions for scantlings for various shell forms employed in the sub sea environment subjected to external pressure. Generally these provisions are in the form of equations using which the thickness for a given external pressure for various shell geometries can be determined. In each of the rulebook, there are another sets of equations, which give the collapse pressure for the known scantlings. Classical solutions are available for linear static analysis of ring stiffened cylindrical shells. Empirical relations are also available to predict the collapse pressure.

The rulebooks considered in the present study are Indian Standard Code for Unfired Pressure Vessels (1977), Lloyd's Register of Shipping (1988) and Det Norske Veritas (1996). The rulebook provisions for externally pressurized shells are used to generate a computer program, so that the designed pressure for the given scantlings can be calculated. The details of the software are available elsewhere (Sreekala, 1997).

B.2 Classical Solutions for Short Stiffened Cylindrical Shell with External Pressure

Classical solutions are available to determine the radial deflection of the stiffened cylindrical shell as well as for the prediction of collapse pressure. Generally the collapse pressure will be the minimum of pressure predicted for inter-stiffener buckling. yielding and general instability.

B.2.1 Radial Deflection

The expression of the radius deflection of the ring-stiffened cylinder with end cover is

$\delta' = p'a^2 / Eh\,\beta\,(\cosh 2\alpha + \cos 2\alpha)/(\sinh 2\alpha + \sin 2\alpha) - \frac{1}{2}\nu\,((\sinh 2\alpha - \sin 2\alpha)/(\sinh 2\alpha + \sin 2\alpha))^2 / (\cosh 2\alpha - \cos 2\alpha)/(\sinh 2\alpha + \sin 2\alpha)\beta$ [Timosheko, 1959] (B.1)

where $p' = p - Ph/A$, $\delta' = \delta - \delta_1$, $\delta = pa^2/Eh$, $\delta 1 = P^r a^2/AE$.

P^r denotes the magnitude of force per unit length of the ring for a uniform external pressure p.

$\alpha = \beta L / 2$, $\beta = \sqrt[4]{3(1-\nu^2)} / \sqrt{ah}$, a = radius, h=thickness, ν =Poisons ratio, L=length, A = area of cross section of the ring stiffener.

An expression for radial deflection of ring stiffened cylinder is given by Flugge (1962) $\delta = ((2-\nu)/2)pa^2/Eh \{1-[(\cosh\xi \sin\xi + \sinh\xi \cos\xi)\cosh\psi x/a \cos\psi x/a + (\cosh\xi \sin\xi - \sinh\xi \cos\xi)\sinh\psi x/a \sin\psi x/a] \times [\cosh\xi(\sinh\xi + \eta\cosh\xi) + \cos\xi(\sin\xi - + \eta\cos\xi)]^{-1}\}$ .....(B.2)

where $\xi = \sqrt[4]{3(1-\nu^2)}l/(2\sqrt{ah})$, $\eta = (2h\sqrt{ah})/A\sqrt[4]{3(1-\nu^2)}$.

B.2.2 Stress Resultants

Flugge has given closed form solution for stress resultants Mx and N_Q

$Mx = (2-\nu)pah/\sqrt[4]{3(1-\nu^2)} - [(\cosh\xi \sin\xi + \sinh\xi \cos\xi)\cosh\psi x/a \cos\psi x/a - (\cosh\xi \sin\xi - \sinh\xi \cos\xi)\sinh\psi x/a \sin\psi x/a] \times [\cosh\xi(\sinh\xi + \eta\cosh\xi) + \cos\xi(\sin\xi - + \eta\cos\xi)]^{-1}\}$ .....(B.3)

$N_Q = pa\{1-(2-\nu)/2) - [(\cosh\xi \sin\xi + \sinh\xi \cos\xi)\cosh\psi x/a \cos\psi x/a + (\cosh\xi \sin\xi - \sinh\xi \cos\xi)\sinh\psi x/a \sin\psi x/a] \times [\cosh\xi(\sinh\xi + \eta\cosh\xi) + \cos\xi(\sin\xi - + \eta\cos\xi)]^{-1}\}$ .....(B.4)

B.2.3 Shell Buckling

Windenburg (1934) has developed an equation, based on von Mises equation to predict the collapse pressure in the following form

$$P_c = \frac{2.24E(t/D)^{5/2}}{(1-\mu^2)^{3/2}[L/D - 4.5(t/D)^{1/2}]} \quad \text{.....(B.5)}$$

B.2.4 Shell Yielding

Von Sanden and Gunther (Cormstock, 1988) have developed two equations to predict the pressure at which yielding of the shell will occur at frame and midbay.

For yielding at frame

$$P = \frac{2\sigma_Y t/D}{0.5+1.815K((0.85-B)/(1+\beta))} \qquad \text{..... (B.6)}$$

Fore yielding at midbay

$$P = \frac{2\sigma_Y t/D}{1+H((0.85-B)/(1+\beta))} \qquad \text{..... (B.7)}$$

B.2.5 General Instability

The expression for critical pressure associated with general instability is developed by Kendrick and modified by Bryant (1970).

$$P_{cr} = Et/R\{m^4/[n^2-1+(m^2/2)][n^2+m^2]2\}+\{[n^2-1]EI/R^3L\} \qquad \text{..... (B.8)}$$

Where $m = \pi R/L_s$

B.3 Software Developement

Software has been modified to predict the collapse pressure integrating the rulebook provisions and classical solutions. This program has been used to make a critical study of code provisions as well as classical solutions to highlight the over estimation or under estimation of strength which may cause conservative or inadequate design.

B.4 Numerical Investigations

Design pressure has been predicted for stiffened cylindrical shells of M1 and M2. Geometric features of stiffened cylindrical shells of submarine M1 and M2 are given earlier in table 3.2 and in fig. 3.6 and fig. 3.7.

Table B.1 Design pressure predicted by Rulebooks for M1 and M2

No.	Rulebook concerned	Design pressure predicted N/mm^2	
		M1	M2
1	IS 2825	3.389	1.864
2	LRS	7.693	6.812
3	DnV	4.103	3.633

Table B.2 Collapse pressure predicted and safety factor from classical solutions for M1 and M2

Model	Classical solution	Collapse pressure (N/mm^2)	Safety factor
M1	Windenburg's formula (shell buckling)	39.978	13.06
	Bryant's formula (general instability)	25.371 (n=2)	8.41
	Yielding at midbay (Von Sanden and Gunther)	16.603	5.51
	Yielding at frame (Von Sanden and Gunther)	13.331	4.42
M2	Windenburg's formula (shell buckling)	19.512	6.34
	Bryant's formula (general instability)	38.230(n=2)	12.68
	Yielding at midbay (Von Sanden and Gunther)	6.724	2.22
	Yielding at frame (Von Sanden and Gunther)	9.459	3.14

B.5 Discussion on Results

The design pressures predicted by various Rulebooks are given in table B.1. The design pressure predicted by IS 2825 are 3.389 N/mm^2 and 1.864 N/mm^2 for M1 and M2 respectively. The corresponding values predicted by LRS are 7.693 N/mm^2 and 6.812 N/mm^2 and by DnV are 4.103 N/mm^2 and 3.633 N/mm^2 for M1 and M2 respectively. On analysing the results a comparative study of various code provisions is made. The critical study of code provisions highlights the over estimation or under estimation of strength which may cause conservative or inadequate design. On analysing the results it may be concluded that IS code is more conservative than LRS and DnV and may be advised for a revision.

The collapse pressure predicted by empirical formulae and the safety factors (the ratio of collapse to design pressure) are given in table A.2. The collapse pressure predicted by Windenburg's formula are 39.978 N/mm^2 and 19.512 N/mm^2 for M1 and M2 and by Bryant's formula are 25.371 N/mm^2 (n=2) and 38.230 N/mm^2 (n=2). For M1 and M2 yielding of the shell will occur at midbay at 13.331 N/mm^2 and 9.459 N/mm^2 and at frame at 16.603 N/mm^2 and 6.724 N/mm^2 respectively. The computed safety factors indicate that the classical solutions the submarine scantling design are conservative.

G9047

PUBLICATIONS BASED ON THE RESEARCH WORK

1. Alice Mathai, Sreekala.K and Nandakumar C.G., Prediction of Collapse Pressure of Submarine Hull, Proc. of International Seminar on Safety and Fire Engineering, Cochin, India, Nov. 24-26,1999.

2. Alice Mathai and Nandakumar C.G., Analytical Investigations on Collapse of Cylindrical Submarine Shells, Proc. of National Conference on Materials Processing and Failure Analysis, National Institute of Technology, Trichy-620 015, June 2003 19-20.

3. Alice Mathai and Nandakumar C.G., Finite Element Analysis of Submarine Hull, Journal of Institution of Engineers (India) Marine Division, Vol.85, pp. 4-8, July 2004.

4. Alice Mathai and Nandakumar C.G., Geometrically Nonlinear Analysis of Cylindrical Submarine Shells, Accepted for International Congress on Computational Mechanics & Simulation, IIT Kanpur, 9-12 December 2004.

5. Alice Mathai and Nandakumar C.G., Collapse Pressure Prediction of Cylindrical Submarine Shells, To be communicated to Journal of Ship Research, The Society of Naval Architects and Marine Engineers, USA.

UNIVERSITY LIBRARY ★ UNIVERSITY OF SCIENCE AND TECHNOLOGY ★ Cochin - 682 022